Spring 1-1-2018

Natural and Artificial Satellite Dynamics and Evolution Around Near-Earth Asteroids with Solar Radiation Pressure

Samantha M. Rieger
University of Colorado at Boulder, samantha.m.rieger@gmail.com

Natural and Artificial Satellite Dynamics and Evolution around Near-Earth Asteroids with Solar Radiation Pressure

by

Samantha M. Rieger

B.S. Purdue University, West Lafayette IN, 2012

M.S., University of Colorado Boulder, Boulder CO, 2015

A thesis submitted to the

Faculty of the Graduate School of the

University of Colorado in partial fulfillment

of the requirements for the degree of

Doctor of Philosophy

Department of Aerospace Engineering Sciences

2018

This thesis entitled:
Natural and Artificial Satellite Dynamics and Evolution around Near-Earth Asteroids with Solar Radiation Pressure
written by Samantha M. Rieger
has been approved for the Department of Aerospace Engineering Sciences

_____

Dr. Daniel Scheeres

_____

Dr. Jay McMahon

_____

Dr. Hanspeter Schaub

_____

Dr. Philip Armitage

_____

Dr. Stephen Broschart

Date _____

The final copy of this thesis has been examined by the signatories, and we find that both the content and the form meet acceptable presentation standards of scholarly work in the above mentioned discipline.

Rieger, Samantha M. (Ph.D., Aerospace Engingeering Sciences)

Natural and Artificial Satellite Dynamics and Evolution around Near-Earth Asteroids with Solar Radiation Pressure

Thesis directed by Dr. Daniel Scheeres

Natural and artificial satellites are subject to perturbations when orbiting near-Earth asteroids. These perturbations include non-uniform gravity from the asteroid, third-body disturbances from the Sun, and solar radiation pressure. For small natural (1 cm-15 m) and artificial satellites, solar radiation pressure is the primary perturbation that will cause their orbits to go unstable. For the asteroid Bennu, the future target of the spacecraft OSIRIS-REx, the possibility of natural satellites having stable orbits around the asteroid and characterize these stable regions is investigated. It has been found that the main orbital phenomena responsible for the stability or instability of these possible natural satellites are Sun-synchronous orbits, the modified Laplace plane, and the Kozai resonance. These findings are applied to other asteroids as well as to artificial satellites.

The re-emission of solar radiation pressure through BYORP is also investigated for binary asteroid systems. Specifically, the BYORP force is combined with the Laplace plane such that BYORP expands the orbit of the binary system along the Laplace surface where the secondary increases in inclination. For obliquities from $68.875^\circ - 111.125^\circ$ the binary will eventually extend into the Laplace instability region, where the eccentricity of the orbit will increase. A subset of the instability region leads to eccentricities high enough that the secondary will impact the primary. This result inspired the development of a hypothesis of a contact-binary binary cycle described briefly in the following. YORP will increase the spin rate of a contact binary while also driving the spin-pole to an obliquity of 90°. Eventually, the contact binary will fission. The binary will subsequently become double-synchronous, thus allowing the BYORP acceleration to have secular effects on the orbit. The orbit will

then expand along the Laplace surface to the Laplace plane instability region eventually leading to an impact and the start of a new cycle with the YORP process.

Dedication

To my parents for teaching me to DTBG... To Danie for listening and being there when I needed it most... To Jeroen, who has always believed in me and inspires me to be my best...

Acknowledgements

First, I would like to thank my advisor, Dan Scheeres. You are a brilliant teacher and always thoughtful in your guidance. Secondly, I would like to thank my committee: Dr. McMahon, Dr. Schaub, Dr. Armitage, and Dr. Broschart for the advice and taking time to help me become a better researcher. Thank you to my NSTRF mentor, Brent Barbee for taking an active interest in my research and reccomending me to work at Goddard. I'd also like to thank Dr. Knipp who met with me after a lackluster preliminary oral exam, your words of advice and encouragement were exactly what I needed. Also, to Dr. Howell, the person who inspired me to pursue a PhD.

I would also like to thank my fellowships. First, NSTRF for funding this research in grant number NNX13AL69H. As well as the Smead Scholar program and its founders Ann Smead and Michael Byram. Both have been greatly supportive of my educational pursuits and helped prepare me for the next step in my career.

Of course, thank you to all the CSML and ORCCA students for the good times and support. Extra thanks to Nicola, Stefaan, and Alex Davis for your friendship and putting up with me while traveling. I'd like to also thank Ann Dietrich for always just getting it when talking about the grad school life. I want to thank Greg and Graham for just being awesome friends and for getting me outside. Danie deserves the biggest thank you, you have been my one costant through college and graduate school. And Jeroen. I am so grateful for you and your overwhelming support. Thank you for always being there.

Mom and Dad, truly the best parents ever. Thank you for providing me all the opportunities to discover and learn whatever I was interested in at that moment, even if it meant

taking me all the way to Alaska or taping every wolf and Titanic special or reading a book to me everynight or sitting through an opera. Thank you to my brothers for toughening me up, and extra thanks to Tbone for letting me live in his house during my internships.

Nomenclature

$\boldsymbol{a}$	=	acceleration (m/s^2)
a_p	=	semi-major axis of orbit (m)
$\boldsymbol{A_n}$ and $\boldsymbol{B_n}$	=	Fourier coefficients describing binary asteroid asymmetry (m^2)
a_s	=	semi-major axis of asteroid's orbit around the Sun (m)
α	=	right ascension $(^\circ)$
b	=	mass-to-area ratio of satellite (kg/m^2)
C_{nm} and S_{nm}	=	gravitational field harmonics
D	=	diameter of satellite (m)
δ	=	latitude or declination $(^\circ)$
$\boldsymbol{e_p}$	=	eccentricity vector of the satellite
$\boldsymbol{e_s}$	=	eccentricity vector of asteroid around the Sun
ϵ	=	asteroid's obliquity $(^\circ)$
G	=	gravitational constant $m^3/kg - s^2$
$\boldsymbol{h_p}$	=	angular momentum vector of the satellite (m^2/s)
h_s	=	angular momentum of asteroid's orbit around Sun (m^2/s)
$\hat{H}_s$	=	unit-vector direction of asteroid's orbit pole
i	=	inclination of satellite $(^\circ)$
J_2	=	oblateness coefficient of asteroid
m_a	=	mass of asteroid(kg)
m_p	=	mass of the satellite (kg)
m_s	=	mass of the Sun (kg)
μ_a	=	gravitational parameter of the asteroid (m^3/s^2)
μ_s	=	gravitational parameter of the Sun (m^3/s^2)
n	=	mean motion of the satellite's orbit (s^{-1})
λ	=	latitude $(^\circ)$

Λ = SRP perturbation angle (°)

Ω = longitude of the ascending node of asteroid (°)

ω = argument of periapsis of asteroid (°)

ω_s = third-body perturbation factor

ω_2 = oblateness perturbation factor

ω_{SRP} = SRP perturbation factor

$\hat{\boldsymbol{p}}$ = unit-vector direction of asteroid's spin pole

P_ϕ = solar radiation constant $(kg - m/s^2)$

ϕ = the Laplace angle (°)

P_{nm} = Legendre functions

R_a = major radius of asteroid (m)

r_L = Laplace radius (m)

ρ = density of asteroid kg/m^3

$\boldsymbol{r}_p$ = vector distance from the asteroid to the satellite (m)

$\boldsymbol{r}_s$ = vector distance from the asteroid to the Sun (m)

$\boldsymbol{r}_{sp}$ = vector distance between the Sun and the satellite (m)

θ = rotation of spin angle of secondary (°)

U = gravitational potential energy $kg - m^2/s^2$

ν = true anomaly of orbit (°)

T_s = period of the asteroid around the Sun (s)

V_{lc} = local circular speed of the satellite around the asteroid (m/s)

Contents

Chapter

Tables

Table

Figures

Figure

Chapter 1

Introduction

1.1 Introduction

The future looks bright for NEA exploration and utilization. However, these small bodies come with a significant share of challenges within the field of astrodynamics. The unique shapes in which asteroids are formed cause the gravity around them to be non-uniform. Often, the low gravity of the asteroid will result in third-body perturbations to have a significant effect on the orbit of a satellite. Both third-body effects and non-spherical shapes of the asteroid cause perturbations of a satellite's orbit around an asteroid. However, for smaller asteroids, the real challenge of orbiting a NEA is due to the solar radiation pressure (SRP). Many NEAs have a very low gravitational acceleration allowing SRP to be the primary perturbation to the motion of a satellite. The research described in this thesis will be looking at natural and artificial satellites around NEA with perturbations from an oblate body, third-body perturbations, and SRP effects.

The research presented in this thesis focuses on satellite motion around near-asteroids with possible extensions of application to the main-asteroid belt. Near-Earth asteroids are a unique subset of asteroids to study for multiple reasons. First, they are generally smaller than other asteroids in our solar-system. Therefore, their gravity field is very small and easy to escape with the smallest of accelerations on the satellite. Second, they are only 1 AU away from the Sun. Since, accelerations due to solar radiation pressure are inversely proportional to the square of the distance from the Sun, the SRP perturbations at a NEA

is much stronger than at a main-belt asteroid. The combination of the low gravity field and high SRP accelerations create complex dynamics for satellites orbiting asteroids. This research looks into the relationship and how to effects long-term stability of satellites. The research will characterize the orbital phenomena that exist to create or destroy long-term stability at NEA as well as determine these satellites orbital evolution. Before discussing the contributions provided in this thesis, it is essential to review history of these bodies and their exploration and the work that has been done previously on the subject. Depending on the satellite orbiting the NEA, there are different ways of approaching the problem. Therefore, each satellite type is discussed in succession: artificial satellites, natural satellites, and binary satellites.

1.1.1 Near-Earth Asteroid Relevant History and Background

Asteroids are rocky fragments that are left over from the creation of our solar system 4.6 billion years ago. Millions of asteroids populate the inner solar system. They exist in a broad range of shapes, sizes, and compositions. The main-belt between Mars and Jupiter holds the largest population of known asteroids, but there also exists many asteroids closer to home. These asteroids are called near-Earth asteroids. NEAs are characterized as any asteroid that has a perihelion distance less than 1.3 AU and an aphelion distance greater than 0.983 AU [1]. Their proximity to Earth makes them convenient to send a spacecraft to or study with radar and telescopes here on Earth. The current near-Earth Object Wide-field Infrared Survey Explorer (NEOWISE) estimates that there are 20,500 $\pm$ 3000 NEAs larger than 100 m [2].

The first NEA to be discovered was Eros in 1898 by a German astronomer G. Witt [3]. This discovery would foreshadow that NEA are a unique key for finding information on our solar system. Using Eros, measurements were made to determine the solar parallax or the distance of the Earth from the Sun. This measurement is found using triangulation between the Earth, Sun, and Eros. Eros was the object of choice to determine the solar parallax in

1901 and 1930/1931 [4, 5]. These values were not improved upon until planetary radar range data in the 1960's [6, 7].

Eros was also the first asteroid which had variations in light curve data that changed with time [8, 9]. This variation was due to the highly elongated shape of Eros [9, 10]. Eros was the first object in the solar system to be found that didn't have a near spherical or slightly ellipsoidal shape. Soon it would come to find many small bodies in the solar system had odd, elongated bodies. Even some asteroids and comets would have the appearance of two different bodies being fused together.

In time, spacecraft missions were being sent to asteroids. The first spacecraft to fly by an asteroid was Galileo in 1991 to main-belt asteroid 951 Gaspra [11]. After that, it performed a flyby of Ida and Dactyl, the first confirmed binary asteroid system [12, 13]. Although Galileo flew by these asteroids on its way to Jupiter, the next spacecraft to visit asteroids would be dedicated entirely to asteroid science. Near Earth Asteroid Rendezvous Shoemaker (NEAR Shoemaker) was the first spacecraft to visit a NEA, insert into an orbit around an asteroid, and land on the asteroid. First NEAR did a flyby of 253 Mathilde. NEAR determined the density of Mathilde, 1.3 ± 0.3 g/cm^3, which is very low and suggested that Mathilde was a "rubble pile" asteroid [14, 15]. A "rubble pile" asteroid is a collection of gravitationally bound rocks and boulders of different sizes with relatively small cohesive forces holding them together [16, 17, 18]. After the Mathilde flyby, NEAR Shoemaker orbited and landed on Eros confirming its elongated ellipsoidal shape [19, 20]. The next mission dedicated to a NEA was JAXA's Hayabusa mission, which was sent to 25143 Itokowa. Hayabusa did an in-depth study of Itokawa to determine its "rubble pile" morphology. Itokawa had a "new" surface, meaning it had no visible impact craters and appeared to be a collection of fragments [21]. In fact, it is theorized that Itokawa is a contact binary, meaning that it was at one time a binary system that eventually collided and now is a single body[22, 23].

Scientists are also observing these asteroids from Earth by telescopes and radar imaging. They also observe asteroids from telescope satellites. For instance, NEOWISE using the

Wide-field Infrared Survey Explorer (WISE) has discovered new NEA. Several astronomical surveys on Earth include Lincoln Near-Earth Asteroid Research (Linear) and Catalina Sky Survey. As of November 1, 2017, 17,017 NEA have been found with diameters between 1 meter to 32 km [24]. Currently, a spacecraft has not visited a NEA binary system, however, through observations from Arecibo Observatory, observers were able to characterize the 1999 KW_4 primary and secondary asteroid components of this binary [25]. The primary (alpha) is the larger of the two binaries, while the secondary (beta) is the smaller asteroid that orbits around the alpha. To date of this thesis submittal, there are 62 known binary NEA, with two asteroids containing two satellites each [26]. These binaries were found using radar or light curve analysis.

Space agencies such as JAXA and NASA continue to survey and explore near-Earth asteroids. There are two missions currently headed to asteroids from both NASA and JAXA. NASA's New Frontier mission, OSIRIS-REx will arrive at 101955 Bennu in 2018 for a sample return mission that will return to Earth in 2023 [27]. JAXA's Hayabusa 2 is expected at NEA 162173 Ryugu in 2018 with a sample return in the year 2020 [28]. The popularity of NEAs as a destination for spacecraft missions will only continue to increase. Sending spacecraft to NEA is more accessible due to their relative proximity to the Earth, where less propellant is needed to travel to the mission destination. Also, compared to planets or moons, the low gravity of asteroids makes it easier to move around, land, and return samples to Earth without using much propellant. Besides their convenience in this respect, there is a myriad of reasons to visit these bodies. First is for the simple scientific reason of understanding asteroids. This includes understanding their composition and structure as well as the evolution and formation of single, binary, and ternary asteroid systems. Beyond this, asteroids also provide information through samples on the formation and evolution of the solar system, planetary formation, and contain organic compounds which led to the formation of life [27, 29].

Studying and visiting asteroids also has applications for future space missions which

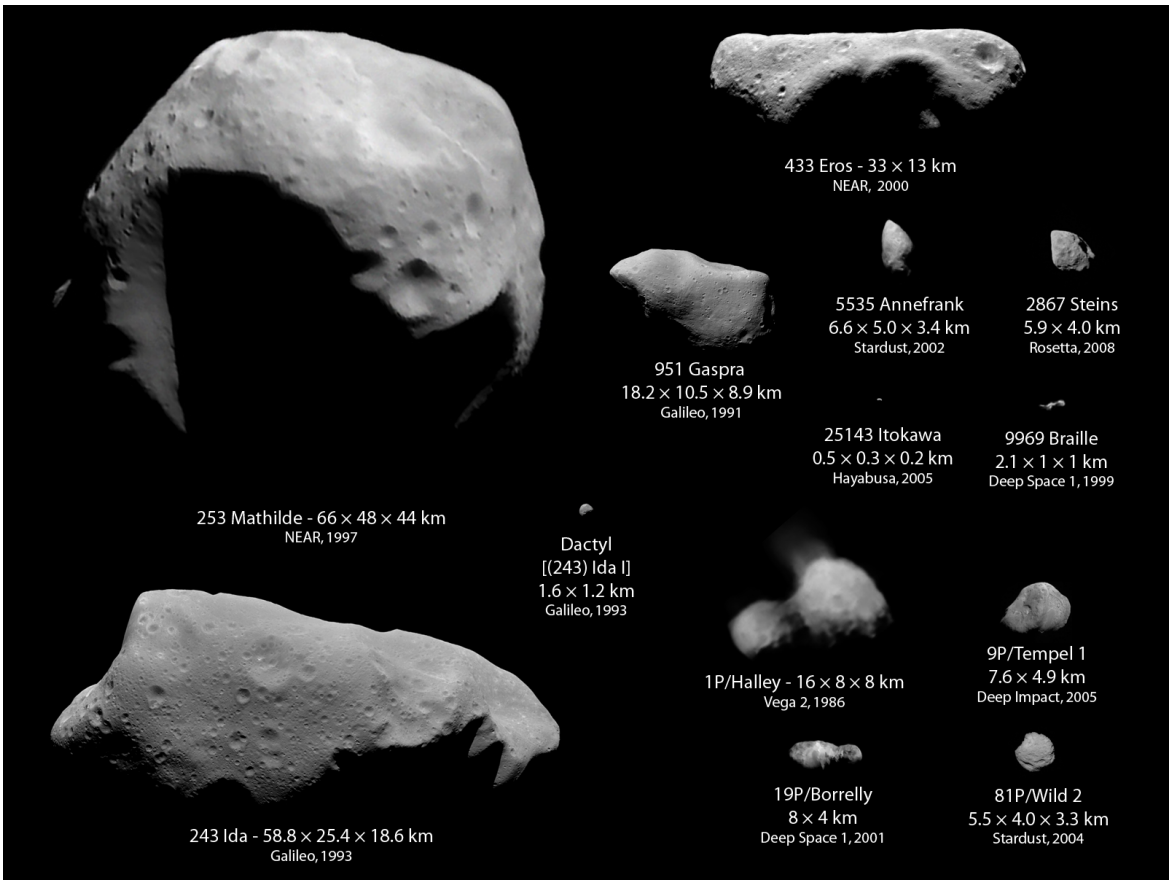

Figure 1.1: Images from spacecraft during missions to the above listed asteroids or comets. Mathilde, Gaspra, Eros, Itokawa, Ida, and Dactyl are specifically discussed in this chapter. *Photo courtesy of the Planetary Society Credits: All images NASA / JPL / Ted Stryk except: Mathilde: NASA / JHUAPL / Ted Stryk; Steins: ESA / OSIRIS team; Eros: NASA / JHUAPL; Itokawa: ISAS / JAXA / Emily Lakdawalla; Halley: Russian Academy of Sciences / Ted Stryk; Tempel 1: NASA / JPL / UMD; Wild 2: NASA / JPL.*

include planetary defense from potentially hazardous asteroids and mining these bodies for resources. AIDA is a conceptual mission that would arrive at NEA binary system 65803 Didymos. It would be the first NEA binary system visited by a spacecraft, but also the NASA portion of the mission would be a technology demonstration of crashing a kinetic impactor onto the Didymos beta. This mission would test the plausibility of using such a method to deflect an asteroid from a collision course with Earth. The mission would be able to measure the trajectory change and momentum transfer due to this impact [30, 31]. This crash would also provide observations of the dust plume of the impact, crater, and exposed new material. These observations will help investigate asteroid composition and will be beneficial to scientists and asteroid mining companies. Although currently not a reality, there are two American asteroid mining companies: Planetary Resources and Deep Space Industries. Both companies are still in the conceptual phases of mission design. In the future, mining asteroids could provide precious metals or water to be processed into in situ propellant for interplanetary flight.

1.1.2 Artificial Satellites

An artificial satellite or spacecraft orbiting around an asteroid will have multiple strong perturbations affecting its orbit. However, depending on the asteroid size and shape or orbit of the spacecraft, the approach to modeling the problem may change. For instance, an asteroid like Eros is the second largest asteroid in the NEA population and has an elongated asymmetrical body. Therefore a spacecraft performing proximity operations around Eros will be more concerned with the non-uniform gravity than SRP. Previous work began with modeling elongated asteroids as a tri-axial ellipsoid. Chauvineau provides information on periodic and synchronous orbits around a tri-axial ellipsoid[32, 33]. He finds that retrograde orbits seem to be more stable to perturbations than prograde orbits [32]. A triaxial ellipsoid is a model that will provide fundamental knowledge on an elongated asteroid, but one can apply shape models of real asteroids using spherical gravity harmonics [34]. This uses a Leg-

endre polynomial series expansion with coefficients describing the gravity harmonics applied to a reference sphere. Spherical harmonics more precisely model the real gravity field at an asteroid than a simple ellipsoid model, but one needs information on the asteroid first to obtain the coefficients needed to use spherical harmonics. When a radar-derived physical model of the complex shaped 4179 Toutatis with a non-principal axis of rotation was developed, Scheeres et al. used spherical harmonics to determine periodic orbits and the escape speed of ejecta on the surface[35]. Next, Scheeres applies his models and analysis to Eros with preliminary information from NEAR. Eros is a uniformly rotating asteroid, which is much more common than the complex spin-state of Toutatis. Therefore, his analysis on Eros can be applied to other asteroids, when information on their shape is obtained. Most important to spacecraft mission design for NEAR and future missions, Scheeres gives computational methods on specific limits on stability against impact[36].

The above research focused on highly elongated asteroids. However, some asteroids approach the shape of an oblate spheroid. Plus, there are plenty of NEAs that are small enough that SRP rivals the gravitational force on the satellite. In these cases, SRP must be modeled. The most straightforward version of this model would be represented best as a two-body problem with a constant force model representing solar radiation pressure. This model was first studied by Dankowicz in 1994 where he found a stable orbit family perpendicular to the direction of the radiation pressure [37]. Dankowicz also derived an equation for the orbit semi-major axis at which the second body would escape the system due to SRP:

$$a_{\max} = \frac{\sqrt{3}}{4}\sqrt{\frac{\mu_a b}{P_\phi}}r_s. \tag{1.1}$$

Where μ is the gravitational parameter of the asteroid, b is the mass-to-area ratio of the satellite, P_ϕ is the solar radiation constant ($1\text{x}10^{17}$ kg $-$ m/s^2), and r_s is the distance of the asteroid from the Sun. The stable orbit families found perpendicular to the direction of SRP also exist when the asteroid body is rotating around the Sun. However, the fixed frozen

orbit can only be seen in the asteroid-rotating frame about the Sun because as the asteroid rotates around the sun, the direction of SRP changes and the frozen orbit must precess to maintain being perpendicular to SRP. The stable orbital families are called terminator orbits because they remain parallel to the terminator line of the asteroid. This also means the terminator orbit is perpendicular to the asteroid-Sun vector[38, 39].

Most models would benefit from modeling both SRP and the higher order gravity of the asteroid. The culmination of this work, where solar tides, spherical harmonics, and SRP are all modeled together was first presented at a conference by Scheeres that defines which perturbation is most substantial depending on the size of the asteroid and the orbit radius of the satellite [40]. Scheeres then published in 2012 a more thorough paper on the topic of these combined perturbations along with the total effects on the terminator plane [41]. This paper also related that if the semi-major axis is less than this value, a terminator plane orbit will not allow the satellite to escape [39]. This equation is

$$a_{\min} = \frac{1}{4}\sqrt{\frac{\mu_a b}{P_\phi}} r_s. \tag{1.2}$$

The terminator orbit has become one of the best options for spacecraft to orbit a small asteroid where SRP is a significant perturbation. A terminator orbit is an orbit that lies perpendicular to the Sun-asteroid radius vector such that its inclination is at $i = 90°$. The orbit lies along the terminator, where the Sun-facing hemisphere meets the hemisphere that is in the dark. For asteroids, the orbit is capable of being stable with large perturbations from solar radiation pressure. For the OSIRIS-REx mission a terminator plane orbit will be used for two different science phases during the mission [42].

1.1.3 Natural Satellites

SRP scales with the mass-to-area ratio of the object. Mass-to-area ratio is the inverse of the more often used area-to-mass ratio. Therefore an object will have larger perturba-

tions from SRP when the area-to-mass ratio increases, while for mass-to-area ratios, larger perturbations from SRP occur when its value decreases. A spacecraft, which is built to have little mass, but has solar panels with large areas to absorb light will generally have a low mass-to-area ratio. For natural objects around an asteroid, a dust particle would be highly perturbed because it has a very low mass-to-area ratio. However, a large boulder, even with a low density, has a high enough mass-to-area ratio not to be perturbed by SRP. Natural satellites are defined as any object that orbits a celestial body that is not human-made. The research in this thesis looks at two types of natural satellites, based on the mass-to-area of these objects, they result in two different models being needed to define their motion correctly. These natural satellites are called natural satellites and binary asteroids. Therefore, the definition of natural satellite for this thesis is a satellite of an asteroid where SRP influences the orbit because the rock, pebble or boulder has a relatively low mass-to-area ratio. The definition of a binary asteroid is a natural satellite large enough that the direct force caused by the SRP is not enough to affect the orbit of the object.

For natural satellites still affected by SRP, the research on artificial satellites is very applicable. The range of mass-to-area ratios for spacecraft going to an asteroid range between 33 kg/m^2 for Hayabusa to 100 kg/m^2 for a CubeSat [29]. While a natural satellite with a density of 2000 kg/m^3 can have a mass-to-area ratio of anything <20,000 kg/m^2. Therefore, natural satellites may be stable in certain orbits where a spacecraft would not. There have been few studies of natural satellites around NEA. There have been studies on the dust ejecta that have been included in research on stable orbits around asteroid and comets, but dust usually is only μm in size [43, 44]. Hamilton and Burns did two studies on objects up to centimeters in size. The first study was on particles around a main-belt asteroid like Amphitrite with third-body perturbations from the Sun. The second paper is the exact same model plus SRP [45, 46]. The second study found particles on the order of cm in size were not perturbed by SRP and stable around the asteroid for tens of years. However, their asteroid model has a 100-km radius and is 2.55 AU away from the Sun. A NEA would be

much smaller than this asteroid and much closer to the Sun. Therefore, SRP would be a stronger perturbation than this study's model and the gravity of the asteroid would be much weaker. Therefore, objects at cm sizes may not be stable for most NEA, but larger objects on the order of meters could be stable. Further analysis would be needed to make such a conclusion on natural satellite stability around NEA.

The purpose of studying artificial satellites may seem more evident than natural satellites, but both need to be understood for spacecraft operations at an asteroid. To plan for a mission to an asteroid, only limited information can be obtained from radar and optical surveys on Earth. There is a certain amount of error in the estimation of the mass, shape, and rotation of the asteroid that will not be clarified until the spacecraft is approaching the asteroid. This is also true for knowing if the asteroid has a natural satellite. For instance, ground-based observations have determined that no object greater than 15 m in diameter is orbiting around Bennu, the NEA to be explored by OSIRIS-REx, but has no constraints on the presence of objects less than this size [47].

Because of the possible risks that are associated with unknown natural satellites upon arrival at an asteroid, it is imperative for a spacecraft to begin scanning the area with its instruments to try and detect natural satellites in orbit. In fact, OSIRIS-REx is performing a natural satellite survey during the approach to Bennu [27]. From the approach distance, large 10 m natural satellites will be easy to quickly spot, however, object less than a 1 m in diameter will be more challenging. With a Hill sphere of 29.5 km, OSIRIS-REx would need to scan $\sim$ 2700 km^2 around the asteroid to conclude whether a natural satellite exists and further analysis if it requires a potential redesign of the spacecraft's trajectory to avoid a collision [48]. Knowing where these natural satellites exist in a stable orbit for long periods of time will constrain the prime search area significantly. Therefore, more time can be allocated to optical imaging of smaller areas around the asteroid, so that quality data can be presented with findings of smaller diameter natural satellites that could significantly impact the mission.

The previous literature summarized gives a summary of what has been studied with regard to natural and artificial asteroids around asteroids. With artificial asteroids, there has been research with various models presented to describe the stability of satellites around asteroids. However, this research does not precisely overlap with natural satellite research where the mass-to-area ratios of these object can be much larger and therefore stable to SRP in certain orbits that are not stable for spacecraft. The natural satellite research that have been previously done is very limited, with only a few studies into millimeter to centimeter sized objects at main-belt asteroids. Therefore natural satellite stability at near-Earth asteroids or even meter sized natural satellites are not very well known. The research presented in this thesis hopes to provide a couple answers on some fundamentals questions that have not been answered such as:

(1) What does natural satellite stability at NEA look like?

(2) Where are centimeter to meter sized natural satellites stable for long periods of time at NEA?

(3) What orbital phenomena can explain the stability or instability of a given natural satellite in an arbitrary orbit around a NEA?

(4) Does any of this research extend to artificial satellites and our knowledge of their stability at NEA?

1.1.4 Binary Asteroid System

For binary asteroid systems with very high mass-to-area ratios, SRP does not have a significant effect on an asteroid's motion. However, thermal re-emission of the heat that comes from SRP on an asteroid can have secular effects on the asteroid over long periods of time. These non-gravitational forces have been theorized and observed to play a critical

role in the formation and evolution of binary asteroid systems in the NEA and main-belt asteroid populations.

The model begins with a single asteroid orbiting the Sun. As the asteroid rotates about its axis, the part of the asteroid facing the Sun will heat up due to the incident photons. As the asteroid rotates, and that specific part of the asteroid is no longer directly facing the Sun, the heat will be re-radiated off the asteroid. Because there is a difference in where the absorption of heat and re-emission of heat occurs on the asteroid, this causes a net force that will change the orbit of the asteroid. If the asteroid is prograde, it will increase the semi-major axis of the asteroid and if it is retrograde the effect will cause the asteroid to reduce in the semi-major axis. This is called the Yarkovsky effect and was studied by Yarkovsky in 1900 [49]. The specific case of the Yarkovsky effect described above is called the diurnal effect and is maximized by the asteroid having an obliquity of 0° or 180°.

There is also the seasonal Yarkovsky effect. The seasonal Yarkovsky effect is also an effect due to thermal re-emission, but because the obliquity is not 0° or 180°. When a hemisphere absorbs more heat in autumn than it does in spring because of the object's obliquity, this will cause a secular decrease in the semi-major axis of the orbit [50]. Rubincam first confirmed this effect with the spacecraft Lageos [51].

Rubincam then defined the Yarkovsky-O'Keefe-Radvieskii-Paddack (YORP) effect. He named the effect to recognize the research of predecessors that studied how the albedo or a body's shape can re-emit radiation in such a way to spin up objects such as tektites or nonmagnetic meteorites till they eventually burst [52, 53, 54]. YORP builds off this idea with an asymmetrical asteroid uniformly rotating such that it asymmetrically scatters SRP re-emissions causing a net torque on the asteroid.

This can cause the asteroid to spin up or spin down while also driving its obliquity to 0°/180° or 90° [55]. Vokrouhlický and Čapek also investigated how YORP drives known models of asteroids and random asymmetrical bodies and found the same results [56]. However, these two studies simplify the analysis by not including thermal conductivity. Once finite

thermal conductivity is added, the obliquity tends to be driven to 0°/180° instead of 90° [57]. Work has also been done to analytically characterize YORP with simple bulk coefficients to understand the general evolution and time to reach a specific end state[58, 59, 60]. YORP has been found in observations as opposed to only being computationally modeled. There have been several observed asteroid spin-rates increasing between periods of observations, these changes have aligned with the predictions of the YORP effect [61, 62, 63].

Recently, YORP has been given the title normal-YORP, as the second type of YORP has recently been theorized called tangential-YORP. Tangential-YORP is "re-emission of absorbed solar light by centimeter to decimeter-sized structures on the asteroid can create a component of the recoil force that is parallel to the surface" [64]. Tangential-YORP is like normal-YORP in that it alters the spin state of the asteroid. With an obliquity of 0°, the tangential YORP can be equal to normal-YORP in magnitude [65]. However, as obliquity increases, the effect of tangential-YORP drops to approximately half of its original value [66]. Recent conference proceedings on the combination of tangential-YORP and normal-YORP with finite thermal conductivity yield results where the obliquity will equally tend towards 0°/180° and 90° [67].

The final non-gravitational force to discuss is BYORP or Binary-YORP. BYORP is an extension of YORP to binary asteroid systems. Many binary asteroids are synchronous, or the time it takes to complete one orbit around the asteroid is equal to the time it takes to revolve one revolution about its axis. The secondary also needs to be asymmetrical, just as with the YORP effect. Using the same principles of thermal reemission with YORP, this will cause secular effects to the secondary's orbit around the primary [68]. BYORP most notably expands or contracts the semi-major axis of the orbit for the binary system. Binary asteroid systems compose 15% of the near-Earth asteroid population [69, 70]. This fact puzzled scientists since the BYORP effect results in a binary lifetime of $\sim 10^5$ years, which is much too short of a timescale to maintain the current population of binary asteroids [71]. Ćuk and Nesvorný modified their model of BYORP to include an elongated secondary and modeled

its libration. They found that eventually as the binary expanded, the secondary's libration would lose synchronous lock and the binary would stop expanding. Eventually, the system would re-gain synchronicity back and begin to contract the orbit [72]. This could rectify why BYORP has a short timescale to expand, but still maintains the large population of binary NEA. Ćuk's model is simply a constant force applied in the body-fixed frame, which is a somewhat inaccurate representation of BYORP. McMahon and Scheeres derive a more accurate model using a Fourier series to model the body's rotation state using coefficients that represent the shape and radiation properties of the body [73]. They then apply this model to 1999 KW_4 and show that this binary's orbit should double in 22,000 years. They also scaled the KW_4 results so that it can be applied to other binary systems without a detailed shape model. Finally, they included an adjusted model for double-synchronous orbits (where double-synchronous is when the secondary's orbit and both binary's rotation about their axes are all equal) [74].

The non-gravitational forces above are used to explain binary asteroid evolution and formation as well as other observed phenomena amongst the NEA and main-belt asteroid population. Observations of the NEA population have found that asteroids greater than 200 m in diameter rarely spin with a period less than 2.2 h [75]. It has also been observed that many objects observed in the NEA population are rubble piles because of their low estimated densities [14, 15, 16, 17, 18, 25]. Therefore, it has been theorized that these objects spin up from YORP until they reach an orbital period of 2.2 hours, where the gravitational forces can no longer keep the rubble pile bound together as centrifugal forces increase. Scheeres considers this process in detail to understand how this event would occur. He finds that each component of the asteroids has a specific spin state at which the component of the body will go into orbit and this is determined by the largest distance between the two mass centers [76]. He then goes on to describe the fission process and what the secondary's orbit might be after separation. He finds that the secondary immediately goes into a chaotic orbit after separation [77]. Jacobson and Scheeres then find that mutual body tides can take the binary

to the next step in the evolution. However, this largely is decided by the mass ratio M_s/M_p of the two components. Mass ratio <0.2 have multiple possibilities after fission [78]:

(1) Binary escape or re-impacts soon after becoming a chaotic binary.

(2) Binary becomes a stable synchronous binary system subject to BYORP.

(3) Multiple fission events lead to a ternary system.

However, with a mass-ratio >0.2, the evolution is simplified because the exchanges through angular momentum and energy through spin-orbit coupling is not severe enough to cause secondary fission or high eccentricities that lead to impact or escape of the secondary [78]. All chaotic binaries with mass ratios $\gtrsim 0.2$ will eventually settle into a double-synchronous orbit with a semi-major axis between 2-8 primary radii [78, 79]. Once in a double-synchronous orbit, BYORP will cause the asteroid to expand or contract in radius. If the orbit expands, it will eventually expand until the secondary escapes the primary and becomes an asteroid pair. Asteroid pairs are two asteroids with heliocentric orbits that if traced backward in time yield to a point where the two asteroids were in each others Hill sphere with small relative speeds [70, 80]. The Hill sphere is the gravitational sphere of influence of a particular body, where outside that sphere a more massive object would have larger gravitational effect on the satellite. Therefore, these asteroid pairs most likely were binaries at some point in the past. If the secondary asteroid contracts, it will end as a contact binary, where two similar sized components of the asteroid rest on each other to create one asteroid. Contact binaries make up >9% of the NEA population[81].

Both binary asteroids and contact binaries make up a significant amount the NEA population and hypotheses to determine what creates and destroys these populations are still being investigated today. Jacobson later proposed that perhaps rubble pile asteroids that contract due to BYORP may not inevitably impact, but instead find an orbit radius where mutual body tides balance the BYORP force that is contracting the secondary [78].

The binary would then stay in a stable orbit at this radius until perturbed perhaps by a planetary encounter. Therefore, if contraction through BYORP does not necessarily mean a contact binary or re-shaped asteroid is the end state; is there a process where expansion through BYORP could lead to an equilibrium or impact as opposed to eventual escape?

The research on binary asteroids have generally assumed that the binary will expand or contract without changing inclination. However, if the primary asteroid has its spin-pole not aligned with its orbit-pole, precession along the Laplace plane will cause the inclination of the orbit to change due to solar tides and the oblateness of the primary [82]. The Laplace plane is an equilibrium between these two perturbations that is stable to secular changes in inclination and longitude of the ascending node of an orbit. This phenomena has been used to describe why ring or moon systems have certain inclinations around planets, but the Laplace plane has never been applied to an asteroid. In this research, a hypothesis is tested on whether a satellite that expands in a binary system will expand along the Laplace plane and therefore change inclination. And if so, does this provide any new information on the theory of binary asteroids or contact binary evolution?

1.2 Organization and Contributions

The research presented in this thesis provides insight into a few questions about NEA and their binary, natural and artificial satellites. The focus will be on natural satellites and binaries, however since the mass-to-area ratios of artificial and natural satellites overlap, conclusions on spacecraft are made as well. The contributions are summarized in the next sections.

1.2.1 Artificial and Natural Satellites

The work in this thesis explores the possible long-term stable orbits that natural satellites may exist in around NEA and what natural phenomena causes it to be stable in these regions. This involves modeling third-body dynamics from the Sun, spherical harmonics of

the asteroid, and solar radiation pressure. The initial models only include J_2 for spherical harmonics, however, continued work also includes some analysis with 4×0 spherical harmonics and 4×4 spherical harmonics. Through a rigorous modeling of the behavior of many different possible orbits around asteroids of various obliquities, it will be determined how large or small natural satellites can exist in long-term orbits at a given radius or inclination from the asteroid. These results can be used to reduce the necessary search area around an asteroid (specifically the asteroid Bennu is evaluated) to determine the most efficient way to search for natural satellites.

From a subset of this work, spacecraft stability in these long-term orbits are also observed. One natural phenomenon that is stable to SRP, J_2, and third-body perturbations is the modified Laplace plane. The modified Laplace plane is a frozen orbit that balances the three perturbations by leveraging the different directions of precession each perturbation possesses when an asteroid has a non-zero obliquity [83]. The modified Laplace plane could be a stable orbit that has not been utilized around NEA before and could be of use for spacecraft missions if the asteroid has enough mass. It is determined that the minimum mass of the asteroid needed to maintain a stable orbit for a spacecraft with a low mass-to-area ratio. The contributions included in this thesis are:

(1) Characterize and understand the phenomena that provide stability for natural satellites around the near-Earth asteroid Bennu.

(2) Understand how higher-fidelity modeling of spherical harmonics changes orbits very near (<3 km) the asteroid.

(3) Extend understanding to various asteroids of differing mass and obliquities.

(4) Apply finding to spacecraft and investigate asteroid mass required for a long-term stable modified Laplace plane orbit.

1.2.2 Binary Asteroids

The contributions to binary asteroid evolution include utilizing the classical Laplace plane with BYORP in binary asteroid evolution. The classical Laplace plane is a simplified version of the modified Laplace plane where SRP is not included in the model [82]. It has been that a binary can expand with BYORP and change inclination to maintain the stability of the classical Laplace plane. If the primary has a high enough obliquity, the binary may enter a cycle where the expansion of the binary may eventually lead to an eventual impact through increasing eccentricity of the orbit. This provides a method of contact binary formation through a cycle to maintain the current contact binary population. The contributions for binary asteroids included in this thesis are modeling secondary BYORP expansion along the classical Laplace plane and presenting a hypothesized contact binary-binary cycle through BYORP expansion along the classical Laplace plane.

Thesis Statement

> Binary, natural, and artificial satellites at near-Earth asteroids are modeled with non-gravitational forces such as SRP and re-emission of SRP to develop a theory on the stability, evolution, and formation of binary, natural and artificial satellites. Natural satellites are stable for long periods of time in a multitude of orbits around NEA, where the modified Laplace plane, Kozai resonance, and Sun-synchronous orbits provide orbital phenomena to explain satellite stability or instability. Binary asteroids with an expanding binary will expand along the classical Laplace plane and therefore increase in inclination as orbital radii increases. A binary on the Laplace plane with a high obliquity primary will be subject to a binary-contact binary cycle that subjects a contact binary to fission, binary processes, and re-impact.

1.2.3 Journal Papers

The following journal papers resulted from the work done for this thesis:

- Rieger, S. M., Scheeres, D. J., Barbee, B., "Orbital Stability Regions for Hypothetical

Natural Satellites of 101955 Bennu (1999 RQ_{36})", In Prep., 2017.

- Rieger, S. M., Scheeres, D. J., "High Obliquity Contact Binary Evolution from the Classical Laplace Plane", In Prep., 2017.

1.2.4 Conference Papers

The following conference papers resulted from the work done for this thesis:

- Rieger, S. M., Scheeres, D. J., "Laplace Plane Dynamics with Solar Radiation Pressure in the Vicinity of an Asteroid", AIAA/AAS Astrodynamics Specialist Conference. San Diego, California, August 2014.

- Rieger, S. M., Scheeres, D. J., Barbee, B., "Orbital Stability Regions for Hypothetical Natural Satellites of 101955 Bennu (1999 RQ_36)", 26th AAS/AIAA Space Flight Mechanics Meeting, Napa Valley, California. February 2016

- Rieger, S. M., Scheeres, D. J., Barbee, B., "Orbital Stability Regions for Hypothetical Natural Satellites", International Symposium on Space Flight Dynamics. Matsuyama, Japan. June 2017.

1.2.5 Abstracts and Invited Talks

The following abstracts resulted from the work done for this thesis:

- Rieger, S. M., Scheeres, D. J., "High Obliquity Contact Binary Evolution from the Classical Laplace Plane, Division of Dynamical Astronomy Meeting. Pasadena, California. May 2015.

- Rieger, S. M., Scheeres, D. J., Barbee, B., "Orbital Stability Regions for Natural Satellites of 101955 Bennu", MIT-Stanford Women in Aerospace Symposium. Cambridge, Massachusetts. May 2016.

- Rieger, S. M., Scheeres, D. J., "Evolution of binary asteroids under the BYORP effect, 4th Workshop on Binaries in the Solar System. Prague, Czech Republic. June 2016.

- Rieger, S. M., Scheeres, D. J, Barbee, B., "Orbital Stability Regions for Natural Satellites of 101955 Bennu" International Astronautical Congress 2016. Guadalajara, Mexico. September 2016.

- Rieger, S. M., Scheeres, D. J. "A Contact Binary Asteroid Evolutionary Cycle driven by BYORP and the Classical Laplace Plane", Asteroid, Comets, Meteors 2017. Montevideo, Uruguay. April 2017.

- Rieger, S. M., Scheeres, D. J. "A Contact Binary Asteroid Evolutionary Cycle driven by BYORP and the Classical Laplace Plane", 49th Annual Divisions of Planetary Sciences Meeting. Provo, Utah. October 2017.

1.2.6 Organization

The second chapter discusses and derives the mathematical models used for both binary systems and natural/artificial satellites. The chapter includes a derivation of the Sun third-body perturbations, spherical harmonics, SRP, and BYORP. Next, chapter 3 shows the averaged equations of motion derived and used to obtain the classical Laplace plane and modified Laplace plane. Analysis of the classical Laplace plane instability region is discussed in this chapter. Chapter 4 begins with an analysis of stability of natural satellites around Bennu. This discussion goes into the orbital phenomena causing stability or instability. This chapter also includes changes in spherical harmonics modeling and its effect on the stability of natural satellites. Chapter 5 discusses the extension of this research to other asteroids with various masses and obliquities as well as a discussion on artificial satellite stability analysis. This chapter also includes work on the modified Laplace plane and its possibility of being a stable orbit for future spacecraft missions to asteroids. Next, Chapter 6 proposes

the possibility of a binary-contact binary cycle from the expansion of the secondary's orbit through BYORP along the classical Laplace plane. The final chapter, Chapter 7 summarizes the conclusions.

Chapter 2

Numerical Equations of Motion

In this chapter, the mathematical models used to approach the research on natural, artificial, and binary asteroid systems is discussed. For all satellites, the same model was used for third-body dynamics from the Sun and spherical harmonics. However, there are two separate models for SRP and BYORP that will also be discussed. For an asteroid the size of Bennu, 492 m, the SRP model is only used for natural ($d < 15$ m) and artificial satellites, while the BYORP model is used on large secondaries. Their isn't an obvious point where the natural satellite no longer needs to model SRP, however for a satellite with $d = 150$ m, the averaged equations of motion and numerical simulations discussed below have sub-meter differences in their orbital positions. Therefore, an object greater than this size at a Bennu-sized asteroid is not perturbed by SRP and modeling BYORP over longer time scaled will give a better approximation of the evolution of the orbit.

The model is set in the asteroid orbit-centered inertial frame. Therefore, the $x - y$ plane will be in the same plane as the asteroid's orbit around the Sun. However, since the asteroid is the origin of the frame, it will appear that the Sun is orbiting in retrograde around the asteroid. It is important to specify if in the asteroid-orbit centered frame because sometimes it is also convenient to model the motion in the asteroid-equator centered frame. These two frames are always different in this work because how the asteroid's obliquity will change the dynamics of the satellite is investigated. Both frames are inertially fixed with the asteroid as the origin. The asteroid-orbit centered frame has the $x-y$ plane in the same

plane as the asteroid's orbit around the Sun, while the equator frame lies along the equator of the asteroid. Therefore, the z-axis for the asteroid centered inertial-orbit frame is aligned with the angular momentum of the asteroid's heliocentric orbit. The z-axis for the asteroid centered inertial equatorial-orbit frame is aligned with the spin-pole of the asteroid. These two frames are define in Figure 2.1. The difference is defined by the obliquity, ϵ.

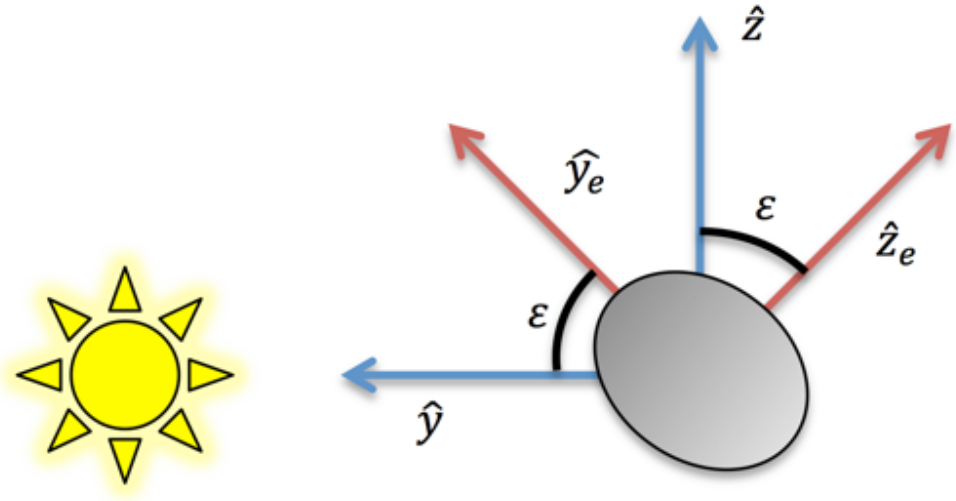

Figure 2.1: Difference between asteroid orbit-centered frame and asteroid equator-centered frame is from rotating the orbit frame by the obliquity, ϵ, about the $\hat{x}$-axis.

2.1 Third Body Perturbations

Third body dynamics from the Sun may not be the largest perturbation on a satellite at an asteroid, but it does influence the dynamics over long time periods. An example of third-body perturbations affecting a satellite's orbit is the Kozai mechanism. If there is a binary system with a massive object, such as the Sun perturbing the satellite, it will cause an exchange between the satellite's eccentricity and inclination [84]. Three-body equations of motion can be derived using Newtonian mechanics from the equation $\boldsymbol{F} = m\boldsymbol{a}$. The n-body

problem can be written as

$$m_i \frac{d^2 \boldsymbol{r_i}}{dt^2} = \sum_{\substack{j=1 \\ j \neq i}}^{n} \frac{G m_i m_j (\boldsymbol{r}_i - \boldsymbol{r}_j)}{|\boldsymbol{r}_j - \boldsymbol{r}_i|^3} = \frac{\partial U}{\partial \boldsymbol{r}_i}. \tag{2.1}$$

This problem has three bodies: the Sun, an asteroid, and a satellite. It is assumed that the mass of the satellite is negligible such that it does not affect the other two body's orbit. Since the asteroid is the origin of the frame, the vector $\boldsymbol{r_a}$ is equivalent to zero and not included in the naming scheme of the radius and velocity vectors. This gives the equation

$$\ddot{\boldsymbol{r}}_p = \frac{\mu_s}{|\boldsymbol{r}_s|^3}\boldsymbol{r}_s - \frac{\mu_s}{|\boldsymbol{r}_{sp}|^3}\boldsymbol{r}_{sp} - \frac{\mu_a}{|\boldsymbol{r}_p|^3}\boldsymbol{r}_p, \tag{2.2}$$

where μ_s is the gravitational parameter or the Sun, μ_a is the gravitational parameter of the asteroid, $\boldsymbol{r}_s$ is the distance from the asteroid to the Sun, $\boldsymbol{r}_p$ is the distance from the asteroid to the point-mass or satellite, and $\boldsymbol{r}_{sp}$ is the distance from the Sun to the point-mass/satellite. The above equation is the sum of the two-body motion between the satellite and the asteroid and the third body perturbations. Therefore only the third-body perturbations is

$$\boldsymbol{a}_{sun} = \frac{\mu_s}{|\boldsymbol{r}_s|^3}\boldsymbol{r}_s - \frac{\mu_s}{|\boldsymbol{r}_{sp}|^3}\boldsymbol{r}_{sp}. \tag{2.3}$$

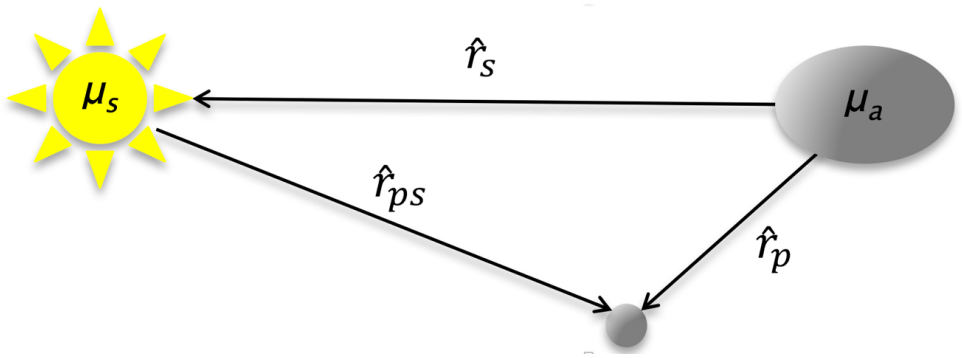

Figure 2.2: Relationship between the 3 bodies modeled in this problem: the Sun, an asteroid, and a satellite.

2.2 Spherical Harmonics

Asteroids exist in many different irregular shapes. These non-spherical mass distributions provide complex dynamics for a satellite orbiting the asteroid. If a point mass particle is orbiting any mass distribution, the potential can be computed from a differential mass element over the body [29],

$$U(\boldsymbol{r}) = G \int_B \frac{dm(\boldsymbol{\mathcal{R}})}{|\boldsymbol{r} - \boldsymbol{\mathcal{R}}|}, \tag{2.4}$$

where $\boldsymbol{\mathcal{R}}$ is the position vector of the differential mass element dm, B is the collection of all mass elements, and G is the gravitational constant (6.673×10^{-11}) $\mathrm{m}^3/\mathrm{kg}\cdot\mathrm{s}^2$. From here, you can derive Poisson's equation,

$$\bigtriangledown^2 U = -4\pi G\rho(\boldsymbol{r}). \tag{2.5}$$

Satellites are always orbiting outside the body where there is no mass density, Poisson's equation then reduces to Laplace's equation, $\bigtriangledown^2 U = 0$. It is assumed that the sphere has a constant density and mass, M for this model. Therefore the integration of the potential of a satellite yields:

$$U = \frac{GM}{|\boldsymbol{r}|} \quad r > R. \tag{2.6}$$

Any function that satisfies Laplace's equation is called a harmonic. Using separation of variables to solve Laplace's equations, the Laplace's equation in rectangular coordinates are:

$$\bigtriangledown^2 U = 0 = \frac{\partial^2 U}{\partial^2 x} + \frac{\partial^2 U}{\partial^2 y} + \frac{\partial^2 U}{\partial^2 z}. \tag{2.7}$$

However, spherical gravity harmonics are derived using spherical coordinates. Spherical coordinates are related to Cartesian coordinates by:

$$r = \sqrt{x^2 + y^2 + z^2}, \tag{2.8}$$

$$\sin\delta = \frac{x}{r}, \tag{2.9}$$

$$\tan\lambda = \frac{y}{x}, \tag{2.10}$$

where δ is the latitude and λ is the longitude. Solving for Laplace's equation in these coordinates gives

$$\nabla^2 U = \frac{1}{r^2}\frac{\partial}{\partial r}\left(r^2\frac{\partial U}{\partial r}\right) + \frac{1}{r^2\cos\delta}\frac{\partial}{\partial\delta}\left(\cos\delta\frac{\partial U}{\partial\delta}\right) + \frac{1}{r^2\cos^2\delta}\frac{\partial^2 U}{\partial\lambda^2} = 0. \tag{2.11}$$

Solving this equation gives the full gravitational potential in terms of spherical harmonics,

$$U = \frac{GM}{r}\sum_{n=0}^{\infty}\left(\frac{R_a}{r}\right)^n\sum_{m=0}^{n}P_{nm}\left(\sin\delta\right)\left[C_{nm}\cos m\lambda + S_{nm}\sin m\lambda\right], \tag{2.12}$$

where R_a is the normalizing radius or the maximum radius of the asteroid. P_{nm} are the associated Legendre functions and C_{nm} and S_{nm} are the gravity field harmonic coefficients. These coefficients represent the mass distribution of the body that is defined up to degree n and order m. The associated Legendre functions are defined by

$$P_{nm}(\sin^2\delta) = (1-\sin^2\delta)^{m/2}\frac{d^m}{d(\sin\delta)^m}\left(P_{n0}(\sin^2\delta)\right), \tag{2.13}$$

where $P_{n0}(\sin\delta)$ are defined as

$$P_{n0} = \frac{1}{2^n n!}\frac{d^n}{d(\sin\delta)^n}(\sin^2\delta - 1)^n. \tag{2.14}$$

The problems analyzed in this research begin with only needing J_2 of the asteroid to be derived. It is assumed that the asteroids analyzed in this research have uniform density, and therefore their spherical harmonic coefficients can be determined from the shape and

size of the asteroid if the asteroid is assumed to be a tri-axial ellipsoid. The symmetry of an ellipsoid makes it relatively easy to determine the spherical harmonics. All $S_{nm} = 0$ and odd order or degrees will have a zero value C_{nm} coefficients. Therefore the first few even C_{nm} coefficients can be determined by

$$\begin{aligned} C_{20} &= \frac{1}{5R_a}\left(\gamma^2 - \frac{\alpha^2+\beta^2}{2}\right), \\ C_{22} &= \frac{1}{20R_a^2}\left(\alpha^2 - \beta^2\right), \\ C_{40} &= \frac{15}{7}\left(C_{20}^2 + 2C_{22}^2\right), \\ C_{42} &= \frac{5}{7}C_{20}C_{22}, \\ C_{44} &= \frac{5}{28}C_{22}^2, \end{aligned} \tag{2.15}$$

where α is the semi-major axis, β is the semi-intermediate axis, and γ is the semi-minor axis of the asteroid. The simplest gravity model for an asteroid is to assume it is an oblate spheroid, therefore only the J_2 coefficient needs to be modeled. $J_2 = -C_{20}$, where C_{20} can be determined by the length of its three principal axes as shown in equation Equation 2.15 [41].

Therefore Equation 2.11 for an oblate spheroid in our model can be written as

$$U = \frac{\mu_a}{r_p}\left[1 + \left(\frac{R_a}{r_p}\right)^2\left\{C_{20}\left(1 - \frac{3}{2}\cos^2\delta\right)\right\}\right]. \tag{2.16}$$

The model typically is in the asteroid orbit-centered frame, and since there is a non-zero obliquity, it is easier to work with spherical harmonics in a vector format. Therefore the gravity potential of J_2 can be expressed as

$$R_2(\boldsymbol{r}_p) = -\frac{\mu_a}{2|\boldsymbol{r}_p|^3}C_{20}R_a^2[1 - 3(\hat{\boldsymbol{r}}_p \cdot \hat{\boldsymbol{p}})^2], \tag{2.17}$$

where $\hat{\boldsymbol{p}} = [0,\ \sin\epsilon,\ \cos\epsilon]$, or the spin pole of the asteroid in the inertial asteroid orbit-centered frame. $R_2 = U - \frac{\mu}{r}$ and $\ddot{r} = \frac{\partial U}{\partial r}$, therefore the partial derivative of the potential will

give the acceleration due to J_2 [41]. To find the acceleration of R_2, first the equation can be rewritten as

$$R_2(\boldsymbol{r}_p) = -\frac{\mu_p}{2|\boldsymbol{r}_a|^3} C_{20} R_a^2 [1 - \frac{3(\boldsymbol{r}_p \cdot \hat{\boldsymbol{p}})^2}{|\boldsymbol{r}_p|^2}]. \tag{2.18}$$

The partial derivative of the potential is

$$\frac{\partial U}{\partial \boldsymbol{r}_p} = \frac{3}{2} \frac{\mu_a}{|\boldsymbol{r}_p|^5} C_{20} R_a^2 \left(1 - \frac{3}{|\boldsymbol{r}_p|^2} (\boldsymbol{r}_p \cdot \hat{\boldsymbol{p}})^2\right) \boldsymbol{r}_p - \frac{\mu_a}{|\boldsymbol{r}_p|^3} C_{20} R_a^2 \left(\frac{6}{|\boldsymbol{r}_p|^4} (\boldsymbol{r}_p \cdot \hat{\boldsymbol{p}})^2\right) \boldsymbol{r}_p. \tag{2.19}$$

with some simplification this equation becomes

$$\boldsymbol{a}_{J_2} = \frac{\partial U}{\partial \boldsymbol{r}_p} = \frac{3}{2} \frac{\mu_a}{|\boldsymbol{r}_p|^5} C_{20} R_a^2 \boldsymbol{r}_p - \frac{15}{2} \frac{\mu_a}{|\boldsymbol{r}_p|^7} C_{20} R_a^2 (\boldsymbol{r}_p \cdot \hat{\boldsymbol{p}}) \boldsymbol{r}_p + 3 \frac{\mu_a}{|\boldsymbol{r}_a|^5} C_{20} R_a^2 (\boldsymbol{r}_p \cdot \hat{\boldsymbol{p}}) \hat{\boldsymbol{p}}. \tag{2.20}$$

Finally, it has been mentioned that eventually, our model will include 4×0 and 4×4 gravity harmonics. The fourth degree and order is used because the model of the spherical harmonics is around Bennu, which has been surveyed from Earth. The current OSIRIS-REx mission created a 16×16 coefficient model for their analysis [48]. However, the higher degrees and orders are arbitrary and will not be completely characterized, even after completing the mission at the asteroid. Therefore degree and order is limited to four, because these values have been roughly determined from the model created by Earth observations. However, The higher order gravity harmonics becomes computationally taxing because the model needs to take the partial derivatives of Equation 2.12 and the model needs to include rotation since odd degrees and orders are not symmetric. Therefore the Gravity Potential Derivatives Calculator (GPDC) is used to determine the partials numerically for these models [85]. In this case, it was more convenient to integrate the model in the inertial asteroid-equatorial frame.

2.3 Solar Radiation Pressure Perturbations

The final perturbation to be included is SRP. A simple Cannonball model will be used [83]. The Cannonball model assumes the satellite presents a constant area perpendicular to

the Sun-line [29]

$$\boldsymbol{a}_{SRP} = -(1+\rho)\frac{P_\Phi}{r_{ps}^2 b}\hat{\boldsymbol{r}}_{ps}, \tag{2.21}$$

where ρ is the reflectance, b, or m/A, is the mass-to-area ratio in kg/m^2, and P_Φ is the solar radiation constant and is approximately 1×10^8 km^3/s^2/m^2[83]. Generally, for the natural satellite models, it is assumed that the satellite is a sphere and the area that SRP transfers momentum to is a circle. This model provides easy calculations of the mass-to-area ratio, volume, and mass. Although, in reality, these objects will have complex shapes.

2.4 Equations of Motion for Natural and Artificial Satellites

The equations of motion used for the numerical analysis is just merely the sum of the perturbations and the two-body motion:

$$\boldsymbol{a} = -\frac{\mu_a}{|\boldsymbol{r}_p|^3}\boldsymbol{r}_p + \boldsymbol{a}_{sun} + \boldsymbol{a}_{J_2} + \boldsymbol{a}_{SRP}. \tag{2.22}$$

The equation of motion is

$$\begin{aligned}\ddot{\boldsymbol{r}}_p = -\frac{\mu_a}{|\boldsymbol{r}_p|^3}\boldsymbol{r}_p + \frac{\mu_s}{|\boldsymbol{r}_s|^3}\boldsymbol{r}_s - \frac{\mu_s}{|\boldsymbol{r}_{sp}|^3}\boldsymbol{r}_{sp} + \frac{3}{2}\frac{\mu_a}{|\boldsymbol{r}_p|^5}C_{20}R_a^2\boldsymbol{r}_p - \frac{15}{2}\frac{\mu_a}{|\boldsymbol{r}_p|^7}C_{20}R_a^2\left(\boldsymbol{r}_p\cdot\hat{\boldsymbol{p}}\right)\boldsymbol{r}_p \\ +3\frac{\mu_a}{|\boldsymbol{r}_p|^5}C_{20}R_a^2\left(\boldsymbol{r}_p\cdot\hat{\boldsymbol{p}}\right)\hat{\boldsymbol{p}} - (1+\rho)\frac{P_\Phi}{r_{ps}^2 b}\hat{\boldsymbol{r}}_{ps}.\end{aligned} \tag{2.23}$$

2.5 BYORP model

One can use a Fourier series with higher order coefficients to determine the exact direction and magnitude of the acceleration due to BYORP [73]. The derivation presented here is from a combination of research papers written by McMahon and Scheeres in 2010. A very simplified version of this model is used, where only the 0^{th} order coefficient is modeled and apply it only in the direction that causes the secular growth of the semi-major axis of the

binary system. Some assumptions need to be made to model BYORP. First, the secondary's motion is at least synchronous. Therefore one revolution around its spin-axis takes the same amount of time as one revolution in its orbit around the primary. Second, the secondary's spin-pole is aligned with its orbit pole, so the secondary has no obliquity. It has been found that solar radiation force can be expressed as a Fourier series by this equation [58].

$$\boldsymbol{F}_{SRP} = P(r_{ps}) \sum_{i=1}^{N} \boldsymbol{f}_i(\lambda_s) = P(r_{ps}) \sum_{n=0}^{\infty} \left[\boldsymbol{A}_n(\delta_s) \cos(n\lambda_s) + \boldsymbol{B}_n(\delta) \sin(n\lambda_s) \right], \tag{2.24}$$

where N is the number of surface elements used to describe the body and $P(r_{ps})$ is the solar radiation pressure at a given distance from the Sun, r_{ps}. $P(r_{ps})$ is defined by

$$P(r_{ps}) = \frac{P_\phi}{r_{ps}^2}. \tag{2.25}$$

The Fourier coefficients $\boldsymbol{A}_n$ and $\boldsymbol{B}_n$ have units of area (m^2) and represent the secondary's body shape, the secondary's reflective properties, and the position of the Sun in the body frame with respect to the secondary. The Sun's position can be defined by λ_s, the solar longitude, and δ_s, the solar latitude.

The Fourier series, using different coefficients, can also be modeled as a function of the satellite spin angle:

$$\sum_{i=1}^{N} \boldsymbol{f}_i(\theta) = \sum_{n=0}^{\infty} \left[\boldsymbol{A}'_n \cos(n\theta) + \boldsymbol{B}'_n \sin(n\theta) \right] : \tag{2.26}$$

The coefficients can be generalized as

$$\begin{aligned} \boldsymbol{A}'_n &= \cos(n(\lambda_{s_0} - \theta_0))\boldsymbol{A}_n + \sin(n(\lambda_{s_0} - \theta_0))\boldsymbol{B}_n, \\ \boldsymbol{B}'_n &= \cos(n(\lambda_{s_0} - \theta_0))\boldsymbol{B}_n + \sin(n(\lambda_{s_0} - \theta_0))\boldsymbol{A}_n, \end{aligned} \tag{2.27}$$

Where λ_{s_0} is the initial solar longitude and θ_0 is the initial rotation angle about the pole of the secondary. The initial solar longitude can be related to the Keplerian elements of the

primary's heliocentric orbit by

$$\begin{aligned} \lambda_{s_0} &= \Omega_{s_0} + \lambda_\nu, \\ \tan\lambda_\nu &= \cos i_s \tan(\omega_s + \nu_s). \end{aligned} \tag{2.28}$$

Where Ω_{s_0} is the initial longitude of the ascending node of the Sun in the secondary body-fixed frame, λ_ν is the longitude of the Sun due to the true anomaly, i_s is the inclination of the Sun in the body-fixed frame, ω_s is the argument of perihelion in the body-fixed frame, and ν_s is the true anomaly of the Sun in the body-fixed frame. Since the coefficients given in Equation 2.27 are dependent on the true anomaly of the Sun, the coefficients are only valid for one point in the orbit. To obtain the Sun's orbit in the secondary's body-fixed frame, take the Cartesian coordinates and rotate them into the body-fixed frame and then convert the coordinates into Cartesian elements. Here is the heliocentric orbit in relation to the inertial frame:

$$\begin{aligned} \hat{\boldsymbol{X}}_H &= [\cos\omega_H \cos\Omega_H - \sin\omega_H \sin\Omega_H \cos i_H]\, \hat{\boldsymbol{X}}_{\boldsymbol{I}} \\ &\quad + [\cos\omega_H \sin\Omega_H + \sin\omega_H \cos\Omega_H \cos i_H] \hat{\boldsymbol{Y}}_{\boldsymbol{I}} \\ &\quad + \sin\omega_H \sin i_H \hat{\boldsymbol{Z}}_{\boldsymbol{I}} \\ \hat{\boldsymbol{Y}}_H &= -[\sin\omega_H \cos\Omega_H + \cos\omega_H \sin\Omega_H \cos i_H] \hat{\boldsymbol{X}}_{\boldsymbol{I}} \\ &\quad + [-\sin\omega_H \sin\Omega_H + \cos\omega_H \cos\Omega_H \cos i_H] \hat{\boldsymbol{Y}}_{\boldsymbol{I}} \\ &\quad + \cos\omega_H \sin i_H \hat{\boldsymbol{Z}}_{\boldsymbol{I}} \\ \hat{\boldsymbol{Z}}_H &= \sin\Omega_H \sin i_H \hat{\boldsymbol{X}}_{\boldsymbol{I}} - \cos\Omega_H \sin i_H \hat{\boldsymbol{Y}}_{\boldsymbol{I}} + \cos i_H \hat{\boldsymbol{Z}}_{\boldsymbol{I}}, \end{aligned} \tag{2.29}$$

where the heliocentric frame is denoted by an H subscript and the inertial frame by an I

subscript. The body-fixed frame of the secondary is related to the inertial frame by

$$\begin{aligned}
\hat{\boldsymbol{x}}_b &= -[\sin\alpha\cos\theta + \cos\alpha\sin\theta\sin\delta]\hat{\boldsymbol{X}}_I + [\cos\alpha\cos\theta - \sin\alpha\sin\theta\sin\delta]\hat{\boldsymbol{Y}}_I + \sin\theta\cos\delta\hat{\boldsymbol{Z}}_I \\
\hat{\boldsymbol{y}}_b &= -[\sin\alpha\sin\theta + \cos\alpha\cos\theta\sin\delta]\hat{\boldsymbol{X}}_I + [\cos\alpha\sin\theta - \sin\alpha\cos\theta\sin\delta]\hat{\boldsymbol{Y}}_I + \cos\theta\cos\delta\hat{\boldsymbol{Z}}_I \\
\hat{\boldsymbol{z}}_b &= \cos\alpha\cos\delta\hat{\boldsymbol{X}}_I + \sin\alpha\cos\delta\hat{\boldsymbol{Y}}_I + \sin\delta\hat{\boldsymbol{Z}}_{\boldsymbol{I}},
\end{aligned} \tag{2.30}$$

where α is the right ascension and δ is the declination of the secondary's rotation pole. The body rotates about the $\hat{\boldsymbol{z}}_b$-axis. However, these relations are only needed if coefficients of $n > 0$ are being modeled. For our simplified model, only A_0 is being modeled. Therefore for Equation 2.27, $n = 0$ and therefore $A_0 = A_0'$ [73].

Next, the Fourier coefficients need to be transferred in the secondary's orbit frame so that the model can be simply added to the J_2 and third-body perturbations derived above. If the primary is synchronous, the transformation from the rotation angle of the spin pole can be used, because it is equivalent to one orbit revolution. Therefore the transfromation matrix is

$$T = \begin{bmatrix} \cos\theta & -\sin\theta & 0 \\ \sin\theta & \cos\theta & 0 \\ 0 & 0 & 1 \end{bmatrix}. \tag{2.31}$$

The Fourier series then becomes

$$\sum_{i=1}^{N} T\boldsymbol{f}_i(\theta) = \sum_{n=0}^{\infty}[T\boldsymbol{A}_n'\cos(n\theta) + T\boldsymbol{B}_n'\sin(n\theta)]. \tag{2.32}$$

Therefore the Fourier series can be described in new coefficients as

$$\sum_{i=1}^{N} T\boldsymbol{f}_i(\theta) = \sum_{n=0}^{\infty}[\boldsymbol{A}_n''\cos(n\theta) + \boldsymbol{B}_n''\sin(n\theta)]. \tag{2.33}$$

The new coefficients can just be described by the old coefficients, where $\boldsymbol{A}'_n = [A'_n(1)\ A'_n(2)\ A'_n(3)]^T$. The new coefficients are expressed as:

$$\boldsymbol{A}''_0 = \frac{1}{2}\begin{bmatrix} A'_1(1) - B'_1(2) \\ A'_1(2) + B'_1(1) \\ 2A'_0(3) \end{bmatrix}, \tag{2.34}$$

$$\boldsymbol{A}''_1 = \frac{1}{2}\begin{bmatrix} 2A'_0(1) + A'_2(1) - B'_2(2) \\ 2A'_0(2) + A'_2(2) + B'_2(1) \\ 2A'_1(3) \end{bmatrix}, \tag{2.35}$$

$$\boldsymbol{B}''_1 = \frac{1}{2}\begin{bmatrix} -2A'_0(2) + A'_2(2) - B'_2(1) \\ 2A'_0(1) - A'_2(1) + B'_2(2) \\ 2B'_1(3) \end{bmatrix}, \tag{2.36}$$

$$\boldsymbol{A}''_n = \frac{1}{2}\begin{bmatrix} A'_{n-1}(1) + A'_{n+1}(1) - B'_{n-1}(2) - B'_{n+1}(2) \\ A'_{n-1}(2) + A'_{n+1}(2) - B'_{n-1}(1) - B'_{n+1}(1) \\ 2A'_n(3) \end{bmatrix}, \tag{2.37}$$

$$\boldsymbol{B}''_n = \frac{1}{2}\begin{bmatrix} -A'_{n-1}(2) + A'_{n+1}(2) + B'_{n-1}(1) + B'_{n+1}(1) \\ A'_{n-1}(1) - A'_{n+1}(1) + B'_{n-1}(2) + B'_{n+1}(2) \\ 2B'_n(3) \end{bmatrix}. \tag{2.38}$$

However, since only A_0 is used for our model, this simplifies the new Fourier series to

$$\boldsymbol{a}_{BYORP} = P(r_{ps})\left[\left(A_0(1)\cos(n\theta) - A_0(2)\sin(n\theta)\right)\hat{\boldsymbol{x}} + \left(A_0(1)\sin(n\theta) - A_0(2)\cos(n\theta)\right)\hat{\boldsymbol{y}} + A_0(3)\hat{\boldsymbol{z}}\right]. \tag{2.39}$$

2.5.1 Normalized Coefficients

In Figure 2.3, the yearly averaged coefficients for A_0 and some higher orders for the binary system KW_4 are presented [74]. These values are used to model A_0 for our binary

system. However, KW_4 does not have a binary with a mass-ratio greater than 0.2. If the size of the primary or secondary is changed and similar timescales for BYORP expansion is maintained, the BYORP model for KW_4 used in McMahon and Scheeres needs to be normalize. The normalizing factor is just simply the mean radius of the secondary,

$$\mathcal{A}_n = \frac{\boldsymbol{A}_n}{r_m^2}, \tag{2.40}$$

where the mean radius can be determined from the volume of the secondary, $\sqrt[3]{\frac{3V}{4\pi}}$, and the volume can be determined from its density and mass. The new coefficients for an arbitrary system would then be determined by multiplying this non-dimensional factor by the square of the new mean radius to be modeled [74].

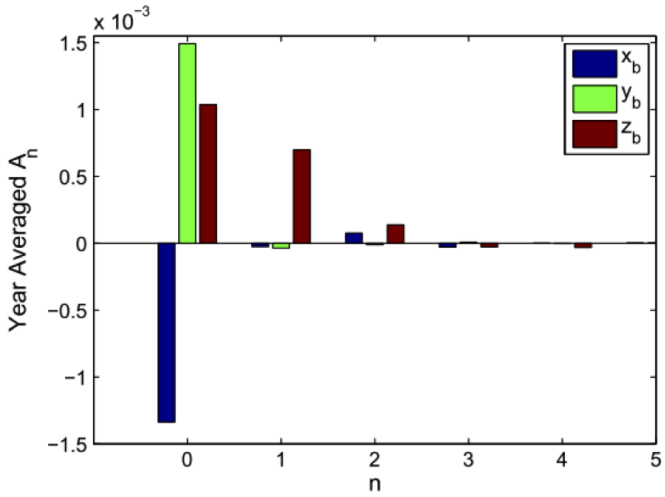

Figure 2.3: Yearly averaged body-frame A_n coefficients for KW_4 from McMahon and Scheeres, 2010.

2.5.2 Double-Synchronous Binary Systems

Any asteroid that has a mass-ratio greater than 0.2 will be double-synchronous [78]. This means the rotation rate of both asteroids and the secondary's orbit around the primary are all equal. Therefore a model is needed to correctly describe how the mutual synchronous

rotations between the primary and secondary affect BYORP. Therefore, the research needed to model BYORP expansion/contraction will include syncronous orbits for mass-ratios <0.2 and double-synchronous for mass-ratios > 0.2. The equations of motion of the secondary around the primary would be

$$\ddot{\boldsymbol{r}}_{\boldsymbol{p}} = \ddot{\boldsymbol{r}}_p - \ddot{\boldsymbol{r}}_a = -\frac{G(m_p + m_a)}{r_p^3}\boldsymbol{r}_p + \frac{\boldsymbol{F}_p}{m_p} - \frac{\boldsymbol{F_a}}{m_a}. \tag{2.41}$$

where the primary asteroid is at the origin of our model, so $r_a = 0$. The disturbing accelerations due to SRP, $\boldsymbol{F}_s$ and $\boldsymbol{F}_a$ can be combined.

$$\boldsymbol{a} = \frac{\boldsymbol{F}_p}{m_p} - \frac{\boldsymbol{F_a}}{m_a} = \frac{1}{m_r}\left[(1 - f_m)\boldsymbol{F}_p - f_m\boldsymbol{F}_a\right], \tag{2.42}$$

where $m_r = \frac{m_a m_p}{m_a + m_p}$ and $f_m = \frac{m_p}{m_a + m_p}$. From Equation 2.24, the model of these two forces separately can be combined using the equation above. Therefore, the two forces can be modeled as Fourier series

$$\begin{aligned}
\boldsymbol{F}_{a,BYORP} &= P(r_s)\left[\boldsymbol{A}\boldsymbol{a}_0'' + \sum_{n=1}^{\infty}\boldsymbol{A}\boldsymbol{a}_n''\cos(nM) + \boldsymbol{B}\boldsymbol{a}_n''\sin(nM)\right], \\
\boldsymbol{F}_{p,BYORP} &= P(r_{ps})\left[\boldsymbol{A}\boldsymbol{p}_0'' + \sum_{n=1}^{\infty}\boldsymbol{A}\boldsymbol{p}_n''\cos(nM) + \boldsymbol{B}\boldsymbol{p}_n''\sin(nM)\right],
\end{aligned} \tag{2.43}$$

where M is the mean anomaly of the secondary's orbit, which is best used in these equations for future purposes of averaging using Gauss's equations [74]. The secondary is orbiting in close proximity to the primary asteroid, therefore the approximation that $r_{ps} = r_s$ can be made. The total acceleration on the secondary can be found by inserting Equation 2.43 into Equation 2.42 such that

$$\begin{aligned}
\boldsymbol{a}_{BYORP} &= \frac{P(r_s)}{m}\left[(1 - f_m)\boldsymbol{A}\boldsymbol{p}_0'' - f_m\boldsymbol{A}\boldsymbol{a}_0''\right], \\
&+\frac{P(r_s)}{m} \times \sum_{n=1}^{\infty}((1 - f_m)\boldsymbol{A}\boldsymbol{p}_n'' - f_m\boldsymbol{A}\boldsymbol{a}_n'')\cos(nM) + ((1 - f_m)\boldsymbol{B}\boldsymbol{p}_n'' - f_m\boldsymbol{B}\boldsymbol{a}_n'')\sin(nM).
\end{aligned} \tag{2.44}$$

The double-synchronous BYORP model can then be deduced from this expression as

$$\begin{aligned} \boldsymbol{AC}_0'' &= (1-f_m)\boldsymbol{Ap}_0'' - f_m\boldsymbol{Aa}_0'', \\ \boldsymbol{AC}_n'' &= (1-f_m)\boldsymbol{Ap}_n'' - f_m\boldsymbol{Aa}_n'', \\ \boldsymbol{BC}_n'' &= (1-f_m)\boldsymbol{Bp}_n'' - f_m\boldsymbol{Ba}_n''. \end{aligned} \tag{2.45}$$

These coefficients can be used then to determine the acceleration on the secondary by

$$\boldsymbol{a}_{BYORP} = \frac{P(r_s)}{m}\left[\boldsymbol{AC}_0'' + \sum_{n=0}^{\infty}\boldsymbol{AC}_n\cos(nM) + \boldsymbol{BC}_n\sin(nM)\right]. \tag{2.46}$$

For our model, where $n = 0$, the equation for BYORP in a double-synchronous orbit will be

$$\begin{aligned} \boldsymbol{a}_{BYORP} = P(r_s)\left[\left(AC_0(1)\cos(nM) - AC_0(2)\sin(nM)\right)\hat{\boldsymbol{x}}\right] \\ +P(r_s)\left[\left(AC_0(1)\sin(nM) - AC_0(2)\cos(nM)\right)\hat{\boldsymbol{y}}\right] \\ +P(r_s)\left[AC_0(3)\hat{\boldsymbol{z}}\right]. \end{aligned} \tag{2.47}$$

This equation is the exact expression used earlier in Equation 2.39, except using mean anomaly instead of the rotation angle of the secondary. However, since the orbit is synchronous and circular, these values will yield equivalent results. Therefore, one only needs to alter the coefficients to model a synchronous or double-synchronous orbit. The double-synchronous orbit coefficients given in Equation 2.45 show that a double-synchronous orbit can either reduce or enhance BYORP. If the coefficients are similar and have the same sign, BYORP will be reduced. If the coefficients are similar and opposite in sign, BYORP will be enhanced.

2.5.3 Constant Force BYORP Model

In this section, the model derived above will be simplified and derived for a BYORP model where only the 0^{th} order is derived. This requires only one coefficient, A_0 to describe

the asymmetry of the asteroid. It is sometimes advantageous to use a constant force model in the correct direction to yield the secular changes needed to demonstrate the process. This allows for a simple demonstrations of the BYORP model that can be easily applied to primaries and binaries of varying sizes, as well as using A_0 as a simple gage for altering the overall asymmetry of the binary. The secular variation that is most interesting is the expansion of the semi-major axis, and by varying A_0, it can be simply demonstrated how this effects BYORP expansion or the evolution of the binary system. In McMahon and Scheeres, they derived the yearly averaged rates for a secular increase of the semi-major axis [74].

$$\bar{\dot{a}} = \frac{P_\phi}{a_s^2\sqrt{1-e_s^2}} \frac{2a_p\sqrt{\mu p}}{m_p\mu} \left[\hat{\boldsymbol{y}}_b \cdot \bar{\boldsymbol{A}}_0'\right], \tag{2.48}$$

where μ is the mutual gravitation between the primary and secondary. From this equation, it can be seen that the secular expansion of the semi-major axis is only altered by BYORP acceleration in the $\hat{y}_b$ direction. The BYORP model is only applied as a constant force in the $\hat{y}_b$ direction in the body-fixed frame. The orbital angular momentum is in the same direction as the rotation pole in the body-fixed frame, or $\hat{H}_p = \hat{z}_b$. Because the body is synchronous, $\hat{x}_b$ is always pointed towards the radius of the secondary around the primary. Therefore the simplified model with a constant force is

$$\boldsymbol{a}_{BYORP} = \frac{P(r_s)A_0'(2)}{m_p} \hat{\boldsymbol{H}}_{\boldsymbol{p}} \times (-\hat{\boldsymbol{r}}_p). \tag{2.49}$$

Chapter 3

The Laplace Plane

In 1805, Laplace published his theory that the satellites of Jupiter and the rings and moons of Saturn maintain a nearly constant inclination relative to the local invariable plane under the perturbing effects of solar tides and oblateness [86]. This became known as the Laplace plane. When a satellite is subject to perturbations due to the oblateness of the main-body, the orbit will precess around the planet's rotation pole. Likewise, perturbations due to third-body effects from the Sun will cause the satellite to precess around the heliocentric orbit-pole of the planet. With both perturbations and a planet with a spin-pole not aligned with its orbit-pole, there will exist an inclination where the precession due to these perturbations will be in balance such that the orbit has a constant inclination. If the orbit of the satellite is offset from this inclination, the orbit will instead precess around a mean pole that lies between the planet's rotation and orbit poles. This intermediate pole defines the classical Laplace plane, and the orbit with an orbit-pole aligned with this intermediate pole will be "frozen" to perturbations [82, 87]. For a satellite with an orbit very close to the planet, the Laplace plane will lie approximately on the planet's equatorial plane, while distant satellites will lie approximately on the planet's orbit plane. In between these two extremes, the Laplace plane lies at a given intermediate angle at a specific semi-major axis. There exists one significant semi-major axis called the "Laplace radius" and it is the semi-major axis where the Laplace plane bisects the equator and orbit plane or the perturbation forces due to J_2 and the Sun are equal. The sum of all the possible intermediate orientations

between the two extremes (equator and orbit plane) creates the Laplace surface [82, 88, 89] The surface can be observed in Figure 3.1. These frozen orbits all share similar nodes, do not have secular precession and remain in a circular orbit. The Laplace plane is an essential concept in planetary science because many planetary satellites orbit near the Laplace plane. The satellites that are near the Laplace plane are assumed to have been formed by circum-planetary gas disks. The satellites in orbits far from the Laplace plane are thought to be captured from heliocentric orbits or some other unusual event [82].

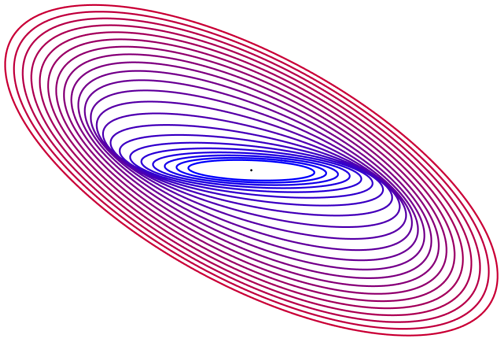

Figure 3.1: Laplace Surface is the collection of stable classical Laplace plane frozen orbits. As the semi-major axis of the satellite's orbit gets larger, the inclination of the orbit moves from the equator to the orbit plane.

3.1 Averaging of Milankovitch Orbital Elements

The Milankovitch orbital elements are simply the angular momentum vector and the vector $\boldsymbol{b} = \mu \boldsymbol{e}$, where μ is the gravitational parameter of the central body and $\boldsymbol{e}$ is the eccentricity vector[90]. The angular momentum vector and eccentricity vector give a complete set of integration constants for an unperturbed Kepler problem where the equations only need the initial position of the satellite in its orbit [90]. Using the averaged equations of motion of the Milankovitch orbital elements, the Laplace plane equilibrium can be easily derived. For

the Laplace plane, the semi-major axis is constant and thus simplifies the problem to[90]

$$\begin{aligned} \boldsymbol{h_p} &= \frac{1}{\sqrt{\mu_a a_p}} \boldsymbol{r_p} \times \boldsymbol{v_p}, \\ \boldsymbol{e_p} &= \frac{1}{\mu_a} \boldsymbol{v_p} \times \boldsymbol{H_p} - \frac{\boldsymbol{r_p}}{|\boldsymbol{r_p}|}, \end{aligned} \tag{3.1}$$

where $\boldsymbol{h}_p$ is the angular momentum of the satellite and $\boldsymbol{e}_p$ is the eccentricity vector of the satellite. To get the rates of the above equations the Lagrange planetary equations is used.

$$\begin{aligned} \dot{\boldsymbol{h_p}} &= \boldsymbol{h}_p \times \frac{\partial \bar{R}^*}{\partial \boldsymbol{h_p}} + \boldsymbol{e_p} \times \frac{\partial \bar{R}^*}{\partial \boldsymbol{e_p}}, \\ \dot{\boldsymbol{e_p}} &= \boldsymbol{e}_p \times \frac{\partial \bar{R}^*}{\partial \boldsymbol{h_p}} + \boldsymbol{h_p} \times \frac{\partial \bar{R}^*}{\partial \boldsymbol{e_p}}, \end{aligned} \tag{3.2}$$

where $\bar{R}^* = \bar{R}(\boldsymbol{h_p}, \boldsymbol{e_p})/\sqrt{\mu_a a_p}$ is the scaled averaged disturbing function of the perturbation, that is independent of time. The average disturbing function is

$$\bar{R}(\boldsymbol{h}_p, \boldsymbol{e}_p) = \frac{1}{2\pi} \int_0^{2\pi} R(\alpha, M) dM, \tag{3.3}$$

where α is a set of orbital elements excluding the mean anomaly, M.

3.2 Planetary Oblateness

The oblateness of the asteroid can be defined as

$$R_2 = \frac{\mu_a J_2 R_a^2}{2 r_p^3} [1 - 3(\hat{\boldsymbol{r}}_p \cdot \hat{\boldsymbol{p}}^2)]. \tag{3.4}$$

Averaging over the orbital motion, and scaling the function by $\sqrt{\mu_a a}$ the new equation is

$$\bar{R}_2^* = -\frac{n_p J_2 R_a^2}{4 a_p^2 h_p^2} [1 - 3(\hat{\boldsymbol{r}}_p \cdot \hat{\boldsymbol{p}}^2)], \tag{3.5}$$

where $n_p = \sqrt{\frac{\mu_a}{a_p^3}}$ is the satellite's mean motion. This equation can now be substituted back into Equation 3.2. Therefore the scalar perturbations due to oblateness are

$$\begin{aligned} \dot{\boldsymbol{h}}_2 &= -\frac{\omega_2}{h^5}(\hat{\boldsymbol{p}} \cdot \boldsymbol{h}_p)\hat{\boldsymbol{p}} \times \boldsymbol{h}_p, \\ \dot{\boldsymbol{e}}_2 &= -\frac{\omega_2}{2h_p^5}\left\{\left[1 - \frac{5}{h_p^2}(\hat{\boldsymbol{p}} \cdot \boldsymbol{h}_p)^2\right] \times \boldsymbol{h}_p + 2(\hat{\boldsymbol{p}} \cdot \boldsymbol{h}_p) \times \hat{\boldsymbol{p}}\right\} \cdot \boldsymbol{e}_p, \end{aligned} \tag{3.6}$$

where $\omega_2 = \frac{3n_p J_2 R_a^2}{2a_p^2}$ is the oblateness perturbation factor.

3.3 Sun Third-Body Perturbations

Our satellite will always be much closer to the asteroid than the Sun, therefore $r_p \ll r_s$. The quadrupolar perturbation function from the Sun's gravity on the satellite is [91]

$$R_s = \frac{\mu_s}{2r_s^3}\left[3(\boldsymbol{r_p} \cdot \boldsymbol{r_s})^2 - r_s^2\right]. \tag{3.7}$$

To average this equation for secular effects, one must consider that there are two different timescales for the dynamical motion: the asteroid's orbit around the sun and the satellite's orbit around the asteroid. If the satellite's period is way less than the period of the asteroid around the Sun, you can assume the Sun's motion is kept constant. Therefore, the equation is averaged over the orbital rate of the satellite, n_p.

$$\bar{R}_s^* = -\frac{3\mu_s}{8n_p a_s h_s^3}\left[5(\hat{\boldsymbol{H}}_s \cdot \boldsymbol{e_p})^2 - (\hat{\boldsymbol{H}}_s \cdot \boldsymbol{h_p})^2 - 2e_p^2\right], \tag{3.8}$$

where $h_s = \sqrt{1 - e_s^2}$, $\hat{\boldsymbol{H}}_s$ is a unit vector aligned with the asteroid's orbit pole. Using the Lagrange planetary equations given in Equation 3.2 on Equation 3.8, the secular equations of motion for the Sun's gravity perturbations are

$$\begin{aligned} \dot{\boldsymbol{h}}_{sun} &= -\omega_s \hat{\boldsymbol{H}}_s \cdot (5\boldsymbol{e}_p\boldsymbol{e}_p^T - \boldsymbol{h}_p\boldsymbol{h}_p^T) \times \hat{\boldsymbol{H}}_s, \\ \dot{\boldsymbol{e}}_{sun} &= -\omega_s\left[\hat{\boldsymbol{H}}_s \cdot (5\boldsymbol{e_p}\boldsymbol{h_p^T} - \boldsymbol{h_p}\boldsymbol{e_p^T}) \times \hat{\boldsymbol{H}}_{\boldsymbol{s}} - 2\boldsymbol{h}_p \times \boldsymbol{e}_p)\right], \end{aligned} \tag{3.9}$$

where $\omega_s = \frac{3\mu_s}{4n_p a_s^3 h_s^3}$ is the third-body perturbation factor.

3.4 Solar Radiation Pressure

The satellite is modeled with the Cannonball model, therefore the satellite is a sphere with constant optical properties. Making the same assumption as with third-body perturbations $r_p \ll r_s$, the disturbing function for solar radiation pressure is [29]

$$R_{srp} = -\frac{(1+\rho)P_\phi}{br_s^2}\boldsymbol{r_s}\cdot\boldsymbol{r_p}. \tag{3.10}$$

It should also be noted; spacecraft going into the shadow of the asteroid is ignored. Generally, the modified Laplace plane has a longitude of the ascending node that is fixed at 0° or 180°, and therefore in one asteroid orbit will orbit in the asteroids shadow for portions of the year. Generally, for this research the stability of a natural satellite in modified Laplace plane is analyzed. Therefore, this assumption may only be invalid for a small subset of satellites that are barely stable in the orbit due to SRP. However the general trends concluded in the research remain intact with this assumption in place. Also, for our model, it is assumed that $\rho = 0$. Although having an albedo of zero is unlikely, the albedo value is ignored because it would only change the answer by a factor of two, and therefore can be built into the approximation of the size of a satellite. Once again, similar to the solar third-body perturbations, the timescale of the asteroid's orbit around the Sun is constant, and averaged over the satellite's orbital rate around the asteroid as

$$\bar{R}^*_{srp} = \frac{3}{2}\sqrt{\frac{a_p}{\mu_a}}\frac{P_\phi}{br_s^2}\hat{\boldsymbol{r}}_s\cdot\boldsymbol{e}_p. \tag{3.11}$$

The equations of motion can then be found using Equation 3.2 such that

$$\begin{aligned}\dot{\boldsymbol{h}}_{srp} &= -\frac{H_s\tan\Lambda}{r_s^2}\hat{\boldsymbol{r_s}}\times\boldsymbol{e}_p,\\ \dot{\boldsymbol{e}}_{srp} &= -\frac{H_s\tan\Lambda}{r_s^2}\hat{\boldsymbol{r_s}}\times\boldsymbol{h}_p,\end{aligned} \tag{3.12}$$

where $H_s = \sqrt{\mu_s a_s (1 - e_s^2)}$ is the specific angular momentum of the asteroid around the Sun and Λ is the SRP perturbation angle. Λ is defined as

$$\tan \Lambda = \frac{3P_\phi}{2bV_{lc}H_s}, \tag{3.13}$$

in which V_{lc} is the local circular speed of the satellite about the asteroid. As Λ approaches $\pi/2$ the perturbation due to SRP is strong, while when Λ is close to zero, the perturbations due to SRP are weak. Because SRP does change a substantial amount over the course of one orbit around the Sun, one cannot assume the time variation of the Sun's orbit can be held constant. If averaged again using the Lagrange planetary equations, the perturbations due to SRP would vanish, which is not true. Therefore a different method is used where the equations are rotated in the Sun-rotating frame, and the asteroid's heliocentric true anomaly is used in the single averaged equations of motion [41]. Where the final secular equations of motion from SRP are [83]

$$\begin{aligned} \dot{\boldsymbol{h}}_{srp} &= -\omega_{srp} \hat{\boldsymbol{H}}_s \times \boldsymbol{h}_p, \\ \dot{\boldsymbol{e}}_{srp} &= -\omega_{srp} \hat{\boldsymbol{H}}_s \times \boldsymbol{e}_p. \end{aligned} \tag{3.14}$$

These equations are the averaged orbital behavior where ω_{srp} is

$$\omega_{srp} = \frac{2\pi(1 - \cos \Lambda)}{T_s \cos \Lambda}, \tag{3.15}$$

in which T_s is the asteroid's orbital period.

3.5 Classical Laplace Plane

The classical Laplace plane is derived from the averaged equations of motion defined above with only J_2 and third-body perturbations. The derivation begins with the total averaged equation of motion of the Milankovitch orbital elements.

$$\begin{aligned}
\dot{\boldsymbol{h}}_p &= -\frac{\omega_2}{h_p^5}\left(\hat{\boldsymbol{p}}\cdot\boldsymbol{h}_p\right)\hat{\boldsymbol{p}}\times\boldsymbol{h}_p - \omega_s\hat{\boldsymbol{H}}_s\cdot\left(5\boldsymbol{e_p}\boldsymbol{e_p}^T - \boldsymbol{h_p}\boldsymbol{h_p}^T\right)\times\hat{\boldsymbol{H}}_s \\
\dot{\boldsymbol{e}}_p &= -\frac{\omega_2}{2h_p^5}\left\{\left[1-\frac{5}{h_p^2}\left(\hat{\boldsymbol{p}}\cdot\boldsymbol{h_p}\right)^2\right]\times\boldsymbol{h}_p + 2\left(\hat{\boldsymbol{p}}\cdot\boldsymbol{h_p}\right)\times\hat{\boldsymbol{p}}\right\}\cdot\boldsymbol{e}_p \\
&\quad - \omega_s\left[\hat{\boldsymbol{H}}_s\cdot\left(5\boldsymbol{e_p}\boldsymbol{h_p}^T - \boldsymbol{h_p}\boldsymbol{e_p}^T\right)\times\hat{\boldsymbol{H}}_s - 2\boldsymbol{h_p}\times\boldsymbol{e_p}\right]
\end{aligned} \tag{3.16}$$

The equations above are invariant under transformations [82]. For example, the above equation is invariant when $(\hat{\boldsymbol{p}}\rightarrow-\hat{\boldsymbol{p}})$ or the obliquity of the asteroid can be restricted in range from $(0,\pi)$ to $(0,\pi/2)$. Therefore, the solutions are the same for a given obliquity and its retrograde complement. This is also true for when $(\hat{\boldsymbol{H}}_s\rightarrow-\hat{\boldsymbol{H}}_s)$, $(\hat{\boldsymbol{e}}\rightarrow-\hat{\boldsymbol{e}})$, or $(\hat{\boldsymbol{h}}\rightarrow-\hat{\boldsymbol{h}},\ t\rightarrow-t)$.

If it is assumed that $\boldsymbol{e}=0$, a complete general solution to Equation 3.16 exists [82]

$$\dot{\hat{\boldsymbol{h}}}_p = -\omega_2\left(\hat{\boldsymbol{p}}\cdot\hat{\boldsymbol{h}}_p\right)\hat{\boldsymbol{p}}\times\hat{\boldsymbol{h}}_p - \omega_s(\hat{\boldsymbol{H}}_s\cdot\hat{\boldsymbol{h}}_p)\hat{\boldsymbol{H}}_{\boldsymbol{s}}\cdot\hat{\boldsymbol{h}}_p. \tag{3.17}$$

The solutions to the Laplace equilibria from the above equation yields five types of equilibria for the system determined by different orientations of the angular momentum and eccentricity vectors. These are explored in Tremaine et al. [82]. Our work is only concerned with the circular Laplace equilibrium. The condition for equilibrium with $\dot{\boldsymbol{e}}=0$ and $\dot{\boldsymbol{h}}=$ constant is

$$\omega_2\left(\hat{\boldsymbol{p}}\cdot\hat{\boldsymbol{h}}_p\right)\hat{\boldsymbol{p}}\times\hat{\boldsymbol{h}}_p + \omega_s(\hat{\boldsymbol{H}}_s\cdot\hat{\boldsymbol{h}}_p)\hat{\boldsymbol{H}}_{\boldsymbol{s}}\cdot\hat{\boldsymbol{h}}_p = 0. \tag{3.18}$$

There are two relationships that will yield solutions to the above equilibrium. They are

$$\begin{gathered}
\hat{\boldsymbol{h}}_p\cdot\hat{\boldsymbol{p}} = \hat{\boldsymbol{h}}_p\cdot\hat{\boldsymbol{H}}_s = 0, \\
\text{or} \\
\hat{\boldsymbol{h}}_p\cdot\left(\hat{\boldsymbol{p}}\times\hat{\boldsymbol{H}}_s\right) = 0.
\end{gathered} \tag{3.19}$$

The first case the angular momentum is perpendicular to the principal plane and is called the "orthogonal" Laplace equilibrium. The second case, the angular momentum lies in the principal plane and is called the "coplanar" Laplace equilibrium. In the coplanar Laplace equilibrium, the equilibrium vector can instead be described simply by an azimuthal angle ϕ, where the equilibrium condition can be represented as:

$$\omega_s \sin 2\phi + \omega_s \sin 2(\phi - \epsilon) = 0, \tag{3.20}$$

where ϵ is the obliquity and ϕ, or the Laplace angle can be explicitly solved by

$$\tan 2\phi = \frac{\sin 2\epsilon}{\cos 2\epsilon + (r_L/a_p)^5}, \tag{3.21}$$

where r_L is the Laplace radius. The Laplace radius is defined by

$$r_L^5 = 2J_2 R_a^2 a_s^3 h_s^3 \frac{\mu_a}{\mu_s}. \tag{3.22}$$

Equation 3.20 has four solutions for ϕ in a 2π interval, therefore ϕ, $\phi \pm \pi/2$, and $\phi + \pi$ are all solutions [82].

3.6 Laplace Plane Stability

The classical Laplace plane eigenvalues equations are [82]

$$\begin{aligned}
\lambda_h^2 &= -\omega_2^2 \cos^2\phi - \omega_s^2 \cos^2(\epsilon - \phi) - \frac{\omega_2 \omega_s}{2}\left[\cos 2\phi + \cos 2(\epsilon - \phi) + 2\cos 2\epsilon\right], \\
\lambda_e^2 &= -\frac{\omega_2^2}{4}(5\cos^4\phi - 2\cos^2\phi + 1) - \frac{\omega_s^2}{2}[7\cos 2(\epsilon - \phi) - 5] \\
&\quad - \frac{\omega_2 \omega_s}{16}[2 + 3\cos 2\epsilon + 6\cos 2\epsilon + 6\cos 2(\epsilon - \phi) + 15\cos 2(\epsilon - 2\phi)].
\end{aligned} \tag{3.23}$$

From these equations and the equilibrium condition given in Equation 3.20, the possible solutions to the Laplace plane and whether these solutions are stable can be determined. These equations give the eigenvalues, which if $\lambda_h^2 > 0$ or $\lambda_e^2 > 0$, the Laplace plane is unstable.

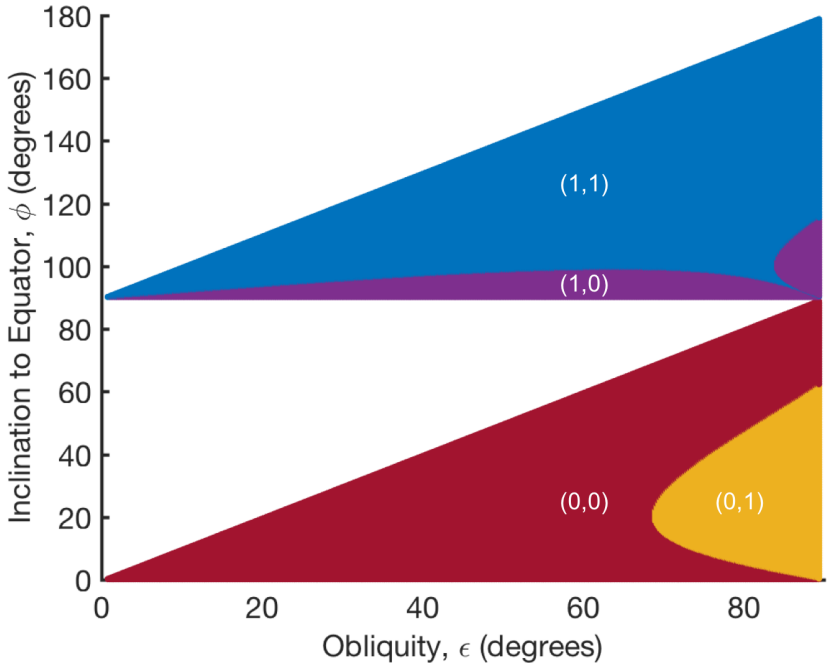

Figure 3.2: Stability and instability regions for the classical and orthogonal Laplace equilibria. A "0" or "1" denotes if the region is stable or unstable respectively. The first number gives the stability in the angular momentum, while the second number gives the stability for the eccentricity.

Varying the values of the obliquity, ϵ, and the inclination of the orbit, ϕ, the conditions for a stable or unstable Laplace plane can be found. The results which were published in Tremaine et al. 2009, and Rosengren & Scheeres, 2014 are in Figure 3.2. The instability region in yellow in Figure 3.2 is unstable for obliquity angles above $68.875° - 111.125°$ and Laplace radii from 0.8 to 1.25. The orthogonal Laplace equilibria are always unstable; however, there is a small region where it is stable to eccentricity as seen in Figure 3.2.

3.7 Modified Laplace Equilibria

With the inclusion of the SRP perturbation terms in Equation 3.18, the Laplace equilibrium is now [83, 90]

$$\omega_2 \left(\hat{\boldsymbol{p}} \cdot \hat{\boldsymbol{h}}_p\right) \tilde{\hat{\boldsymbol{p}}} \cdot \hat{\boldsymbol{h}}_p + \omega_s \left(\hat{\boldsymbol{H}}_{\boldsymbol{s}} \cdot \hat{\boldsymbol{h}}_p\right) \tilde{\hat{\boldsymbol{H}}}_{\boldsymbol{s}} \cdot \hat{\boldsymbol{h}}_p + \omega_{srp} \tilde{\hat{\boldsymbol{H}}}_{\boldsymbol{s}} \cdot \hat{\boldsymbol{h}}_p = 0. \tag{3.24}$$

In terms of obliquity and the Laplace angle the equilibrium is [83]

$$\omega_2 \sin 2\phi + \omega_s \sin 2(\phi - \epsilon) + 2\omega_{srp} \sin(\phi - \epsilon) = 0. \tag{3.25}$$

The solutions for this equilibria are not symmetric. Therefore retrograde orbits will not necessarily have the same inclination as the prograde orbits as was the case with the classical Laplace plane. The modified Laplace plane is not invariant when ($\hat{\boldsymbol{h}} \rightarrow -\hat{\boldsymbol{h}}$, $t \rightarrow -t$). The modified Laplace plane may also not have four solutions, but rather the roots of the equation above vary in number with the strength of SRP [83].

As the mass-to-area ratio increases, SRP increases. And, as SRP increases, the Laplace angle increases in inclination for constant orbital radii. It is assumed that $\rho = 0$ and mass-to-area ratios of $b = 10$, 100, 1000, 10,000 kg/m^2, and no SRP are compared. The difference can be seen in Fig. 3.3. Figure 3.3 gives the Laplace angle or inclination of the natural satellite as a function of semi-major axis normalized by the Laplace radius for mass-to-area ratios of 10, 100, 1000, and 10,000 kg/m^2 at Bennu. For no SRP, the Laplace radius is

equivalent to 1 at the bisection of the obliquity (4°) such that the Laplace angle is 2°. For an increase in the mass-to-area ratio the bisection occurs at a lesser semi-major axis. For reference, a natural satellite with a mass-to-area ratio of 10 kg/m^2, 100 kg/m^2, 1000 kg/m^2, and 10,000 kg/m^2 is 0.75 cm, 7.5 cm, 0.75 m and 7.5 m in diameter respectively.

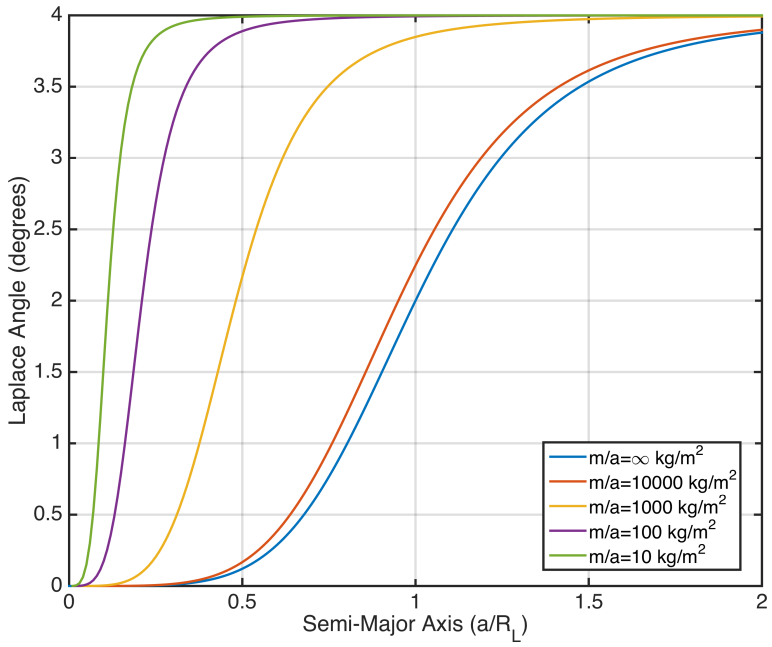

Figure 3.3: The Laplace angle for varied mass-to-area ratios for given semi-major axes.

Chapter 4

Hypothetical Natural Satellites around 101955 Bennu

4.1 Introduction

The Origins, Spectral Interpretation, Resource Investigation, Security-Regolith Explorer (OSIRIS-REx) mission to return a sample from potentially hazardous near-Earth asteroid (NEA) 101955 Bennu (1999 RQ_{36}) is NASA's third New Frontiers mission and launched in September, 2016. During its time at Bennu, the spacecraft will occupy two distinct Sun-terminator plane orbits at radii between 1 km and 2 km [42]. Thus, there is interest in whether Bennu might possess any natural satellites in long-term stable orbits that could interfere with spacecraft operations in Bennu's vicinity. Bennu has been the target of an extensive ground-based observation campaign since its discovery in 1999. Those observations have established that there are no natural satellites larger than 15 m in diameter. [47, 48]

Because of the possible risks that are associated with unknown natural satellites upon arrival at an asteroid, it is imperative for a spacecraft to begin scanning the area with its instruments to try and detect natural satellites in orbit. In fact, OSIRIS-REx is doing a natural satellite survey during approach to Bennu [27]. From the approach distance, large 10 m natural satellites will be easy to quickly spot, however objects less than a 1 m in diameter will be more challenging. With a Hill sphere of 29.5 km, OSIRIS-REx would need to scan $\sim$ 2700 km^2 area around the asteroid to conclude whether a natural satellite exists that requires a potential redesign of the spacecraft's trajectory to avoid a collision. This research

will provide knowledge of where these natural satellites are able to exist in a stable orbit for long periods of time. Thus constraining the necessary search area significantly. Therefore, more time can be allocated to radar imaging of smaller areas around the asteroid, so that more quality data can be presented with findings of smaller diameter natural satellites that could significantly impact the mission.

There has been interest in the possibility of natural satellites or smaller material such as dust or pebbles in orbit around asteroids [45, 46]. Most millimeter to centimeter sized objects will not be stable due to solar radiation pressure. This still leaves a large range of objects that could be stable at Bennu that radar observations haven't discovered.

To investigate whether natural satellites <15 m exist around Bennu, initial conditions are varied for semi-major axis, inclination and longitude of the ascending node to find a range of possible orbits that are stable. It is define that unstable orbits as those that end in a collision or escape, while stable orbits do not impact/escape during the simulation. Eccentricity is not varied as an initial condition, but with perturbations from the Sun the eccentricity may increase. Because highly eccentric orbits with large semi-major axes may intersect near the surveying orbits of OSIRIS-REx; semi-major axes from 1 km to the Hill sphere ($\sim$29.5 km) are analyzed.[48] These initial conditions are evaluated for multiple sized satellites up to 15 m in diameter. Each initial condition is simulated for 1000 years or until the natural satellite escapes or collides with Bennu. If there is escape or collision, these initial conditions are considered to be unstable. Stable natural satellites are in orbits capable of being stable for more than tens of thousands of years. The longer an orbit is stable for a natural satellite, the more likely it may have a natural satellite in orbit when OSIRIS-REx arrives at Bennu. However, sweeping through as many possible initial orbit conditions at Bennu for 10,000 to 100,000 years is computationally exhaustive. Therefore, 1000 years was a compromise to find a preliminary idea of where such long-term orbits exist. It was found that most orbits stable for 1000 years are also stable for 10,000 years, but there are exceptions. These exceptions are simulated for 10,000 years and discussed in the results if necessary. By

extending several test cases to 10,000 years, it was found that only a special subset of high inclination orbits were unstable due to the Kozai resonance. All other solutions that were stable for 1000 years were stable for 10,000 years. The results are trusted because they give an idea of which orbits allow for long term stability of natural satellites, and therefore the longer an object is stable in that orbit, the higher the probability a natural satellite will exist in this orbit when a spacecraft arrives.

There are possible stable orbits expected to exist for varying diameter satellites. The first possible stable region will be due to the modified Laplace plane (MLP). Tremaine defines the classical Laplace plane as "...normal to the axis about which the pole of a satellite's orbit precesses"[82]. The perturbations on the satellite in the Laplace plane are caused by a third-body and an oblate primary. The MLP also includes solar radiation pressure (SRP) in the perturbation model [83]. It has already been determined that two characteristics of the MLP around Bennu [92]. First, the MLP becomes less stable as the distance between the satellite and primary increases. Second, the MLP is less stable as the diameter of the satellite decreases. For a more in depth discussion and derivation on the Laplace plane, please refer to Chapter 3. It should be noted that Scheeres also did work on orbits that are frozen with just a model of oblate asteroid and SRP [40]. He first looks at this frozen orbit separately for each perturbation, with the frozen orbit being stable in the orbit-plane when only SRP is modeled and the frozen orbit being stable on the equator when only the oblateness is modeled. The paper then goes on to explain when both perturbations are modeled that this frozen equatorial orbit is best at small semi-major axes where oblateness is the dominating force. Once, the semi-major axis is large enough, there precession of the orbit changes and SRP will cause the orbit to go unstable as it becomes the dominating force. This work he describes seems to be the modified Laplace plane, however the mass-to-area ratios he investigated were quite small, so the MLP would only exist at very small semi-major axes where oblateness is the dominating force.

Second, the Kozai resonance may be responsible for stable and unstable regions for

natural satellites. The third-body perturbations from the Sun on the satellite causes the Kozai resonance. This resonance causes libration of the satellite's argument of periapsis. The libration produces an exchange between eccentricity and inclination such that the satellite's angular momentum projection normal to the Sun-Bennu orbit plane is conserved [84].

Finally, an orbit can be stable if in a Sun-synchronous orbit. These orbits have bounded variations in the Keplerian orbital elements except the longitude of the ascending node. Due to solar radiation torques, the longitude of the ascending node will precess at a rate equivalent with Bennu's orbit around the Sun [41].

By constructing and executing an array of detailed simulations modeling the evolution of natural satellite orbits over thousand-year time scales, the possible sizes, distances from Bennu, and orbital orientations of long-term stable orbits is assessed. It is noted note that theories proposing credible mechanisms for the in situ formation or capture of such natural satellites are also required, but those studies are purposefully outside our dynamical investigations. From these data, conclusions are drawn on the likelihood of Bennu possessing natural satellites either in the past or during the current epoch. It is determined that whether these satellites might interfere with the OSIRIS-REx spacecraft operations around Bennu. And if so, which specific regions near Bennu that the OSIRIS-REx team may wish to focus their efforts to search for natural satellites during the spacecraft's approach to Bennu.

4.2 Implementation

4.2.1 Approximate escape semi-major axis

Before beginning analysis, it is important to understand at what distance from the asteroid the spacecraft will escape. The Hill radius suffices for determining this distance with third-body motion. But with the strength of the SRP perurbation in a small body's low gravity environment, the natural satellite will often escape at a radius less than the Hill sphere. The Hill

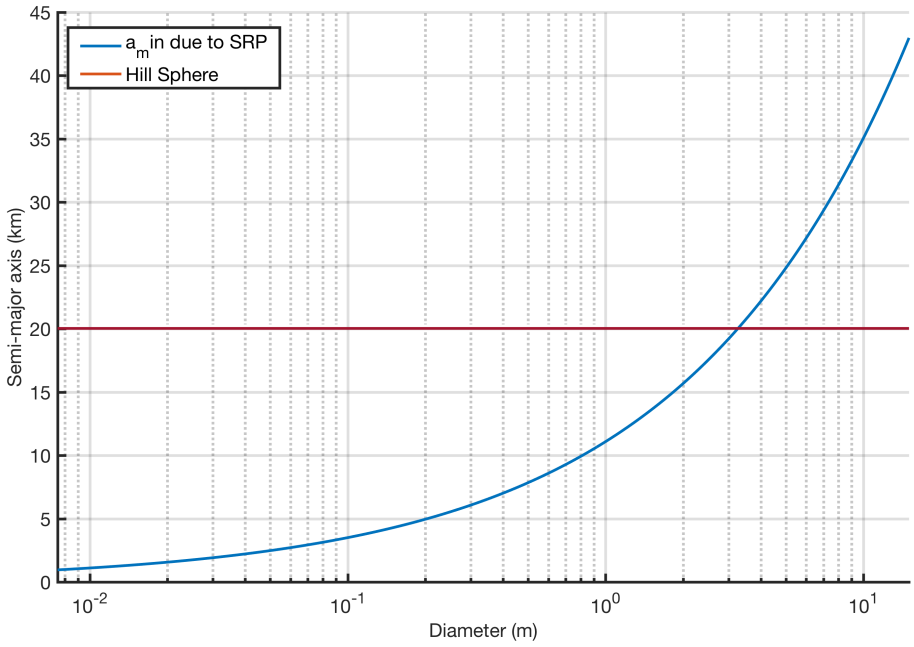

Figure 4.1: The Hill sphere and SRP minimum escape criteria for Bennu.

sphere is defined as [41]

$$r_H = a_s(1-e)^3 \left(\frac{m}{3m_s}\right)^{1/3}. \tag{4.1}$$

The minimum diameter where a natural satellite of a given mass-to-area ratio will escape the system is defined by: [41]

$$a_{min} = \frac{1}{4}\sqrt{\frac{\mu_a}{(1+\rho)P_\Phi/b}}a_s. \tag{4.2}$$

The equations above are an approximation and some satellites at a semi-major axis less than a_{min} may escape. This equation's relationship to various natural satellite diameters can be seen in Fig. 4.1. For satellite diameters below $\sim$ 3 m, the SRP escape criterion is a better approximation for the semi-major axis than the Hill sphere.

4.2.2 Numerical Implementation

To help characterize and understand the orbits of possible natural satellites, the parameters studied will be the semi-major axis of the satellite's orbit, the diameter of the satellite, and the time the orbit remains stable. Instability is characterized by impact or escape from Bennu. All parameters for Bennu are held constant. The parameters used in this research are listed in Table 4.1 [27, 47, 48].

Table 4.1: Bennu Parameters

Parameter	Value
Obliquity (with respect to the orbit plane of Bennu), ϕ	176°
Gravitational parameter, μ_a	5.2 m^3/s^2
Assumed density of Bennu satellites , ρ	2000 kg/m^3
Body Major Axis, α	567 m
Body Intermediate Axis, β	535 m
Body Minor Axis, γ	508 m
Heliocentric Orbit Semi-Major axis, a_s	1.126391025996 AU
Heliocentric Orbit Eccentricity, e_s	0.203745112
Heliocentric Orbit Inclination, i_s	6.0349391°
Heliocentric Orbit Arg. of Periapsis, w_s	2.0608668°

The assumed density of Bennu's satellites is larger than the currently estimated density for Bennu of 1250 kg/m^3 [93]. Bennu is a rubble pile and therefore may have space between

the boulders and rocks that comprise it while the natural satellite may be a single boulder or a rubble pile. It is assumed that the natural satellite is a boulder and will be denser than Bennu. With the assumed density of 2000 kg/m^3 for the natural satellites, the approximate size of a natural satellite can be determined. This value is larger than the density of Bennu. This is because Bennu is a rubble pile asteroid, or a collection of lose material bound together by gravity. This rubble pile has large gaps between the rocks and boulders that make up Bennu and therefore creates a very low density object. If a satellite fissions from the asteroid and is small, it doesn't have enough gravity to be a bound rubble pile, and therefore will be a single rock or boulder. Therefore, the assumption of the density will be greater to represent a monolithic rock. Assuming the natural satellite is a sphere, the SRP will only affect the surface area of a circle in the Sun direction. The diameter of the natural satellite in terms of density and mass-to-area ratio is

$$D = \frac{3}{2}\frac{b}{\rho}. \tag{4.3}$$

The semi-major axes studied range from 1 km out to the Hill sphere, this will include any orbits that grow in eccentricity that may intersect with the OSIRIS-REx survey orbits. The mass-to-area ratios will be from the minimum mass-to-area ratio to yield a captured orbit to 20,000 kg/m^2. For the density assumed, this will be up to a 15 m diameter satellite. The actual density of these satellites can vary from the assumed value, so the diameters given are approximate.

The natural satellite orbits are numerically simulated for numerous initial conditions. Our program to simulate these results was written in C. MATLAB was used to analyze simulation outputs. The numerical simulation in C uses the GNU Scientific Library, which has a suite of functions used to integrate ordinary differential equations. Runge-Kutta Prince-Dormand (8, 9) method is the integration method used. Both the absolute and relative tolerances of the integration are 10^{-14} m. The integration time will be 1000 years. One

thousand years is ample time to determine which orbits are stable for long periods of time. But also, short enough that computations are not overly time-consuming. However, there will be case studies on several examples with larger time scales to determine how this changes the results. For the natural satellite around Bennu, the initial orbit is always assumed to be circular for simplicity. Future work will explore a range of eccentricities since eccentricity can cause certain orbits to become more stable [41].

The initial conditions tested will be at semi-major axes of 1-15 km in intervals of 1 km and then at intervals of 5 km up to 30 km. For each semi-major axis, the mass-to-area ratios between 10 kg/m^2 to 20,000 kg/m^2 are tested. This covers a range of natural satellites from 0.0075 m to 15 m in diameter. The mass-to-area ratios from $10 - 90$ kg/m^2 will be analyzed in intervals of 10 kg/m^2, then mass-to-area ratios from $100 - 900$ kg/m^2 will be analyzed in intervals of 100 kg/m^2, and mass-to-area ratios from $1000 - 20,000$ kg/m^2 will be analyzed in intervals of 1000 kg/m^2. For any semi-major axis and mass-to-area ratio, 120 iterations of varying initial conditions are integrated for 1000 years. The 120 iterations vary with $\Omega = 0^\circ, 90^\circ, 180^\circ, 270^\circ$ and inclinations from 0° to 180° in increments of 6 degrees. This gives a total of 62,640 simulations. The next section will provide a summarization on meaningful trends found in these simulations. Certain simulations will provide insight into the physical phenomena that may be responsible for stability/instability for given initial conditions.

4.2.2.1 Spherical Harmonics

For lower orbits, it is found that increasing the gravity field up to 4th order in the zonal harmonics was needed to resolve some of the stability zones. Zonal harmonics are only increased because Bennu is close to rotationally symmetric. This approximation was close enough to sample results with 4×4 spherical harmonics, but with a significant reduction in computation time. At orbits around 1 km, there were some cases where the J_2 only orbits had different stability characteristics than those expanded up to J_4. This can be seen in

Fig. 4.2, which shows the inclination vs. longitude of ascending node for orbits of various initial conditions and $a = 1$ km and $D = 0.6$ m. Stable orbits are in blue, while unstable orbits are in red, where there are stable orbits for J_2 near $90°$ that do not exist for the 4×0 simulation. At orbits higher than 3 km no differences were found between these cases. Thus for orbits less than 3 km a 4th order zonal gravity field was used while for orbits above 3 km J_2 was used.

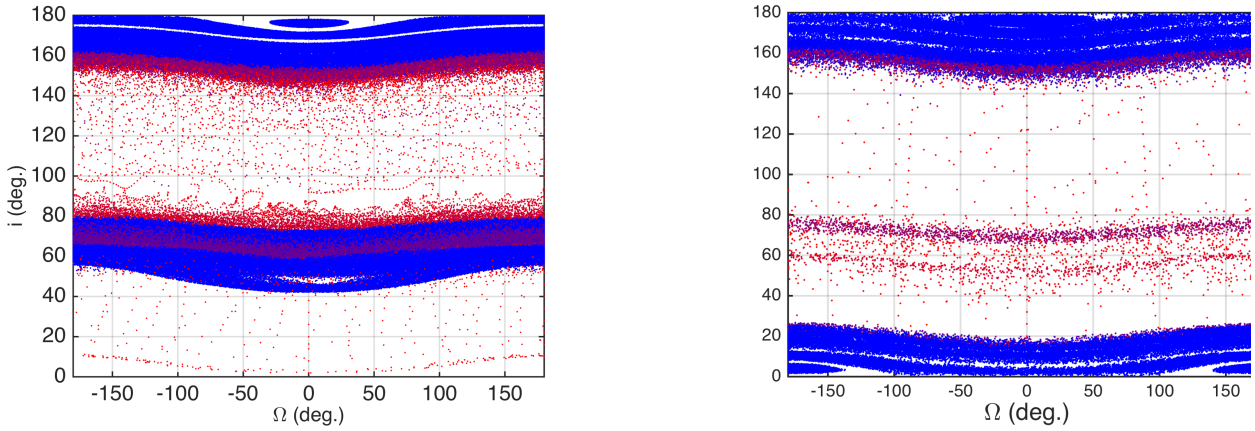

(a) Ω vs. i for J_2 shape model

(b) Ω vs. i for 4×0 shape model

Figure 4.2: Inclination vs. longitude of the ascending node comparison for $a = 1$ km and $D = 0.6$ m for different gravity field expansion orders. Stable orbits are in blue, while unstable orbits are in red. Notice there are stable orbits for J_2 near $90°$ that do not exist for the 4×0 simulation.

4.3 Natural Satellite Stability

A summary of the results is given in Fig. 4.3. This figure represents the results of all simulations with varying semi-major axes, inclinations, longitude of the ascending nodes, and natural satellite diameters. For each semi-major axis and inclination simulated, the minimum natural satellite diameter is determined and shown with a corresponding color, where blue is the smallest diameter to red being the largest. The figure shows the minimum natural satellite diameter stable for 1000 years at each semi-major axis and inclination. Larger diameter objects may exist at the same semi-major axis and inclination. As a satellite

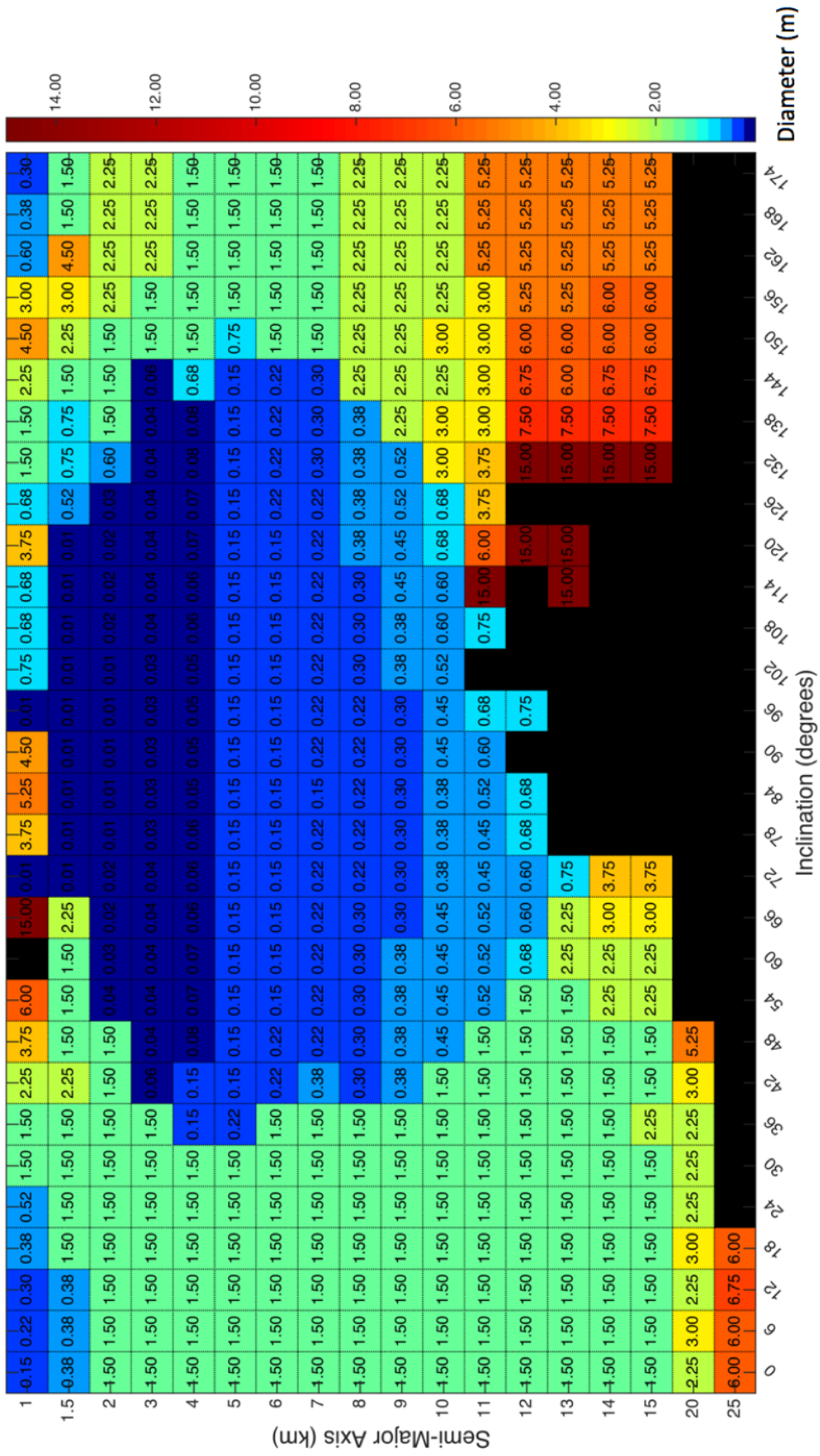

Figure 4.3: This figure summarizes the overall results of the simulations. For each semi-major axis and inclination simulated, the minimum natural satellite diameter is determined and shown with a corresponding color, where blue is the smallest diameter to red being the largest. Larger diameter objects may exist at the same semi-major axis and inclination. Notice that higher inclinations are capable of much smaller diameter object's being stable than more equatorial orbits.

becomes smaller, the more likely it becomes that SRP will disturb its orbit and cause it to go unstable. Therefore, the minimum natural satellite diameter gives the smallest diameter not affected by SRP. Notice that inclinations between 36° and 144° at semi-major axes between 1 and 13 km have significantly smaller diameter natural satellites than the rest of the simulations. Not all objects larger than the minimum diameter are stable. There are regions of instability for larger diameters that can be seen in the Appendix.

A summary of the full results can be seen in Tables A.1 to A.3 in the Appendix. These tables give a list of all diameters of natural satellites stable for 1000 years at a given inclination and semi-major axis. It is important to note that often there are bands of stable diameters. For instance, in Table A.1 at a semi-major axis of 2 km and an inclination of 54° the diameters that are stable are $0.03-0.06$ m and $1.5-15$ m. These ranges of diameters are both stable for two different reasons. As discussed below, the smaller ranges of diameters for natural satellites are stable because they are in a Sun-synchronous orbit. Larger satellites are stable due to SRP not significantly altering the orbit of the satellite.

4.4 Progression of Stability with varying size of natural satellite

The data were analyzed by observing the evolution of stable and unstable orbits at a constant semi-major axis and increasing the size of the natural satellite. Some select examples of these results can be viewed in Fig. 4.4, showing 12 graphs that represent the varying initial conditions. For all figures the semi-major axis of the orbit was kept constant, but each plot represents a different sized diameter at that semi-major axis. Each plot gives 120 different initial conditions for the natural satellite by varying the inclination and longitude of the ascending node for that specific semi-major axis and natural satellite diameter. Each data point represents an inclination and a longitude of ascending node at a specific time in any given orbit. The example case shown in Fig. 4.4 is for a semi-major axis of 4 km in the asteroid-orbit centered frame. The 12 figures increase in natural satellite diameter from 0.75 m to 7.5 m. The sum of all the data yield information on which orbital

regions are stable/unstable or if longitude of periapsis precesses 360° or less for a certain initial condition. It is noted that the color of the data depicts how long the orbit existed before escape or collision. Red shows the natural satellite became unstable in less than 1000 years and blue shows it remained stable until the end of the simulation at 1000 years. The first noticeable observations from Fig. 4.4 is that graphs a, b, and c have stable orbits at inclinations between $50° - 100°$, but graphs d-l are unstable in this region. Graphs a-c are stable in this region due to being in a Sun-synchronous orbit while the instability in the subsequent graphs is due to instability from the Kozai resonance. This is discussed in the subsequent sections. The second noticeable features of graphs d-l are the stable regions at low prograde and high retrograde inclinations that do not precess 360° through Ω, but rather oscillate around $\Omega = 0°$ or $\Omega = 180°$. These points of stability are the modified Laplace plane (MLP) orbits. The MLP is a frozen orbit in both longitude of the ascending node and inclination. Due to short-term perturbations not modeled in the averaged equations of motion, even if the initial conditions were exactly on the MLP; the orbit would still oscillate. Also, initial conditions close to the MLP will also oscillate around the stable region, but with a larger variance in the inclination and Ω. Further discussion on the MLP is in a more detailed section below.

4.5 Range of Sizes possible for a Natural Satellite in a Sun-Synchronous Orbit

Sun-synchronous orbits are orbits that rely on a strong SRP perturbation to cause the node of the orbit to precess at the same rate as the asteroid travels about the sun. These orbits are naturally stable, and oscillate about an eccentric orbit of eccentricity $e = \cos\Lambda$ with orbit angular momentum vector pointing towards or away from the sun. The orbits become more stable as the SRP perturbation grows, to the point where the object is stripped out of orbit. Due to this, such orbits are useful for spacecraft and thus natural satellites trapped in such orbits would be of significant concern.

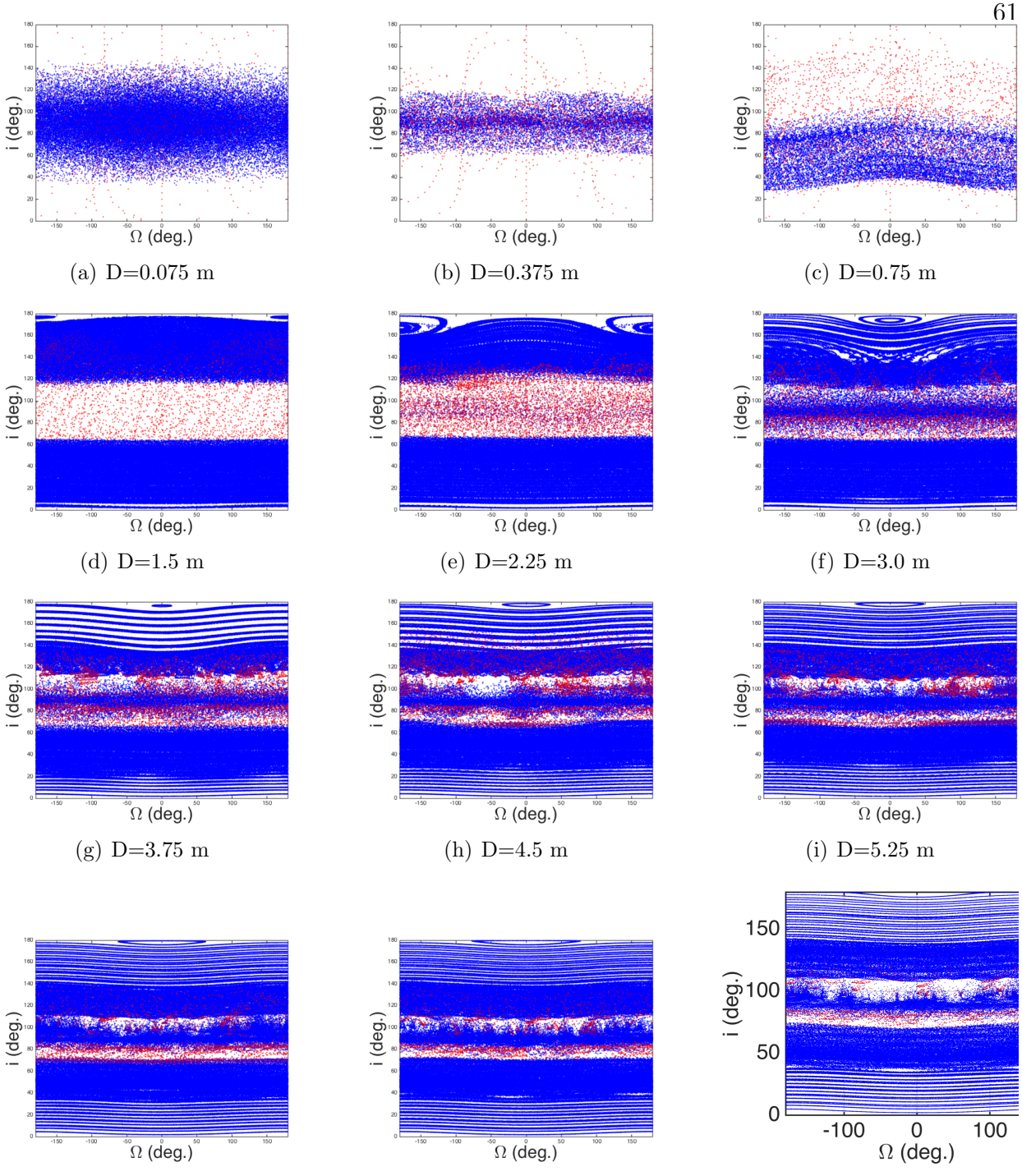

(a) D=0.075 m (b) D=0.375 m (c) D=0.75 m

(d) D=1.5 m (e) D=2.25 m (f) D=3.0 m

(g) D=3.75 m (h) D=4.5 m (i) D=5.25 m

(j) D=6.0 m (k) D=6.75 m (l) D=7.5 m

Figure 4.4: These 12 figures show the numerical results in blue (stable) to red (unstable). These figures are in the asteroid-orbit frame at a semi-major axis of 4 km. Each plot above shows the evolution of the inclination versus the longitude of the ascending node over time for increasingly larger natural satellites, with plot (a) having a diameter of 0.075 m to plot (l) representing a 7.5 m diameter object. Each data point is part of an orbit with varying initial conditions. Orbits lasting 1000 years are in blue, while the initial conditions that ended prior to the 1000 years due to escape or collision are in red.

Sun-synchronous orbits possibly containing natural satellites are especially interesting to OSIRIS-REx as the spacecraft will be in terminator plane orbits between 1 km and 2 km. The terminator plane orbit is a sun-synchronous orbit, but with the advantage of the orbit plane being perpendicular to the Sun-line. This orbit orientation allows the spacecraft to face the Sun. SRP drives the stability of the terminator plane at an asteroid as opposed to J_2 with planetary terminator planes [41]. Because the terminator plane is driven by SRP, it is stable to secular perturbations caused by SRP and therefore is an opportune orbit for spacecraft along with natural satellites.

As stated in the introduction to this chapter, there are no natural satellites orbiting Bennu greater than 15 meters in diameter. So the focus of these results were to determine the minimum natural satetllite diameters that could exist around Bennu. An example is an orbit at 4 km, where the minimum size stable natural satellite is 5.25 cm. This object was stable for 1000 years at a semi-major axis of 4 km, $\Omega = 0°$, and $i = 90° - 108°$. Some Keplerian orbital elements for these 4 orbits can be seen in Fig. 4.5. The semi-major axis, eccentricity, and inclination are constant for the 1000 year period. Longitude of the ascending node precesses a full 360 degrees. These results have the properties of a Sun-synchronous orbit. In Fig. 4.6, an inclination vs. Ω plot is displayed in the Sun-Bennu rotating frame. Sun-synchronous orbits precess in the inertial frame but will remain bounded to $\Omega_R = 0°$ or $\Omega_R = 180°$ in the Sun-Bennu rotating frame. Because the longitude of the ascending node is bounded in Fig. 4.6, the data for the four different orbits all have a precession similar to the rate of Bennu traveling around the Sun.

Sun-Synchronous orbits cause a multitude of < 0.75 m diameter satellites to be stable at inclinations between 36° and 144° or the large blue colored region in Fig. 4.3. These Sun-synchronous orbits oscillate around the terminator plane near $i = 90°$. Therefore, a Sun-synchronous orbit starting at $i = 40°$ will oscillate in inclination between 40° and 140°. If you take these Sun-synchronous orbits away, the summary of stable orbits becomes much different and can be seen in Fig. 4.7. This figure only summarizes natural satellites that were

stable for 1000 years. Therefore the Sun-synchronous orbits are any orbit that maintains a fixed longitude of the ascending node around 0° and 180° and does not precess 360° in the asteroid center orbit rotating frame. Any of these orbits are not included in Fig. 4.7, leaving orbits that do precess 360° in the asteroid centered orbit rotating frame.The figure drastically changes and there are far fewer < 1 m sized satellites that are stable. Objects at inclinations between 78° and 102° are unstable for $a > 4$ km. These Sun-synchronous orbits are stable to SRP. Without being in one of these Sun-synchronous orbits, it is very difficult for smaller objects to remain stable long-term at higher altitude orbits.

The range of values shown in Table 4.2 have a minimum and maximum diameter that is stable at a given semi-major axis. These values correspond directly with the values found by determining the maximum semi-major axis a given mass-to-area ratio can be stable with SRP. This equation is given in Equation 1.1 [37]. The table gives a range of diameters that all have mass-to-area ratios greater than the equations gives for necessary stability at a given semi-major axis. Therefore, the solutions comply with this analytical equation.

Table 4.2: Sun-Synchronous orbits

Semi-major axis (km)	Range of diameters of natural satellite (m)
1	0.0075
1.5	0.0075 - 0.045
2	0.015 - 0.225
3	0.03 - 0.3
4	0.0525 - 0.375
5	0.15 - 0.45
6	0.15 - 0.525
7	0.15 - 0.6
8	0.225 - 0.75
9	0.3 - 0.675
10	0.375 - 0.75
11	0.45 - 0.75
12	0.6-0.75
13	0.75

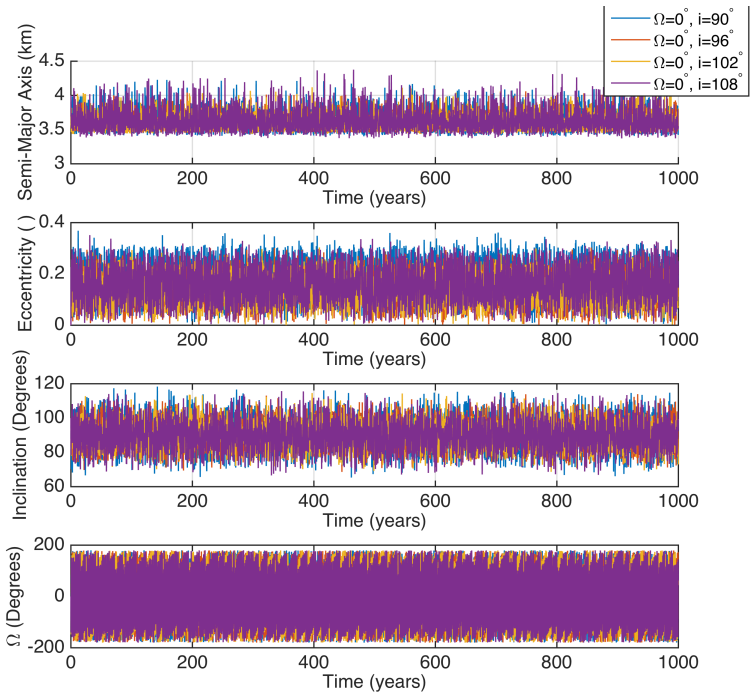

Figure 4.5: Above is the semi-major axis, eccentricity, inclination and longitude of ascending node for the 4 stable orbits for a 5.25 cm satellite at 4 km.

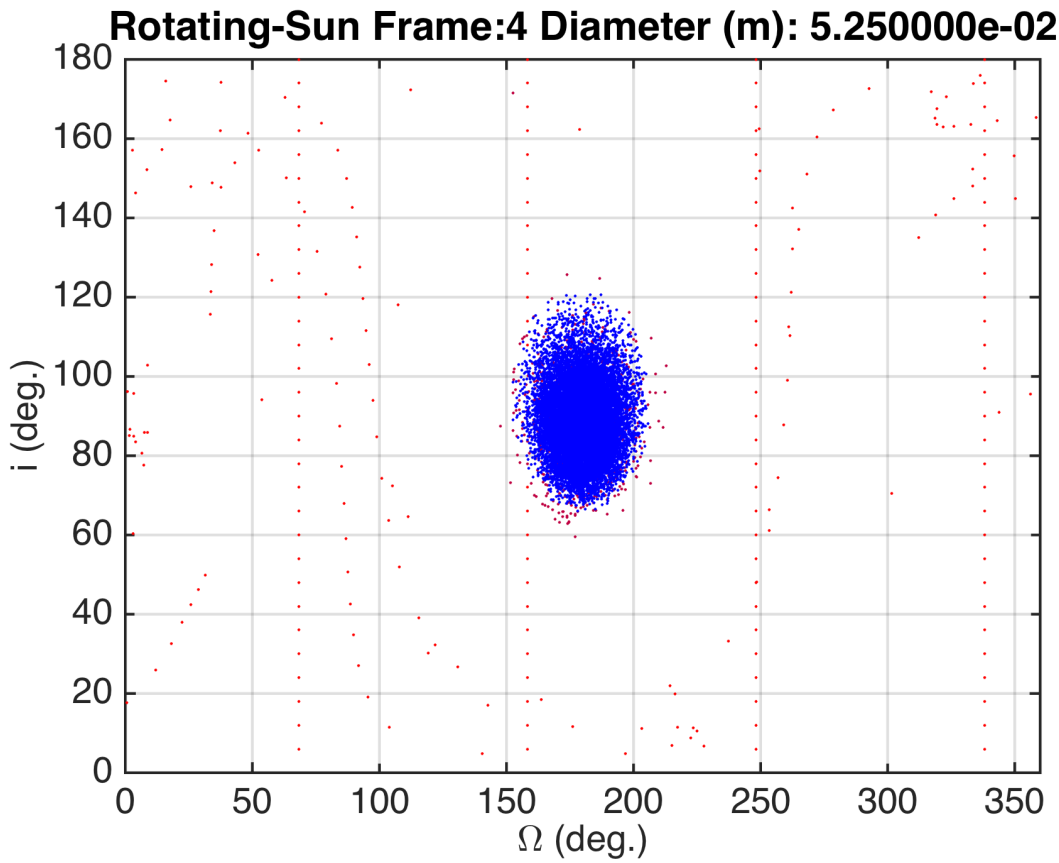

Figure 4.6: This figure gives the motions of inclination vs. longitude of the ascending node for 1000 years for the 4 stable orbits ($i = 84°, 90°96°, 102°$) for a 5.25 cm satellite at 4 km in the rotatings Sun about Bennu frame. These are all bounded to the terminator plane because the precession of Ω is bounded in this frame.

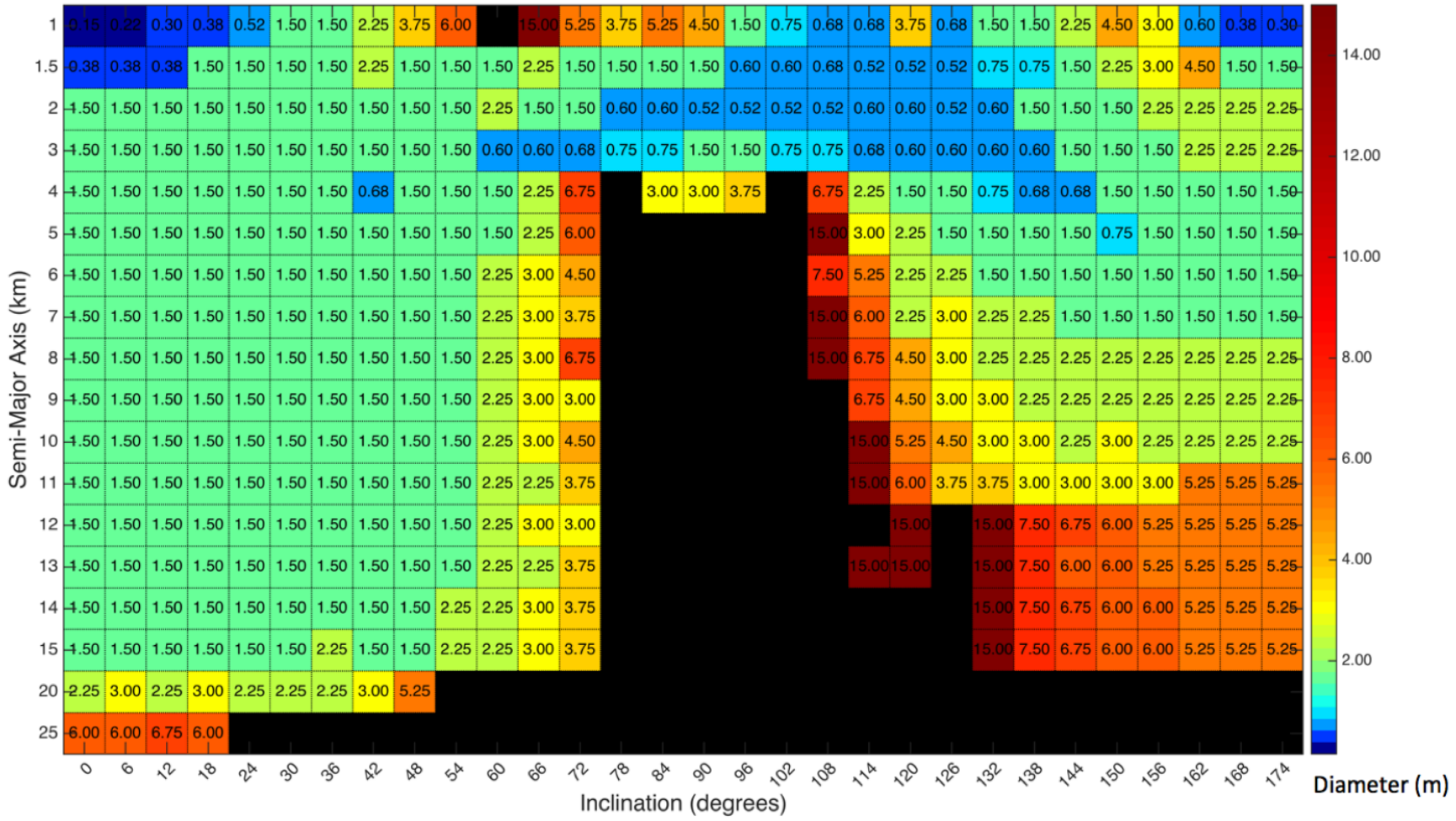

Figure 4.7: Same as Figure 4.3 without Sun-Synchronous orbits. High inclinations around 90° are not stable for semi-major axes greater than 4 km.

4.6 Stability with the modified Laplace plane

As stated in a previous section, the stable points near $\Omega = 0°$ and $\Omega = 180°$ are most likely the results of the modified Laplace plane (MLP) due to the lack of precession in the longitude of the ascending node. A way to confirm this is by comparing the averaged equations shown in Equation (3.16) to the numerical results. In Fig. 4.8a the whole solution set is compared to the averaged equations, but in Fig. 4.8b just the modified Laplace plane and a few other orbits are shown. In Fig. 4.8b, the results for $a = 5$ km, $D = 7.5$ m were compared where just the MLP and two other orbits are plotted. There is a point at $\Omega = 0°$, $i = 3°$ which is the MLP equilibrium. The two other orbits are near enough to the equilibrium that they oscillate around it. In blue are the numerical results. The numerical result for the MLP isn't a point but rather a tight circle with some variance in Ω and inclination. Also, the two neighboring orbits deviate from the averaged equations and have a larger variance in Ω and inclination. It is expected this because the numerical solutions have perturbations that are not modeled with the secular averaged equations of motion.

As the natural satellites decrease in diameter or their mass-to-area ratio decreases, the MLP will cease to be a stable orbit. The averaged equations of motion that model the MLP do not model non-secular motion caused by SRP. Therefore, compared to the example object shown in Fig. 4.8b with $D = 7.5$ m, the object with $D = 1.5$ m in Fig. 4.8c will vary in motion around the MLP more significantly. Eventually, this non-secular motion will be the dominating perturbation, the smaller object will escape or impact Bennu. Also, the variance in motion will change depending on how close to the MLP the initial orbit of the natural satellite may be. If the object's initial conditions are exactly on the modified Laplace, inclination and longitititude of the ascending node are bounded much more than an object displaced a couple degrees in inclination from the MLP.

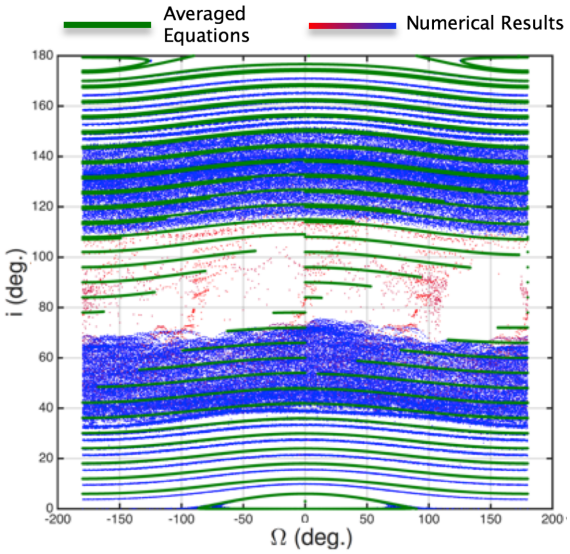

(a) All results

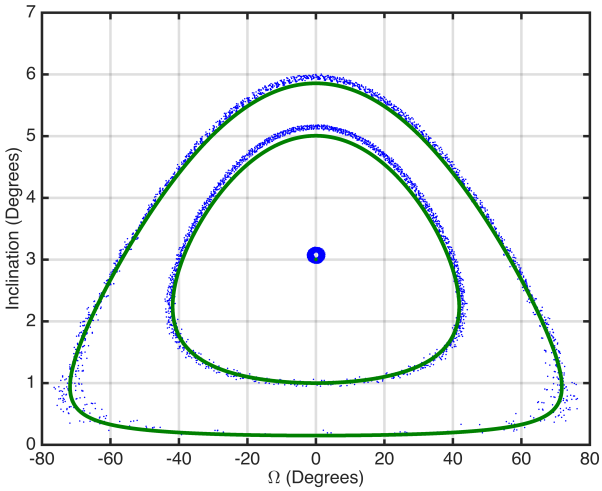

(b) Prograde MLP, D=7.5 m

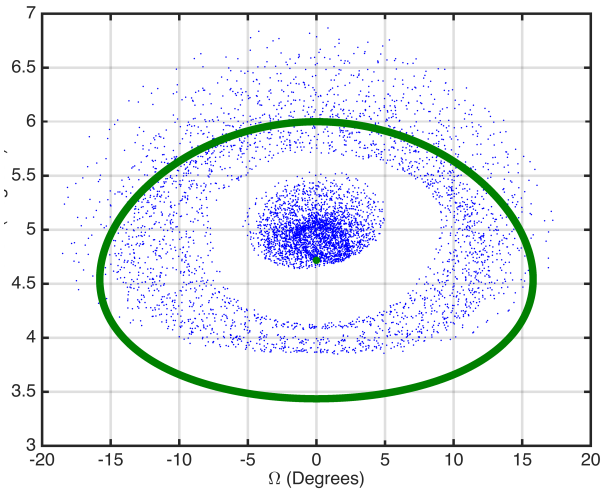

(c) Prograde MLP, D=1.5 m

Figure 4.8: Figures (a-b) Inclination vs. longitude of the ascending node for $a = 5\ km,\ D = 7.5\ m$ for 1000 years. The orbits that existed 1000 years are in blue, while the initial conditions that ended prior to the 1000 years due to escape or collision are in red. In green are the averaged equations of motion results. In plot (a) the whole solution set is compared to the averaged equations, but in graph (b) just the modified Laplace plane and a few other orbits are shown. (c) Is just the MLP and a few other orbits for $a = 5\ km,\ D = 1.5\ m$

4.7 Kozai Resonance

For a Kozai resonance to occur, the satellite has negligible mass compared to the other two bodies in a three-body system. Also, the distance between the primary and the satellite must be much closer than the primary to the Sun. These are both true in this scenario. The orbit's argument of periapsis librating due to perturbations from the Sun causes the Kozai resonance. Using the averaged equations of motion for just third-body dynamics, the angular momentum of the satellite's orbit projected normal to the Sun-Bennu orbit plane is conserved. This can be quantified as

$$H_z = \sqrt{(1 - e^2)} \cos i. \tag{4.4}$$

Therefore, the eccentricity and inclination of the satellite's orbit will vary. As inclination increases, the eccentricity will decrease and vice versa. The Kozai resonance will most likely occur further out from the asteroid such that spherical harmonics will not significantly perturb the system. The satellite needs to be massive enough as to not be perturbed substantially from SRP. Also at high inclinations, the Kozai resonance will cause instability since the eccentricity will be too large. Eccentricity will increase such that it will collide with Bennu or it will escape the Hill sphere.

The Kozai resonance is determined with averaged equations that only include third-body dynamics. In order for the Kozai resonance to occur, the semi-major axis needs to be far enough away from Bennu that perturbations due to J_2 are no longer significant. Plus, the satellite has to be large enough in diameter such that SRP is no longer a dominating force. Therefore, to determine the possibility of a Kozai resonance around Bennu, the example used is both far from Bennu at 10 km and a large satellite at 7.5 m in diameter. In Fig. 4.9, there is a plot of eccentricity as a function of inclination. The numerical results for the orbit of one initial condition at $a = 10\ km,\ D = 7.5\ m,\ \Omega = 0°,\ i = 72°$ is given by the blue data points. The general trend of the data is as eccentricity increases, the inclination decreases,

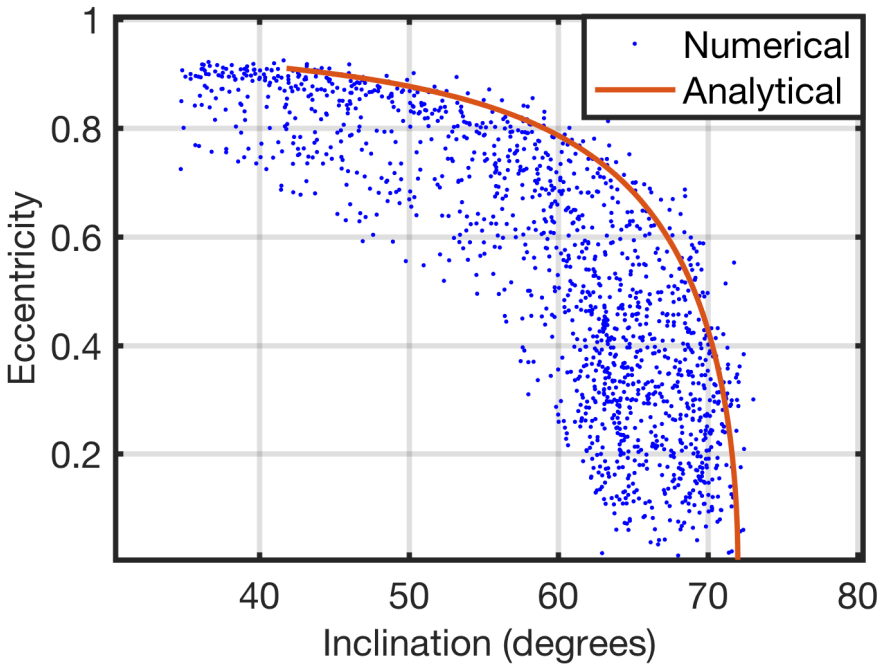

Figure 4.9: The blue data points are the eccentricity as a function of inclination for the numerical equations of motion for initial conditions of $a = 10\ km,\ D = 7.5\ m, \Omega = 0°,\ i = 72°$. In red is the data for the analytical equation between eccentricity and inclination for the Kozai resonance.

a property of the Kozai resonance. Since numerical results of an orbit have multiple perturbations modeled, it cannot be assume H_z or the angular momentum in the $z-$component of the Bennu-Sun orbit plane is constant. Therefore, for the value of H_z, the mean of all the data points was used to determine the value of H_z. Then a range of eccentricities from 0 to 0.8 was used to solve for the inclination. These results are shown in Fig. 4.9 as a red curve. The numerical data follows the same curve as the analytical Kozai resonance equation. But, there is a larger variance in inclination for the numerical results. This may be due to the other perturbative forces on the satellite or higher-order third-body perturbations not accounted for in the averaged equations. Further research will need to be done to verify that this large variation is acceptable and that the orbit can be considered stable for longer periods of time.

The Kozai resonance may also be responsible for the instability regions in Fig. 4.4d-l. The Kozai resonance has a maximum eccentricity value for a given inclination. This relationship is

$$e_{max} = \left(1 - \frac{5}{3}\cos^2 i_{max}\right)^{1/2}. \tag{4.5}$$

For the example orbit with an initial inclination of 72°, the maximum eccentricity is 0.91. The resulting eccentricity from the numerical data appears to go beyond that value to 0.92. As the initial inclination increases, the maximum eccentricity achieved by the Kozai resonance also increases. Eventually, the maximum eccentricity is so high that the satellite may escape the Hill sphere or collide with Bennu. Above an inclination of 72°, there is a critical inclination where the eccentricity will become large enough to cause instability through the Kozai resonance. The same case exists for retrograde orbits near a polar inclination. This givese a band of unstable inclinations between $78° - 102°$.

By looking at Fig. 4.4g-l, there exist stable orbits in the region that are supposed to be unstable due to the Kozai resonance. This may be due to two reasons.

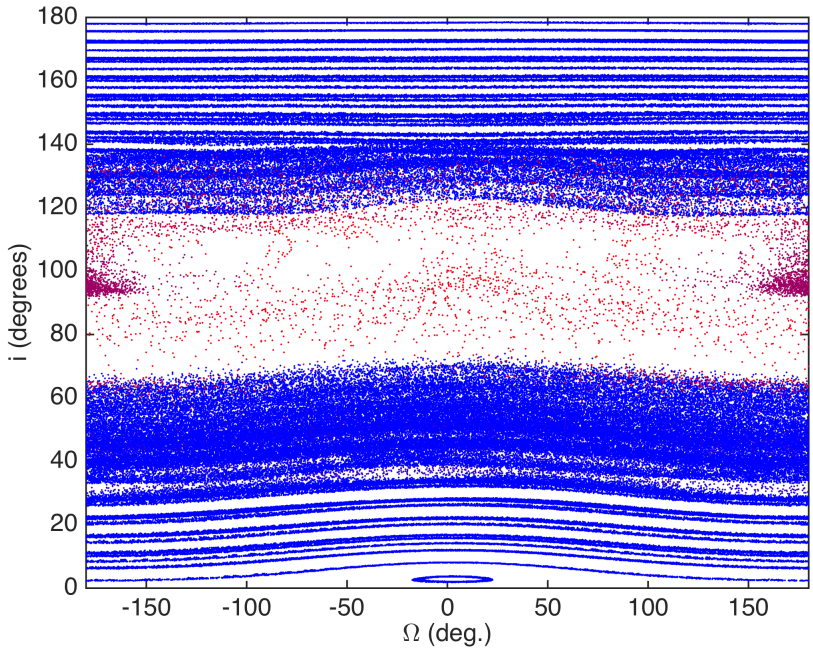

Figure 4.10: Inclination vs. longitude of the ascending node for $a = 4\ km,\ D = 5.25\ m$ for 10,000 years. The orbits that lasted the 10,000 years are in blue, while the initial conditions that ended prior to the 10,000 years due to escape or collision are in red.

First, there are other perturbing forces other than third-body perturbations from the Sun causing the orbits to not reach maximum eccentricity. Second, the simulation did not run for a time period long enough to witness the escape/collision due to the growth in eccentricity. To see if a longer simulation time will yield the escape/collision, Fig. 4.4i with initial conditions $a = 4\ km,\ D = 5.25\ m$ is integrated for 10,000 years. The results are in Fig. 4.10. After 10,000 years all orbits in the $60° - 120°$ range are unstable, which suggests the Kozai resonance is the reason for this unstable region, but the time scales for oscillations between maximum inclination and maximum eccentricity are on longer time scales than 1000 years.

Above it was mentioned that the band of unstable orbits found in Fig. 4.7 for inclinations from $78° - 102°$ for semi-major axes greater than 4 km is attributed to the Kozai resonance. However, if the time of integration was extended to 10,000 years, the Kozai resonance causes instability for all orbits from $60° - 120°$. Therefore, this band of unstable orbits for semi-major axes greater than 4 km, may cover a larger range of inclinations if the integration was on time scales that allowed for maximum eccentricity to be obtained through the Kozai resonance. In future work, it would be advantageous to extend the integration time in this region to see if the Kozai resonance would have this impact.

4.8 Conclusion and Future Work

4.8.1 Conclusion

Simulations were performed for hypothetical natural satellites from 0.0075 m to 15 m at semi-major axes from 1 km to the Hill sphere of 29.5 km [48]. The 120 iterations vary with $\Omega = 0°,\ 90°,\ 180°,\ 270°$ and inclination from 0° to 180° in increments of 6 degrees. A subset of the data was used as an example to show how the stable and unstable orbits evolved as the size of the natural satellite increased at a constant semi-major axis. Multiple observations were made on whether Sun-synchronous, modified Laplace plane, or Kozai resonance could

be used to help understand certain regions.

Sun-synchronous orbits were stable for the smallest natural satellites with diameters from 0.75 cm to 0.75 m. The Sun-synchronous orbits were stable for inclinations from 36° and 144° and semi-major axes from 1.5 km to 13 km. The range of inclinations for these orbits also includes the terminator plane, which means OSIRIS-REx could share an orbit with a natural satellite. The two terminator plane orbits that OSIRIS-REx will be in are at radii between 1 km and 2 km. In this study, no natural satellites stable in the 1 km terminator orbit were found. However, larger objects greater than 4.5 m were found, capable of being stable at 90°, but are not in a terminator or Sun-synchronous orbit. At 1.5 km, there are natural satellites stable in the terminator plane, but they are less than 10 cm in diameter. OSIRIS-REx will only be searching for natural satellites greater than 10 cm in diameter during approach to Bennu.[48] Once again, at a radius of 1.5 km, there are objects larger than 1.5 m capable of orbiting at the same inclination, but not in a Sun-synchronous orbit. These larger objects are not in a frozen like Sun-synchronous orbits and therefore may vary more in their Keplerian orbital elements. At 2 km radii, there are natural satellites with diameters greater than 10 cm in a terminator plane orbit. These objects tend to be eccentric and therefore will intersect the 1.5 km orbit at times. Therefore, OSIRIS-REx will be interested in surveying for natural satellites that may be stable near the terminator plane orbits the spacecraft will be occupying.

For objects greater than 1.5 m in diameter, the modified Laplace plane is a stable frozen orbit where natural satellites may reside for all orbital radii. Because of the low obliquity of Bennu, the modified Laplace plane will only have inclinations differing from the equator of 4° or less. Both prograde and retrograde modified Laplace plane orbits are stable. Natural satellites near the modified Laplace plane may oscillate around the Laplace plane such that RAAN does not precess.

The Kozai resonance created an unstable region for inclinations between $78° - 102°$ for orbital radii greater than 4 km in the 1000 year timespan. The Kozai resonance affects

objects greater than 1.5 m in diameter that are not easily perturbed by SRP.

4.8.2 Future Work

From the data, interesting orbital phenomena capable of occuring to natural satellites around Bennu have been characterized. However, there is interesting work that could be done to further answer some questions on the topic. There is one example of the Kozai resonance occurring at $a = 10\ km,\ D = 7.5\ m, \Omega = 0°,\ i = 72°$, but it is not understood what range of diameters the natural satellite or distance from Bennu that the Kozai resonance occurs. Also, it would benefit OSIRIS-REx to better understand the stability of orbits at 1 km. Observing Fig. 4.3, the minimum diameter natural satellite stable seems random as inclination increases compared to larger orbital radii. One km orbit stability will be heavily affected by spherical harmonics, therefore further investigation in how this affects the lower orbits around the asteroid will be beneficial. Further conclusions can also be made by quantifying the variance in the eccentricity of a given natural satellite orbit. Many of these orbits maintain constant semi-major axis and inclination, but the eccentricity can increase dramatically. Therefore, these satellites make exist at a large range of radii and a large breath or orbits may intersect paths with OSIRIS-REx.

This investigation was purely targeted at the asteroid Bennu for understanding where the stable orbits of a natural satellite may exist. However, this study can be applied to other small bodies or with bodies of varying obliquities, and the dynamics could be very different. Therefore, understanding how the orbital phenomena change from various obliquities or asteroids could help with understanding the dynamical environment of natural satellites for future missions to small bodies. Altering the obliquity of the asteroid and its effects are discussed in the next chapter.

The research completed at Bennu looked at multiple stable orbits such as the modified Laplace plane and Sun-synchronous orbits. However, there are other stable orbits that natural satellites could exist in but require different initial conditions to ensure long-term

stability. The first stable orbit that could potentially be stable for natural satellites are heliotropic orbits. Heliotropic orbits have low inclinations less than 46.378° [94, 95]. These orbits also require a given non-zero eccentricity to maintain being frozen. Generally in the orbit the apoapsis of the orbit is pointed towards the Sun. Therefore $\Pi = \omega + \Omega$ rotates equivalent to the mean motion of the asteroid's orbit to the Sun. In this orbit, the eccentricity, inclination, and semi-major axis are frozen. This orbit was not captured in the initial conditions studied in this research because heliotropic orbits require a precise eccentricity in order to be stable. Therefore, this adds another reason to investigate future work where the eccentricity of the orbit it altered to determine more possible stable orbits. Another interesting possibility is for the orbits of natural satellites to exist in quasi-periodic terminator orbits [96]. These solutions may not necessarily be a simple circular or elliptical orbit, but more complex motion that is periodic and related to the motion around the terminator plane.

Previous work on using FLI (Fast Lyapunov Indicator) to determine stability of terminator plane orbits and there periodic orbit families has been done [97, 98, 99]. This work has been compared to the analytical theory modeling spherical harmonics and SRP. Most notably, the FLI indicators were able to give the range of semi-major axes where a terminator plane may be stable. This range coincided with the analytical equation (Equation 4.2), however for longer time periods the FLI indicators show that the range of stable semi-major axes would decrease. The FLI indicators also investigated how changing other orbit elements such as inclination, eccentricity, argument of periapse and longitude of the ascending node such that the orbit was a near-terminator orbit would effect the stability. FLI indicators prove to be a useful tool to determine stability with more flexibility than the analytical solutions. This would be advantageous to incorporate into future work on natural satellites. The previous work observed spacecraft with low mass-to-area ratios, therefore using FLI indicators for a multitude of mass-to-area ratios would help to understand how the size of the natural satellite effects the range of orbital elements where a natural satellite can be stable

and Sun-Synchronous. Also, FLI indicators give information on how chaotic the motion of the satellite can be. Our work only looked at whether a satellite escaped or impacted within 1000 years, however the orbit could possibly have chaotic motion where a slight deviation in the model would result in an impact/escape that is not detected in our simple definition of stability. Therefore, more comprehensive idea of stability through FLI indicators could be deduced from long-term orbit stability of terminator and Sun-synchronous orbits.

Chapter 5

Artificial and Natural Satellites around Asteroids

This chapter looks into both natural and artificial satellites around multiple asteroids. The chapter is broken into four main sections, each interested in a different focus that complements the work done on natural satellites around Bennu. The first section will introduce the stability of a spacecraft and a one meter in diameter natural satellite around multiple asteroids: KW_4, Bennu, and Vesta. Specifically, this study focuses on the stability of the terminator plane and Laplace plane around these asteroids while changing various parameters. The second section focuses on artificial satellites at Bennu using a subset of mass-to-area ratios from the previous chapter. The third part takes a more in-depth look at the modified Laplace plane and how much mass an asteroid needs for the spacecraft to be stable. Finally, the last section of this chapter looks at various obliquities of an asteroid to see how that changes the overall stability of natural satellites that could orbit a given asteroid. This chapter hopes to gain some insight into artificial and natural satellites at various asteroids and to help advance perspective on general satellite stability around an asteroid.

5.1 Natural and Artificial satellites around multiple asteroids

Initiating and maintaining a spacecraft orbit in the proximity of an asteroid is a significant challenge. The unique and often irregular shapes of asteroids cause their gravity fields to be non-uniform, while the low mass of these bodies results in their gravity fields being relatively weak. Also, solar radiation pressure (SRP) can be a dominating force on a

spacecraft's motion in this weak gravity environment. All of these factors combine to make the orbital motion of a spacecraft about an asteroid potentially unstable over time. Such instability could lead to the spacecraft escaping from the asteroid or crashing into its surface. Therefore it is paramount to determine frozen orbits that exist around an asteroid such that excessive station-keeping can be minimized. Frozen orbits such as the Sun-terminator plane are being used by OSIRIS REx; however, the Modified Laplace Plane may also yield another viable option as a frozen orbit to be utilized by spacecraft [41].

The motion of the spacecraft around an asteroid includes perturbations from J_2, third-body perturbations from the Sun and SRP. To better understand the full capability of the modified Laplace plane, parameters such as the asteroid orbit, mass-to-area ratio of the spacecraft, and obliquity of the asteroid are varied. Three asteroids are studied to determine the effect an asteroids' shape, mass and orbit have on the spacecraft. These asteroids are 66391 (1999KW_4), Bennu, and Vesta. Near-Earth asteroid 66391 (1999 KW_4), hereinafter will be referred to as KW_4. Although Vesta is not a NEA, its comparably larger mass will help contrast the effects of SRP on the other two smaller bodies.

5.1.1 Implementation

There is a multitude of parameters that can be varied to compare how the Laplace equilibrium and other equilibria evolve. The parameters that will be varied are obliquity, semi-major axis, mass-to-area ratio of the spacecraft, the asteroid's mass and J_2. The asteroids being compared are 1999 KW_4, Vesta and Bennu. The parameters for each are listed in Table 5.1.

Table 5.1: Asteroid Parameters

Name	Mass (kg)	SMA (km)	Ecc. ( )	T_s (days)	ϵ (deg)	α (km)	β (km)	γ (km)
Bennu	6.233×10^{10}	1.6844×10^{8}	0.204	436.6	175°	0.3	0.3	0.25
1999 KW_4	2.353×10^{12}	9.6042×10^{7}	0.688	188	3.2°	0.75	0.75	0.65
Vesta	2.5908×10^{20}	3.5328×10^{8}	0.0886	1325	41°	283	279	223

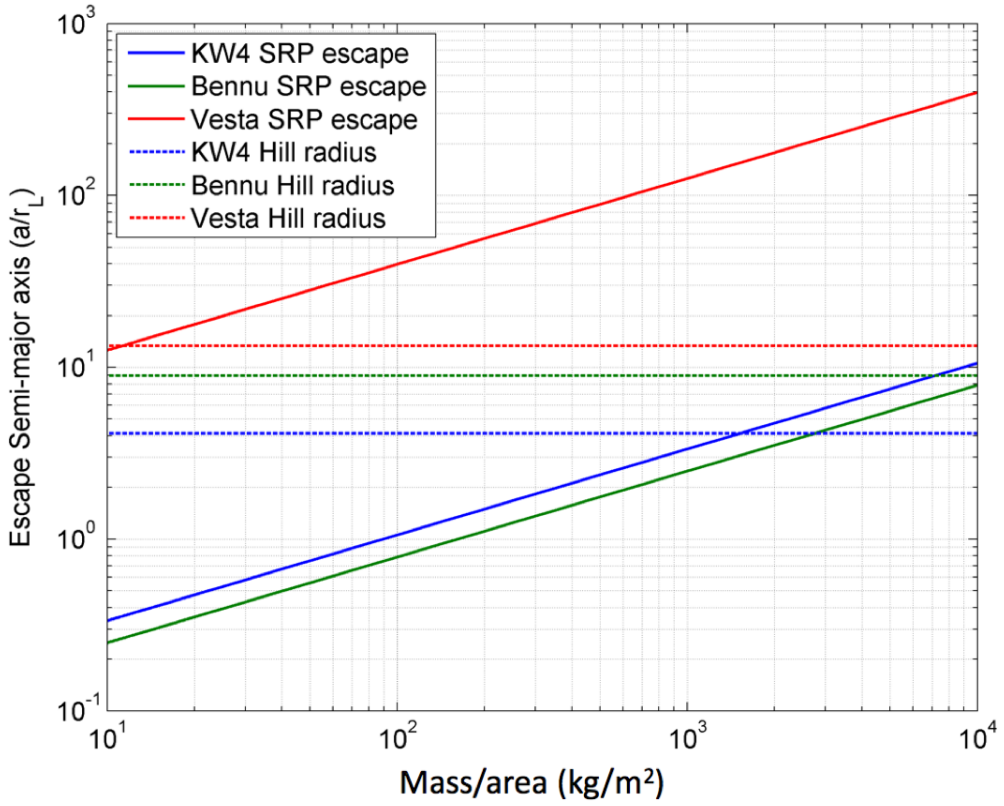

Figure 5.1: The Hill sphere and SRP no-escape criteria for Bennu, KW_4, and Vesta.

Before beginning analysis, it is essential to understand at what distance from the asteroid the spacecraft will escape. The Hill radius usually is sufficient for determining this distance, however with the strength of the SRP perturbation another approximation needs to be established. The Hill sphere is defined as [41]

$$r_H = a_s(1-e_s)^3\left(\frac{m_p}{3m_s}\right)^{1/3}. \tag{5.1}$$

The approximation for what distance SRP will be weak enough the spacecraft will not escape is [41]

$$a_{min} = \frac{1}{4}\sqrt{\frac{\mu_a}{(1+\rho)P_\phi/b}}a_s. \tag{5.2}$$

Although the equations above are an approximation and may result in some semi-major axes less than a_{min} escaping, it gives a more realistic idea of where SRP is a dominating perturbation. The results of these analytic equations for Bennu, KW_4, and Vesta can be seen in Figure 5.1. Notice that for Vesta, a large asteroid with significant mass, the Hill radius is a better approximation of when the spacecraft will escape as opposed to the SRP escape criteria. However, for KW_4 and Bennu, mass-to-area ratios below ~ 1500 kg/m^2 and ~ 3000 kg/m^2 respectively yield the SRP escape criteria as a better approximation. This suggests that SRP is a significant perturbation that will cause instability for the satellite up until at least these mass-to-area ratios.

5.1.2 Overview of Ω and Inclination precession

All trajectories will be compared with a right ascension of the inclination versus ascending node (RAAN) plot. The initial conditions have a RAAN of 0° or 180 ° while the inclinations tested are 0° to 180° in increments of 15°. The initial conditions will also include the prograde and retrograde Laplace plane equilibria. The time will be terminated at escape or collision or after ten years. The change in inclination and RAAN will be mapped over

time for these initial conditions to show general trends in the motion of the spacecraft given its initial orbit parameters. Figure 5.2 can be used as an example for the inclination vs. right ascension of the ascending node map. The numerical results are displayed in colors ranging from blue to green, where the color denotes the time of escape/collision or end of integration; where the green data set represents a trajectory that quickly escapes from or collides with the asteroid. A pure blue set of data denotes the end of integration with no escape of collision. The data that are displayed in red denotes the averaged equations of motion's evolution of RAAN and inclination. Three general trends can be seen in these maps. The first is the modified Laplace plane equilibrium. For the modified Laplace plane the averaged equations in red will be a singular point denoting no changes in inclination or RAAN over time. This can be seen in the three different plots in Figure 5.2 at various inclinations with RAAN of either 0° or 180°. The numerical equations will never result in a singular point when on the modified Laplace plane but rather the data will "orbit" the averaged equation's equilibrium data point due to small precessing in inclination and RAAN. The second trend is where both the averaged equations and numerical equations orbit around the equilibrium. This is when the initial condition is somewhat offset from the modified Laplace plane. This can be seen as a closed singular loop for the averaged equations while the numerical is a closed loop but with oscillations around the averaged equations. These oscillations that don't exist in the averaged model are non-secular motion due to SRP. If this non-secular motion is large enough it will cause the satellite to become unstable. Finally, there exists a case where both the average equations and numerical equations yield an inclination that oscillates within a range of values, but the RAAN precesses through 360° of motion. The numerical data will oscillate about the averaged equations or deviate from the averaged equations over time depending on the strength of the non-secular forces due to SRP.

5.1.3 Obliquity

The obliquity affects where the Laplace angle will lie on the Laplace surface. For comparing varying obliquity, all analysis was completed at 0.25 Laplace radius at Bennu with an object that has a mass-to-area of $b = 1000$ kg/m^2. The analysis was done in the asteroid orbit-frame; therefore the equilibrium in this frame is defined by $i = \epsilon - \phi$. This close to the asteroid the Laplace angle is inclined 1.5° from the equator, which means the Laplace angle is at 29.5° relative to the orbit plane.

It can be seen in Figure 5.2 that as the obliquity increases, so does the inclination of the Laplace surface relative to the orbit plane. There are two Laplace equilibria. First is at $\Omega = 0°,\ i = \epsilon - \phi$ and the second is $\Omega = 180°,\ i = 180° - i$. As the obliquity increases, the two equilibrium are relatively close regarding inclination, till both are at 90° when the obliquity is 90°. This is a special case where the asteroid equator is perpendicular to the orbit pole. It should also be noted, that as the obliquity increases, the further away an orbit can be displaced from the modified Laplace plane and still precess about the Laplace plane as opposed to processing in RAAN a full 360°. When the obliquity reaches 90°, all initial conditions investigated are precessing around the Laplace plane.

5.1.4 Compare different Laplace Angles

A comparison was made of Bennu, Vesta, and 1999 KW$_4$ at $\phi = 5°,\ 15°$, and 25°. The satellite and each asteroid will have $b = 1000$ kg/m^2 and $\epsilon = 30°$. This provides two comparisons. The first is a comparison of all three asteroids at three different points on their Laplace surface. Second, because of the differences in mass, the 3 points of the Laplace surface will be at different radii for each asteroid. This provides an understanding of how the stability of a satellite evolves as it is placed on an orbit further from the asteroid.

In Figure 5.3, the evolution of increasing radii for Vesta can be seen. There is little deviation from the numerical analysis to the averaged equations. Only at $\phi = 25°$ there

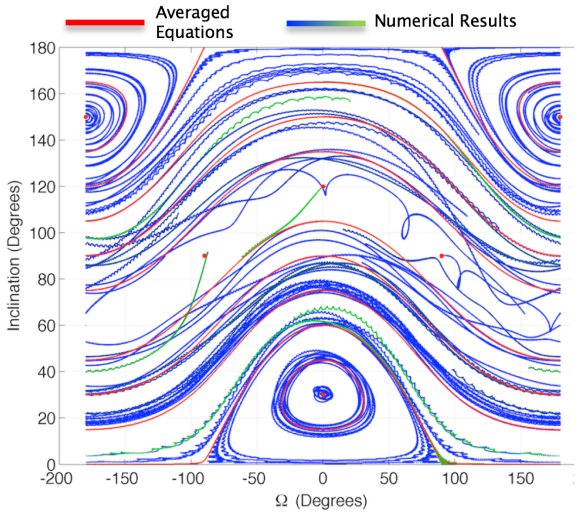

(a) 30° Obliquity

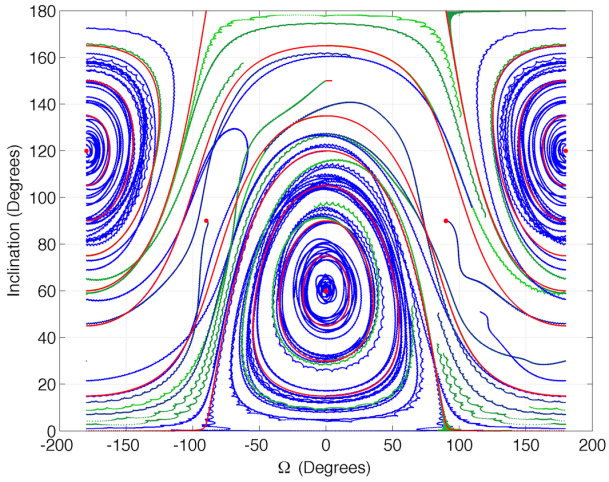

(b) 60° Obliquity

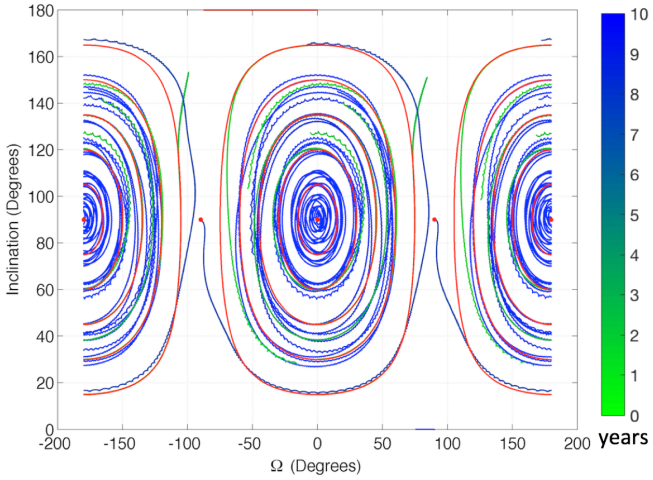

(c) 90° Obliquity

Figure 5.2: These three figures show the numerical results in blue to green and the averaged motion in red. Each plot was evaluated at 0.25 Laplace radii at Bennu with $b = 1000$ kg/m^2. Figure a.) $\epsilon = 30°$ b.) $\epsilon = 60°$ c.) $\epsilon = 90°$ These figures are in the asteroid orbit frame so the equilibria for the Laplace plane is defined by $i = \epsilon - \phi$.

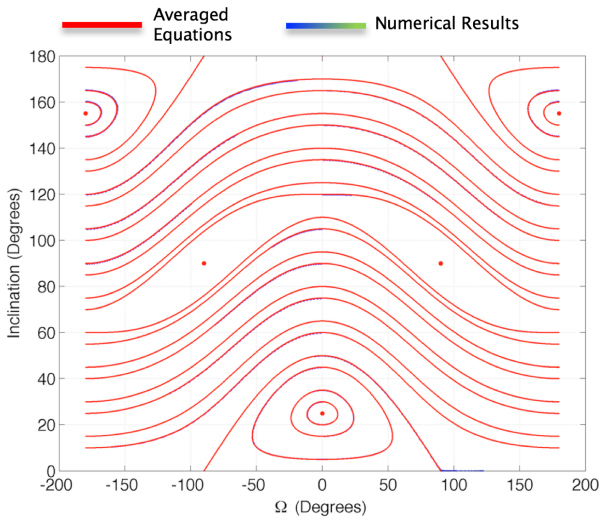

(a) Vesta $\phi = 5°$, $0.743 r_L$

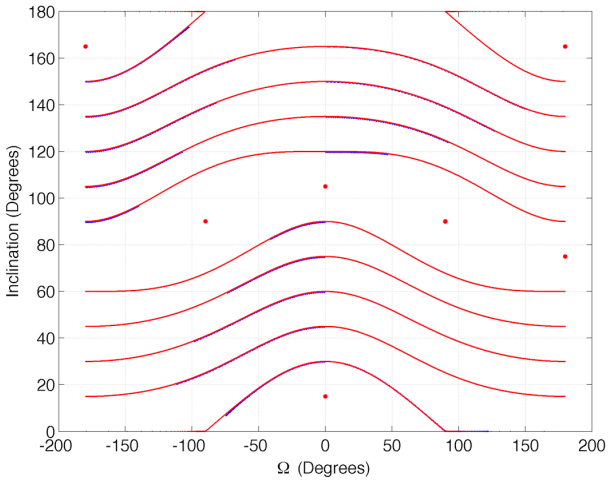

(b) Vesta $\phi = 15°$, r_L

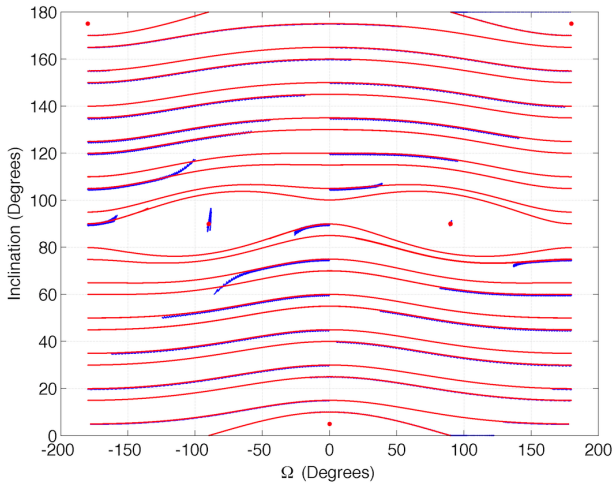

(c) Vesta $\phi = 25°$, $1.345 r_L$

Figure 5.3: These three figures show the numerical results in blue to green and the averaged motion in red. These figures are in the asteroid orbit-frame so the equilibria for the Laplace plane is defined by $i = \epsilon - \phi$. The numerical data is integrated for 100 years, which is not enough time to make a full precession of longitude of the ascending node for a natural satellite orbit around Vesta, Therefore the numerical results only show a portion of the orbital evolution.

exists deviation from the averaged equations that are significant. However, there are no escapes or collisions during the ten years analyzed. This contrasts significantly with Figure 5.4 where the analysis on KW_4 and Bennu are shown. For 1999 KW_4, at $\phi = 5°$ there are significant oscillations about the averaged equations. There is also instability for the prograde modified Laplace plane equilibrium. At $\phi = 15°$ the oscillations increase but few trajectories escape before the end of the analysis time. The Laplace equilibria do not necessarily exist, but some trajectories oscillate in Ω and i around the equilibrium. By $\phi = 25°$, most of the trajectories are unstable and escape. Bennu is even more unstable, even at radii close to the asteroid. The Laplace equilibria is not stable for Bennu except the retrograde MLP at a Laplace angle of 5°.

There are significant differences between the behavior of the satellite around the three asteroids. Vesta is more massive than the other asteroids. This allows for the 2-body motion between Vesta and the spacecraft to dominate and thus SRP perturbation will be relatively weak. The Laplace plane with no SRP has a Laplace angle of $\phi = 15°$ at 1 Laplace radius for the obliquity used in this analysis. For Vesta, the MLP Laplace radius did not change with the addition of SRP. While for Bennu and KW_4 the new radii for $\phi = 15°$ is $0.477r_L$ and $0.787r_L$ respectively. The stronger the SRP perturbation is relative to the other perturbations, the more it will alter the Laplace surface.

5.1.5 Mass-to-Area Ratio

For the asteroid Bennu at $\epsilon = 30°$ and $a = 0.337r_L \approx 3$ km , a comparison of $b = 0,\ 100,$ and 1000 kg/m^2 was made. The results can be seen in Figure 5.5. For increasing mass-to-area ratio, the closer the spacecraft follows the averaged equations. For $b = 100$ kg/m^2, the motion of the spacecraft hardly follows the averaged equations of motion. This is in contrast to no SRP, where the numerical analysis simply oscillates around the averaged equation's precession of inclination and RAAN. From Figure 5.5 it appears the only case where the modified Laplace plane is stable is the retrograde grade case for $b = 1000$ kg/m^2.

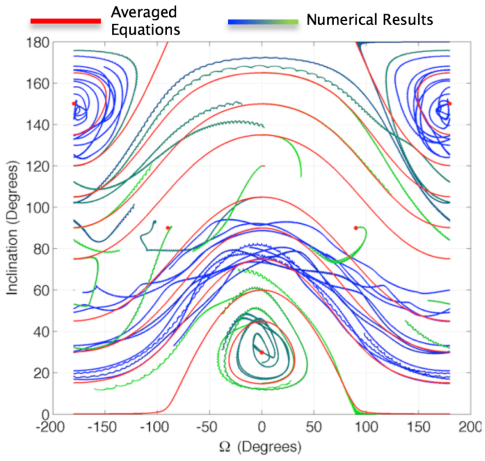

(a) Bennu $\phi = 5°$, $0.337 r_L$

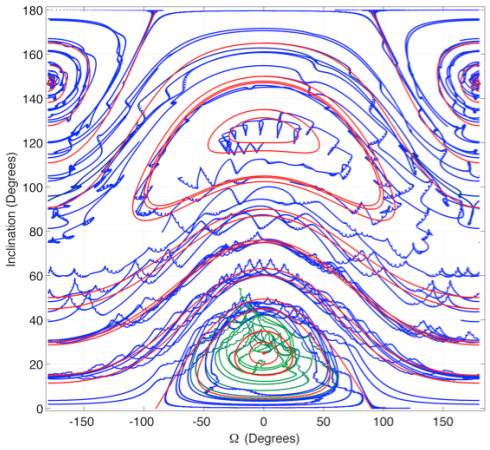

(b) KW4 $\phi = 5°$, $0.565 r_L$

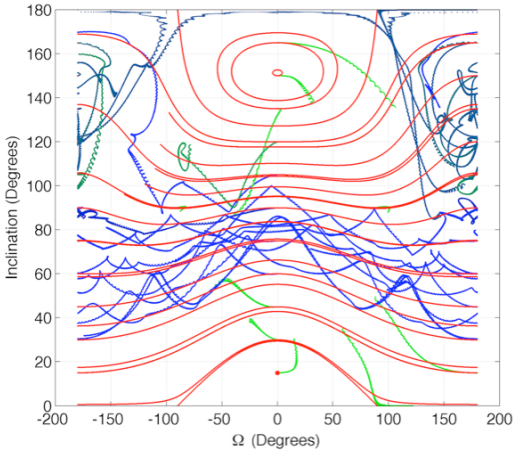

(c) Bennu $\phi = 15°$, $0.477 r_L$

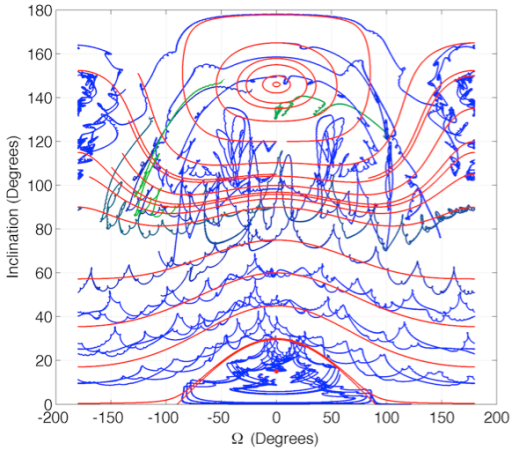

(d) KW_4 $\phi = 15°$, $0.787 r_L$

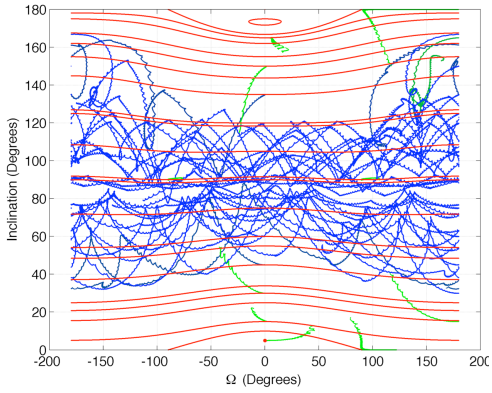

(e) Bennu $\phi = 25°$, $0.673 r_L$

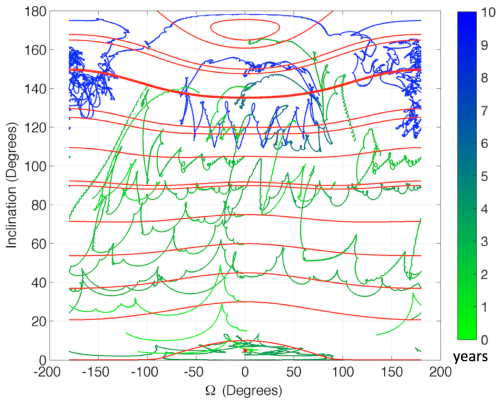

(f) KW_4 $\phi = 25°$, $1.089 r_L$

Figure 5.4: These 6 figures show the numerical results in blue to green and the averaged motion in red. The trajectories go from green to blue, depending how long the trajectory exists without escape or collision. The color scale on plot (f) gives the time scale for the corresponding color. Each plot was evaluated at Bennu with $b = 1000$ kg/m^2.These figures are in the asteroid orbit frame so the equilibria for the Laplace plane is defined by $i = \epsilon - \phi$.

Figure 5.5c shows a large number of stable orbits that oscillate in inclination around 90°. These are Sun-synchronous orbits that are oscillating around the terminator plane.

Figure 5.6 shows the precession of RAAN and inclination for a satellite where $b = 100$ kg/m^2 at the three asteroids. With a mass-to-area ratio that low, the averaged equations of motion are changed significantly for the smaller asteroids, KW_4 and Bennu, than for Vesta. While every initial condition for Vesta is stable including the Laplace plane, the only stable orbits for KW_4 and Bennu are Sun-synchronous orbits with large oscillations around the terminator plane.

5.1.6 Conclusion

The modified Laplace plane equilibria do not create frozen orbits in circumstances where solar radiation pressure is the dominating force in the system. The averaged equations of motion used to derive the MLP only take into account the long-term oscillations in motion for the spacecraft. In a small body system, the short-term perturbations have a greater effect and can cause a collision or escape in approximately 19 days or less. However, for a spacecraft where stationkeeping is involved, the MLP orbit could remain in a useful orbit long enough to still be considered. This could be determined by understanding how the Keplerian motion evolves and comparing that to the well utilized frozen orbits such as the terminator plane. Also, the MLP may not be Lyapunov stable and if there is a small deviation from the equilibrium a possible collision or escape may result.

This preliminary work was initially intended to determine if the modified Laplace plane is a valid stable orbit choice for a spacecraft visiting an asteroid. The answer is unclear because the modified Laplace plane would be very stable at an asteroid the size of Vesta but not anything the size of Bennu or KW_4. Vesta is 8-10 orders of magnitude larger in mass than Bennu and KW_4. Therefore, somewhere in between these objects in mass is the minimum sized asteroid where the modified Laplace plane can be used for a spacecraft. This is answered in section 5.3.

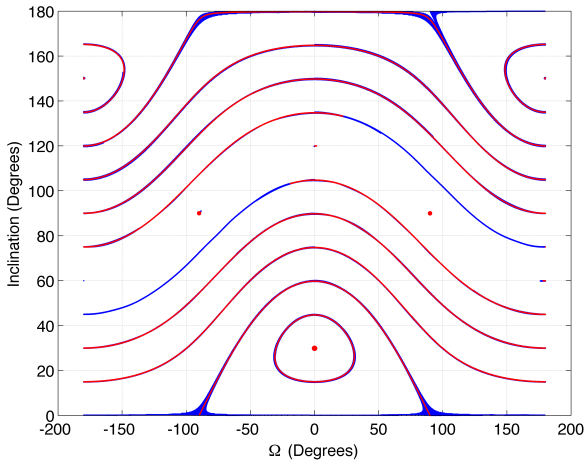

(a) Bennu: $b = 0$ kg/m^2

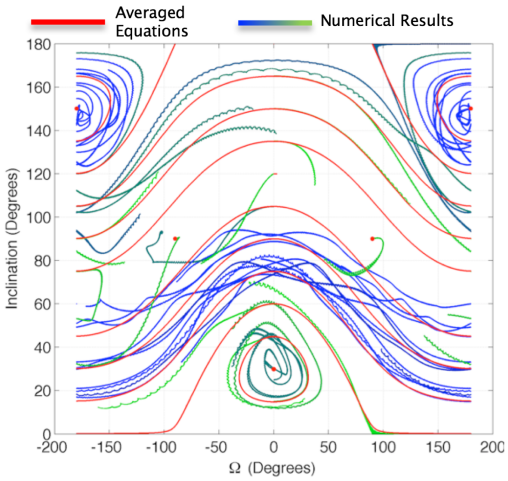

(b) Bennu: $b = 1000$ kg/m^2

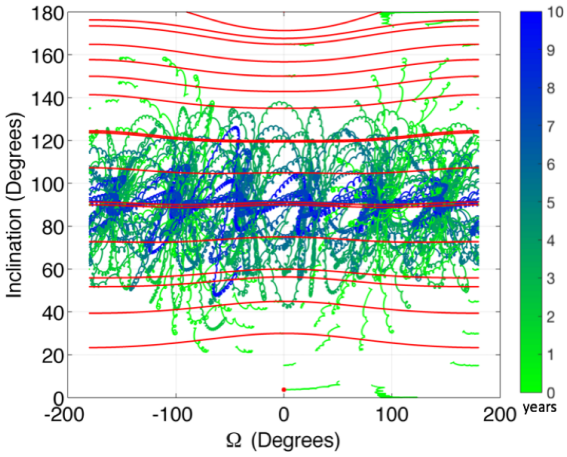

(c) Bennu: $b = 100$ kg/m^2

Figure 5.5: These three figures show the numerical results in blue to green and the averaged motion in red. The trajectories go from green to blue, depending how long the trajectory exists without escape or collision. The colormap on the right gives the time in years that corresponds to a given color. Each plot was evaluated at Bennu at $\epsilon = 30°$ and $a = 0.337 r_L \approx 3$ km. These figures are in the asteroid orbit frame so the equilibria for the Laplace plane is defined by $i = \epsilon - \phi$.

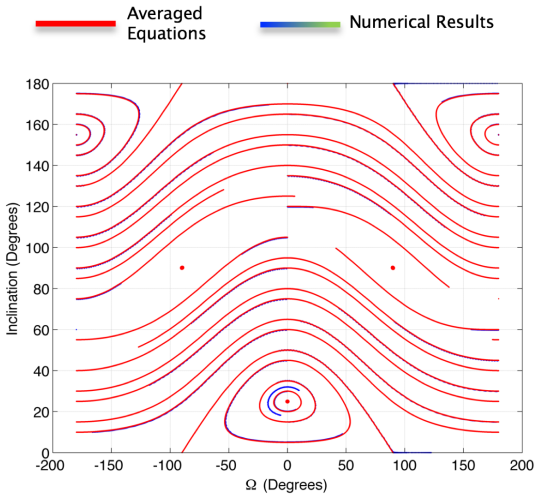

(a) Vesta: $b = 100$ kg/m^2

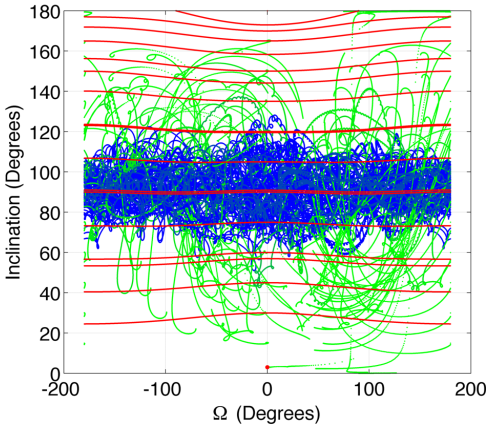

(b) KW$_4$: $b = 100$ kg/m^2

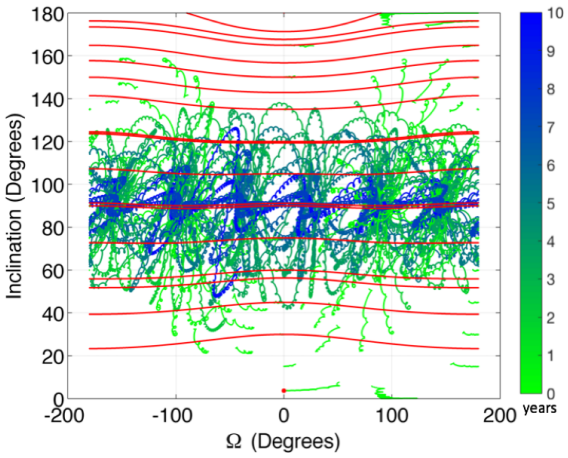

(c) Bennu: $b = 100$ kg/m^2

Figure 5.6: Comparison of a satellite with mass-to-area ratio of 100 kg/m^2 at each asteroid. Each plot was evaluated at the asteroid at $\epsilon = 30°$ and $a = 0.337 r_L$. These figures are in the asteroid orbit frame so the equilibria for the Laplace plane is defined by $i = \epsilon - \phi$.

The second biggest takeaway from this research is that the obliquity of the asteroid changes the precession of an orbit significantly. Ifthe same rigorous initial condition model as in Chapter 4 was implemented, how would the obliquity affect the overall natural or artificial satellite stability for the whole parameter space around a given asteroid.

Finally, it was clear from this study and the previous chapter, to have an artificial satellite at an asteroid like Bennu, the best orbit for stability is a terminator plane orbit or a Sun-synchronous orbit. The data from Chapter 4 overlaps with the mass-to-area ratios of artificial satellites. Although a 1000 year stability isn't required for spacecraft mission design, this subset of data in the next section is discussed to better understand the parameter space where artificial satellites can be stable around Bennu.

5.2 Artificial Satellites at Bennu

This section looks at the subset of data from Chapter 4 that applies to artificial satellites. Typically, spacecraft that are for exploring small bodies have a mass-to-area ratio of approximately $\sim$40 kg/m^2 [29]. This is equivalent to a 3 cm in diameter for a natural satellite discussed in Chapter 4. Also, many CubeSat projects have been looking at exploring small bodies. CubeSats have a mass-to-area ratio of about 100 kg/m^2. Therefore, any of the data with mass-to-area ratios less than 100 kg/m^2 are also useful for understanding long-term spacecraft stability. For comparison, a natural satellite with a mass-to-area ratio of 100 kg/m^2 in this study is less than 10 cm in diameter. Although spacecraft will not need to exist in orbit around an asteroid for 1000 years, an orbit that is stable for 1000 years to multiple perturbations will be a safe choice for a science mission or as a long-term parking orbit.

For spacecraft with mass-to-area ratios less than 100 kg/m^2, all unstable orbits are $<$4 km. The range of inclinations available is from 36° to 144° with most, 73%, reaching a maximum eccentricity above 0.5. The results can be examined closer in Fig. 5.7, where every stable orbit is shown in a histogram providing information on maximum eccentricity

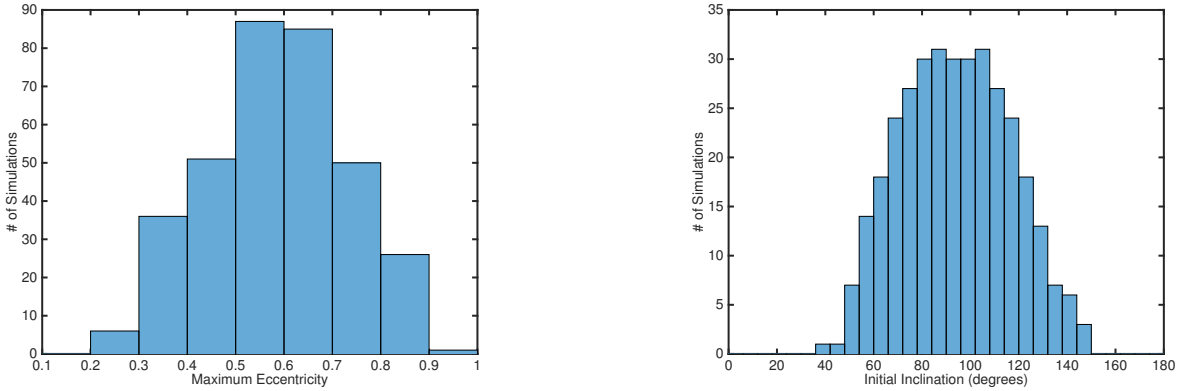

Figure 5.7: $\frac{m}{A} < 100\ kg/m^2$

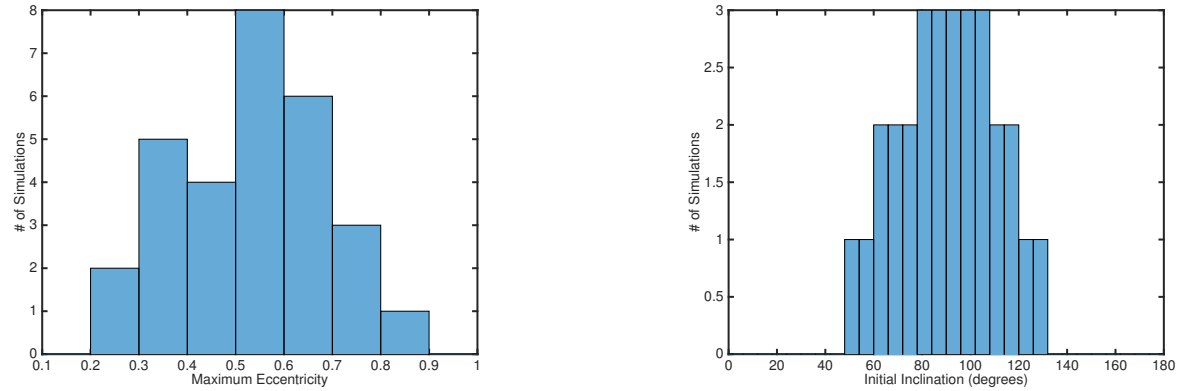

Figure 5.8: $\frac{m}{A} = 40\ kg/m^2$

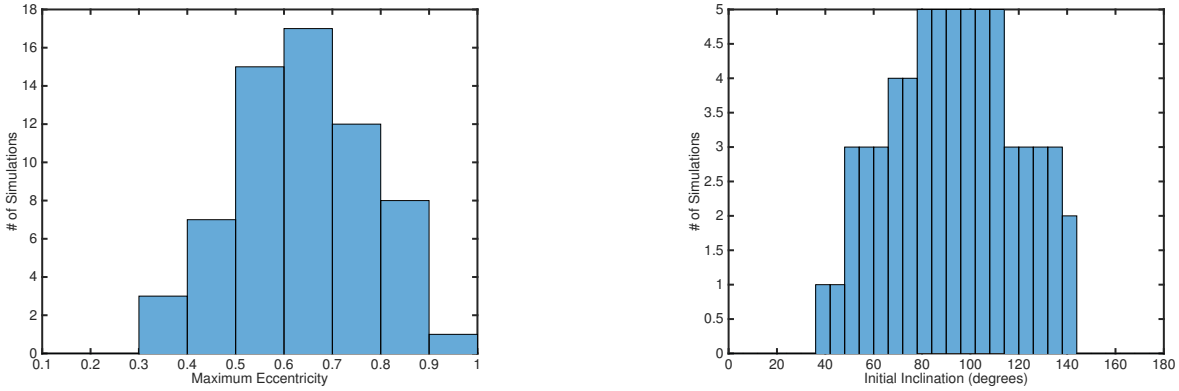

Figure 5.9: $\frac{m}{A} = 100\ kg/m^2$

and inclination. Also in Fig. 5.8 and 5.9, the results for mass-to-area ratios for both a $\frac{m}{A} = 40\ kg/m^2$ spacecraft and $\frac{m}{A} = 100\ kg/m^2$ CubeSat are given. The main difference between these two mass-to-area ratios is that the CubeSat can orbit in a 4 km orbit and a wider range of inclinations for 1000 years,while the spacecraft can only orbit at 2-3 km.

Finally in Figure 5.10 there is a summary of the lowest mass-to-area ratios capable of being stable for 1000 years at each initial inclination and semi-major axis. OSIRIS-REx has a mass-to-area ratio of ~ 63 kg/m^2 and therefore can maintain stability for 1000 years if it's semi-major axis is 1-4 km and has an inclination between $48° - 138°$. However, the Sun-synchronous orbits with an inclination off the terminator plane are not the best options for spacecraft missions. These orbits precess in inclination around the terminator plane, therefore they may be stable to impact/escape, but their inclination can vary by $\sim 30°$ or more. Also, the eccentricity of these orbits can become quite high with a maximum eccentricity of 0.8 and an average eccentricity around ~ 0.4. Therefore it is still in the best interest of spacecraft to stay in an inclination as close to the terminator plane, $i = 90°$, to avoid large precession in inclination. Over the 1000 year period, even the terminator plane orbit will result in a maximum eccentricity of ~ 0.5 and an average eccentricity of ~ 0.2 over the entire simulation. Obviously, these large changes that occur over 1000 years aren't directly applicable to a spacecraft that can do station keeping to maintain this orbit over months, but it still shows that the terminator plane is the most stable option with the least long term growth in eccentricity.

5.3 Artifical Satellite Stability in the Laplace Plane

At the beginning of this chapter, it was investigated whether the modified Laplace plane was an option as an orbit for spacecraft. The asteroids used for the simulation include KW_4, Bennu and Vesta. Both Bennu and KW_4 were not particularly good candidates for the modified Laplace plane, while a spacecraft at Vesta was able to maintain a stable orbit in the MLP. However, the difference in these bodies gravitational parameter is 8-10 orders of

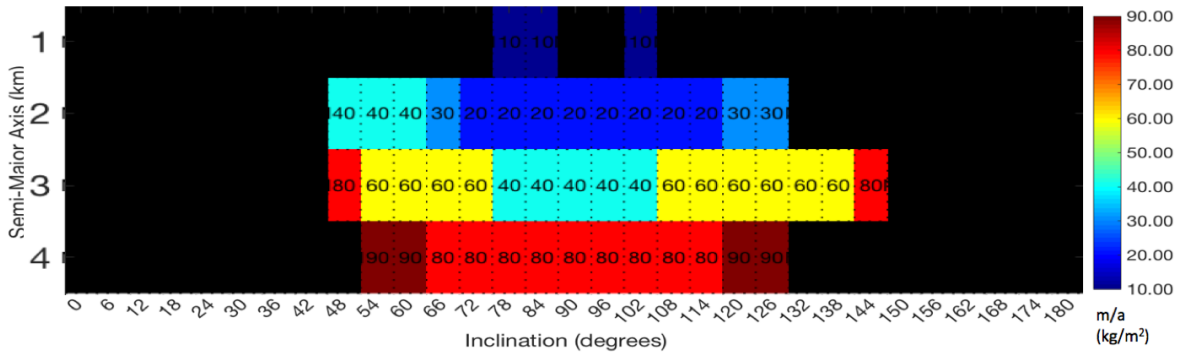

Figure 5.10: The lowest mass-to-area ratio stable in a given orbit for 1000 years for a range of mass-to-area ratios below 100 kg/m^2.

magnitude. Therefore, this section looks into the minimum gravitational parameter necessary for a stable MLP to exist. The model includes J_2, third-body perturbations from the Sun, and SRP. The spacecraft has a mass-to-area of 40 kg/m^2, which is similar to the mass-to-area ratio of NEAR Shoemaker [29]. The asteroid will be orbiting at 1 AU and will have a $J_2 = 0.02798$. The gravitational parameter will vary by increasing its order of magnitude until a MLP that will be stable for 1000 years is found. No spacecraft requires being in orbit for 1000 years, but orbits stable on the order of decades often just did not impact or escape the asteroid yet and were not on the MLP at all. Different obliquities will be observed for the asteroid from $25° - 85°$ in increments of $20°$. The initial conditions of the orbit will be on the modified Laplace plane along with orbits incrementally displaced from the modified Laplace plane by inclination differences of $1°$, $5°$, and $10°$. Also , semi-major axes along the Laplace surface of 0.25 r_L to 1.5 r_L in increments of 0.25 r_L is evaluated.

It was found that for a prograde modified Laplace plane, the minimum gravitational parameter needed is $\mu_a = 10^5$ m^3/kg s^2. This gravitational parameter was stable for the obliquities of $25°$, $45°$ and $65°$ for a semi-major axis of $0.25r_L$. An example of the Laplace plane is in a prograde orbit at $\epsilon = 25°$ is shown in Figure 5.11. An asteroid with $\mu_a = 10^5$ m^3/kg s^2 can have an orbital diameter between ~9.4-12.4 km depending on the density of the

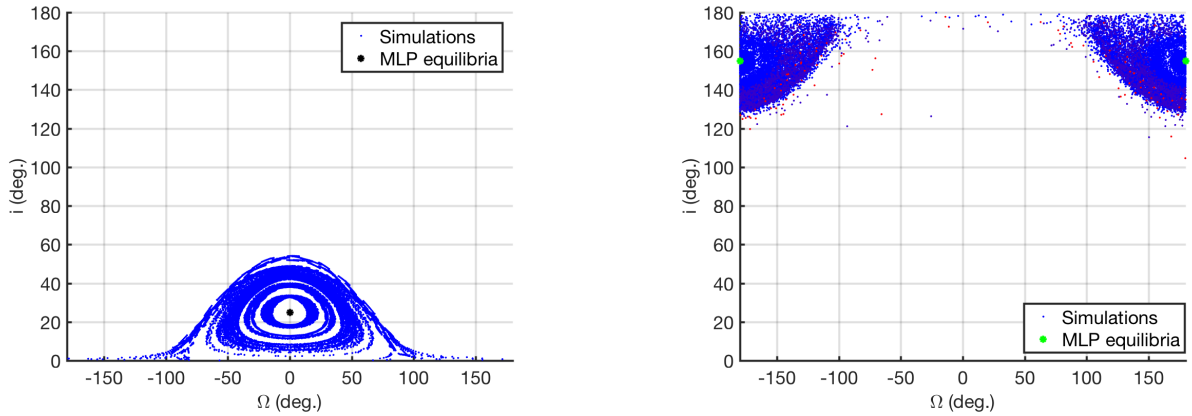

Figure 5.11: Prograde (left) and retrograde (right) modified Laplace plane equilibria. The prograde MLP orbit is for $\mu_a = 100,000$ m^3/kg s^2 at an obliquity of 25° and $a = 0.25r_L$. The retrograde MLP orbit is for $\mu_a = 10,000$ m^3/kg s^2 at an obliquity of 25° and $a = 0.25r_L$.

asteroid. It is assumed a range of densities between 1.2 g/cm^3 to 3.4 g/cm^3, or a rubble pile to a metallic body. The stable orbit would be approximately 25.7 km away. For an obliquity of 85° or semi-major axes greater than $0.25r_L$, the minimum gravitational parameter needs to be $\mu_a = 10^6$ m^3/kg s^2. This would be double the radius of an asteroid with $\mu_a = 10^5$ m^3/kg s^2. An asteroid with $R_a =\sim 5$ km is huge for a near-Earth asteroid. There are NEA with diameters this big, but many of them resemble an ellipsoid as opposed to an oblate spheroid. The modified Laplace plane only takes J_2 into account so that the MLP may be unstable for these tri-axial ellipsoids. Even still, these asteroids are quite rare in the NEA population with only maybe ∼12 asteroids in the NEA population with diameters over 5 km [100]. However, the retrograde modified Laplace plane is stable for asteroids an order of magnitude less in the gravitational parameter at a semi-major axis of $0.25r_L$ ($\sim 16.2km$). This gives an orbital radius of 4.3-6.2 km, which is still very large for NEA.

The MLP may be stable for the main-belt asteroid population which holds more large asteroids and because of their distance from the Sun, also are subjected to smaller perturbations from SRP. Assuming the asteroid had an orbit of 3 AU, the retrograde and prograde MLP was stable at $0.25r_L$ ($\sim$ 10.2 km) for an asteroid with an obliquity of 25° and 45° for

$\mu_a = 1000$ m^3/kg s^2. This is equivalent to an asteroid that is between 2-2.8 km. However, this gravitational parameter is very constrained in spacecraft orbit radius and the obliquity of the asteroid. For the main-belt, there are many asteroids with μ_a that is on the order of $\mu_a = 10^4 - 10^6$ m^3/kg s^2, where the modified Laplace plane would be stable for all obliquities and a larger range of orbital radii for options the spacecraft.

5.4 Natural Satellites around Asteroids of Various Obliquities

In this section,a few different obliquity angles for an asteroid the size of Bennu is observed and determine how the obliquity will change the overall stability of natural satellites orbiting the asteroid. The focus of this research is solely on the existence of stable orbits for a natural satellite and purposefully places how the natural satellite migrated to this orbit outside the bounds of this study. Numerical simulations modeling J_2, third body dynamics, and solar radiation pressure is used on a broad set of initial conditions that vary in semi-major axis, inclination, longitude of the ascending node and natural satellite diameter. To be considered stable, it is required that a set of initial conditions to remain in orbit for greater than 1000 years. Instability is defined as an escape from the asteroid or impact. By constructing and executing an array of detailed simulations modeling the evolution of natural satellite orbits over thousand-year timescales, the possible sizes, distances from Bennu, and orbital orientations of long-term stable orbits is assessed. In Chapter 4 it was found that three orbital phenomena that dictated the stability of natural satellites from a centimeter in diameter to 7.5 m in diameter [101].

In the previous chapter, it was discussed three different orbital phenomena that would cause the natural satellites to be stable or unstable. These were the modified Laplace plane, Kozai resonance, and Sun-synchronous orbits. In this section, each of these orbital phenomena but at varying obliquities is revisited. If there are changes in how the orbital events affect the orbit stability for different obliquities, then this knowledge can be applied to future spacecraft missions.

A summary of the results from Chapter 4 can be seen in Figure 4.3. This figure represents the results for all simulations with varying semi-major axis, inclination, longitude of the ascending node, and natural satellite diameter at Bennu with its true obliquity. The graph shows the minimum natural satellite diameter that is stable for 1000 years at each semi-major axis and inclination. Larger diameter objects may exist at the same semi-major axis and inclination. Therefore the minimum natural satellite diameter gives the minimum diameter not impacted by SRP. Notice that inclinations between 36° and 144° at semi-major axes between 1 and 13 km have significantly smaller diameter natural satellites than the rest of the simulations. These smaller objects are stable due to Sun-Synchronous orbits. If natural satellites that are a stable due to Sun-synchronous orbits are taken away from Figure 4.3, there are no stable orbits for objects with inclinations between 78° and 108° for radial distances greater than 4 km. This can be viewed in Figure 4.7. This instability region is due to the Kozai resonance where higher inclinations correspond to growth in eccentricity that is large enough to cause escape or an impact with Bennu.

The results discussed above and summarized with Figure 4.3, are for a particular asteroid, Bennu. How natural satellite stability changes when an asteroid with different parameters is evaluated. How the obliquity of the asteroid will affect the natural satellite stability is examined. Therefore all parameters are kept the same as in previous work, but with an asteroid precisely the same as Bennu with obliquities of 0°, 45°, 90° and 135°.

5.5 Various Obliquities Summary

The summary of results for various sized natural satellites with different initial conditions: semi-major axis, longitude of the ascending node, and inclination for various obliquities is shown in Figures 5.12-5.15. The first basic observation is that the low obliquity asteroids 0° and 176° both have stable orbits out to 25-29 km, while the high obliquity asteroids have nothing stable after 20 km. This would make visiting an asteroid with high obliquity beneficial because the stable region for all natural satellites is significantly reduced. Also, it

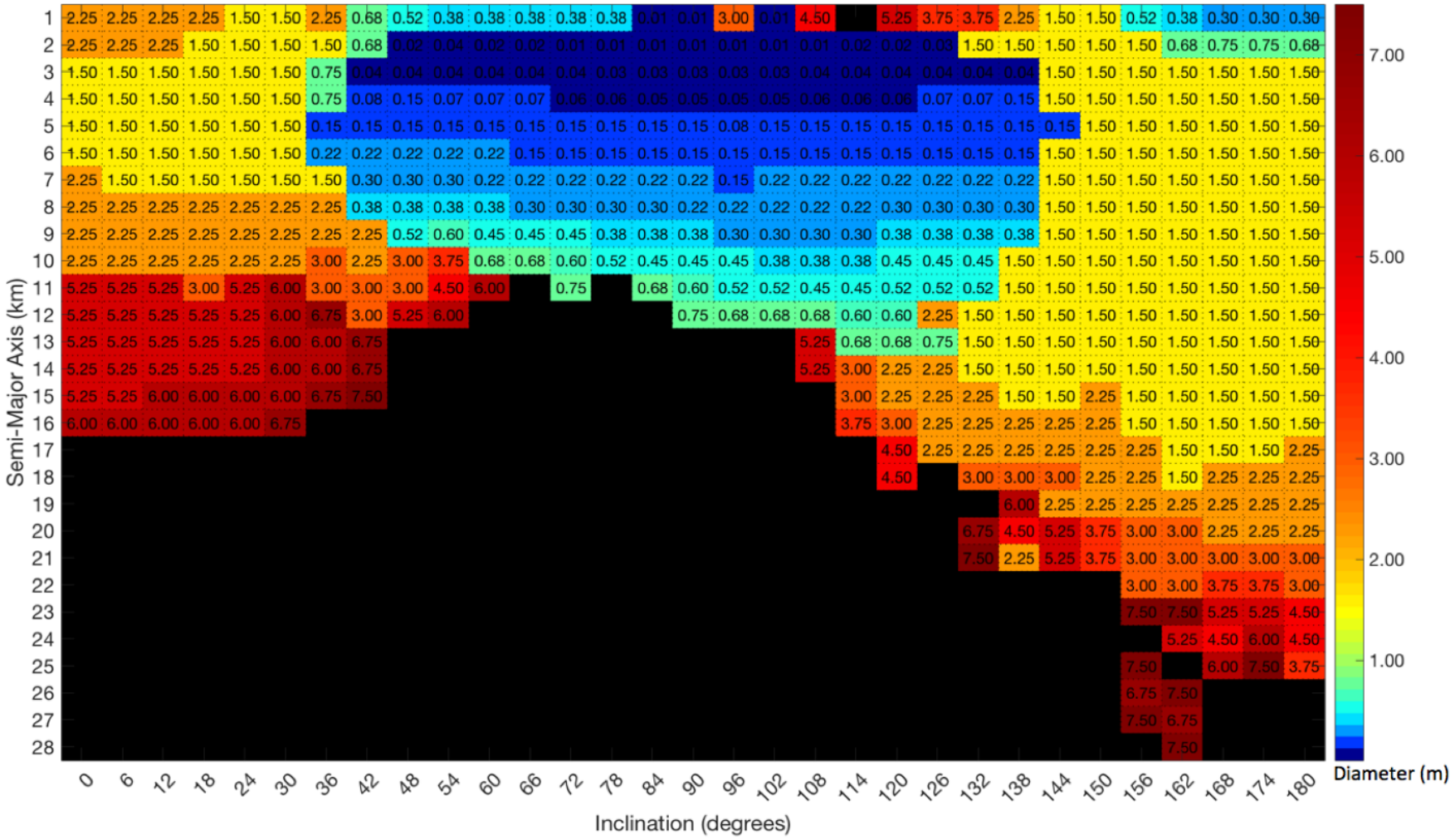

Figure 5.12: This figure summarizes the overall results of the simulations for an asteroid with obliquity of 0°. For each semi-major axis and inclination simulated, the minimum natural satellite diameter is determined and shown with a corresponding color, where blue is the smallest diameter to red being the largest. Larger diameter objects may exist at the same semi-major axis and inclination.

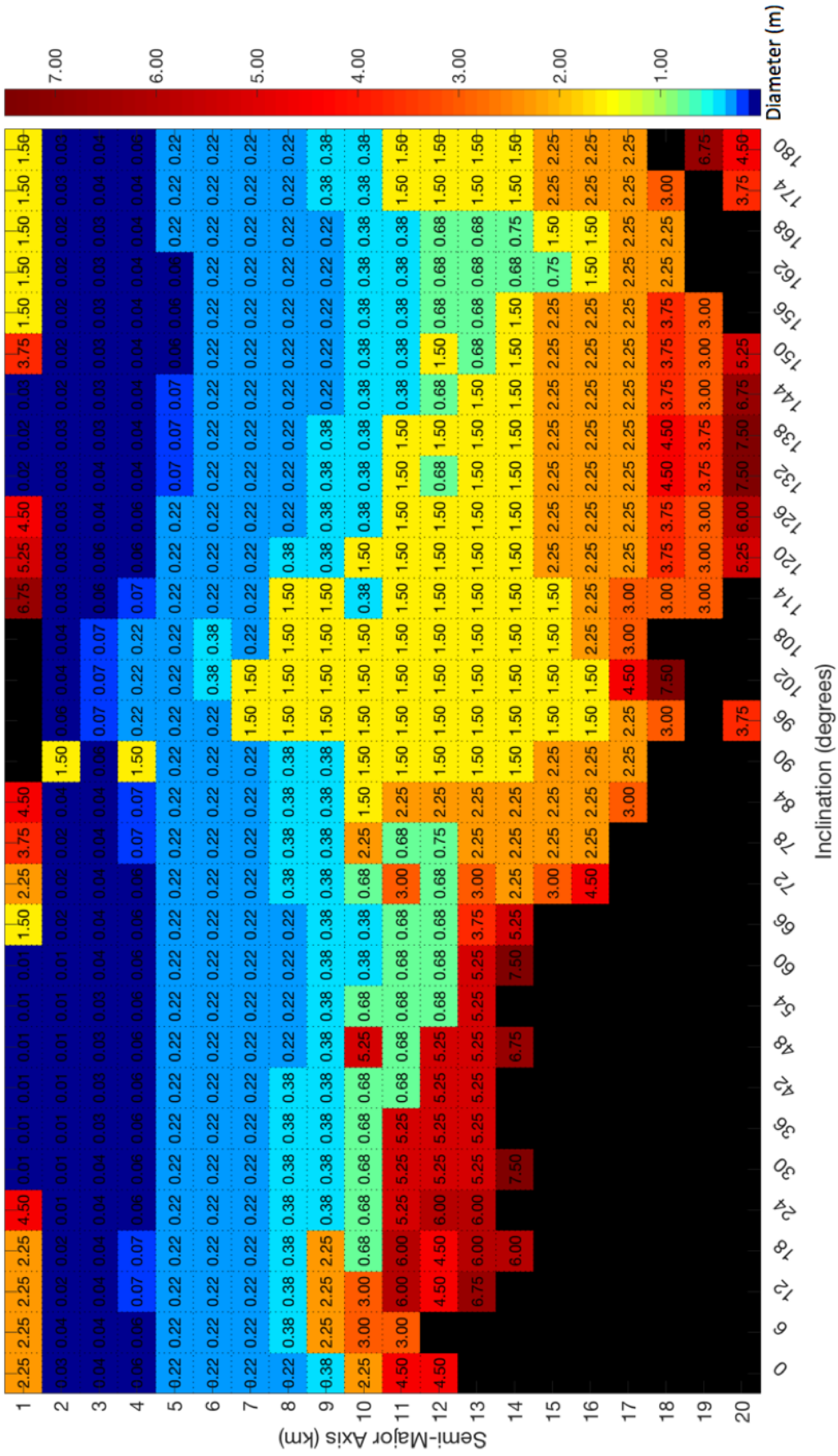

Figure 5.13: This figure summarizes the overall results of the simulations for an asteroid with obliquity of 45°. For each semi-major axis and inclination simulated, the minimum natural satellite diameter is determined and shown with a corresponding color, where blue is the smallest diameter to red being the largest. Larger diameter objects may exist at the same semi-major axis and inclination.

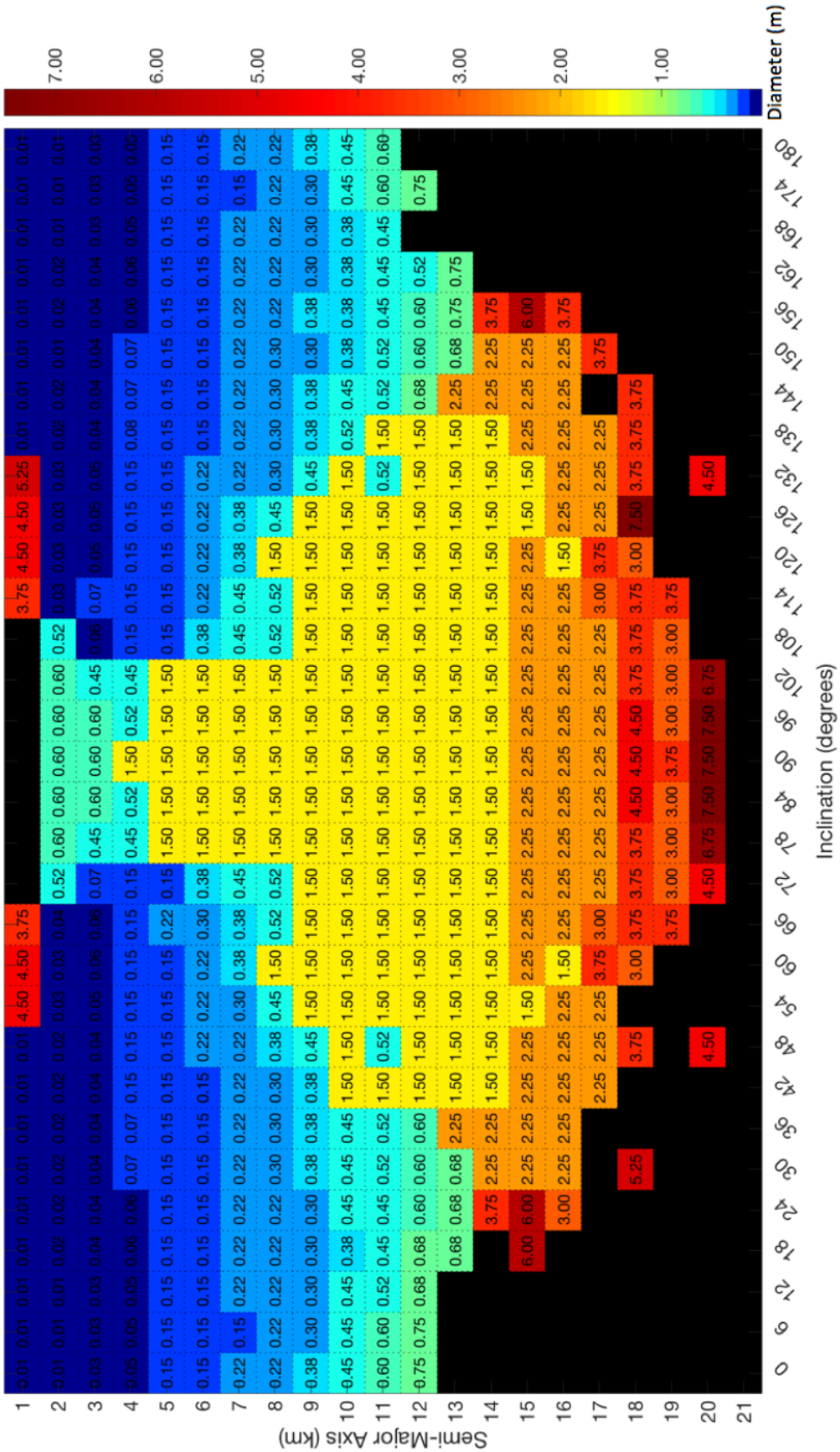

Figure 5.14: This figure summarizes the overall results of the simulations for an asteroid with obliquity of 90°. For each semi-major axis and inclination simulated, the minimum natural satellite diameter is determined and shown with a corresponding color, where blue is the smallest diameter to red being the largest. Larger diameter objects may exist at the same semi-major axis and inclination.

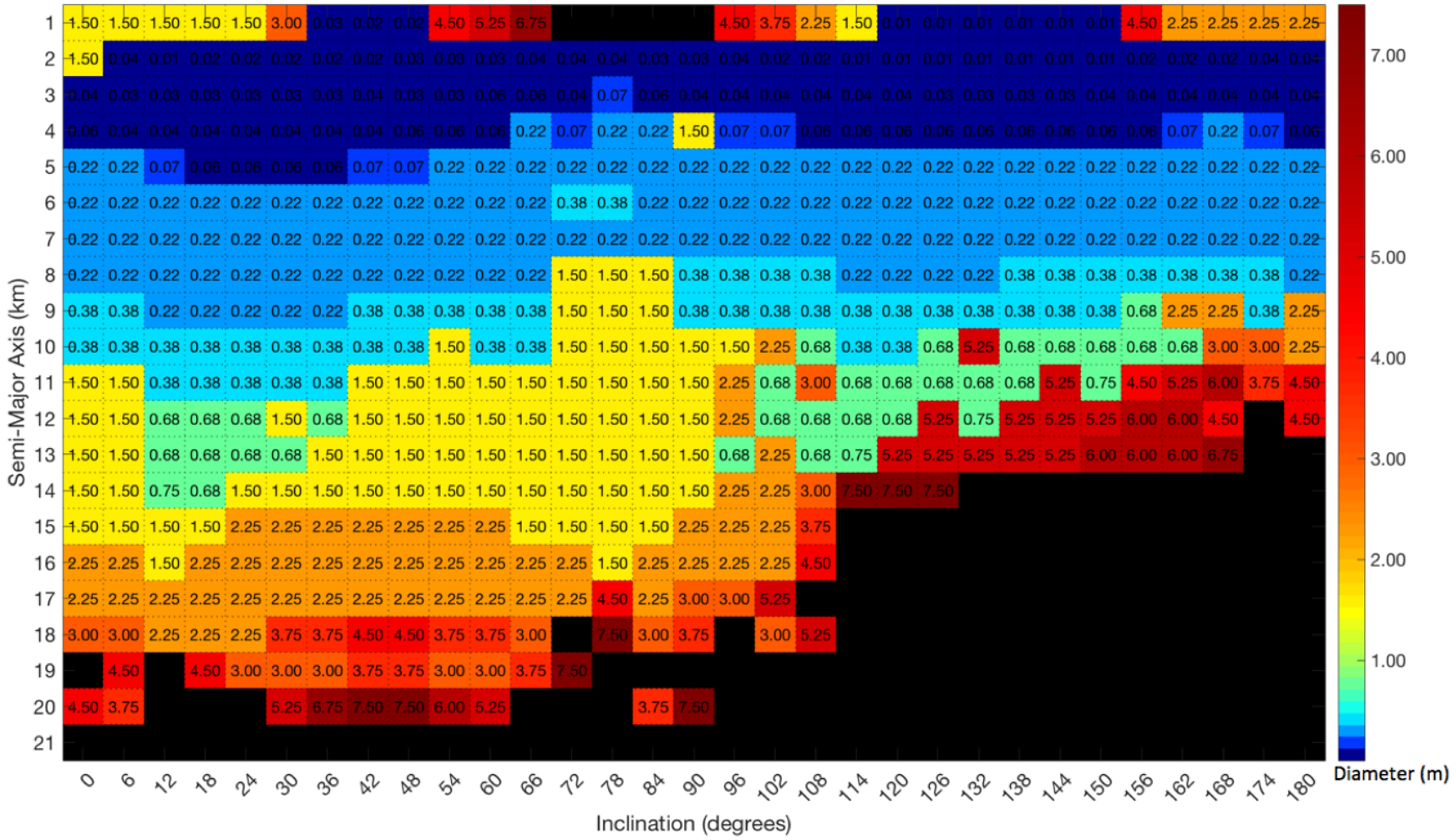

Figure 5.15: This figure summarizes the overall results of the simulations for an asteroid with obliquity of 135°. For each semi-major axis and inclination simulated, the minimum natural satellite diameter is determined and shown with a corresponding color, where blue is the smallest diameter to red being the largest. Larger diameter objects may exist at the same semi-major axis and inclination.

appears the orbit that rotates in the opposite direction of the asteroid's spin will be stable at higher orbital radii. So a prograde obliquity will have more possible orbital radii stable for retrograde natural satellites, while a retrograde obliquity will yield more possible orbital radii stable for prograde natural satellites.

5.5.1 Sun-Synchronous Orbits

The first comparison between the varying obliquities is the difference in their Sun-Synchronous orbits. The Sun-synchronous orbits are easy to determine in the figures because they are most objects with a diameter less than 1 meter. It is also further verified that these are Sun-Synchronous orbits by observing the change in longitude of the ascending node in the Sun-rotating frame. Sun-synchronous orbits precess in the inertial frame but will remain bound to $\Omega_R = 0°$ or $\Omega_R = 180°$ in the Sun-Bennu rotating frame. For the original, $\epsilon = 176°$, Sun-Synchronous orbits exist, for inclinations between 36° and 144° at semi-major axis between 1 and 13 km. For $\epsilon = 45°$, Sun Synchronous orbits exist for a semi-major axis between 1 and 15 km but exist for all inclinations. Finally, for $\epsilon = 135°$, the Sun-Synchronous orbits exist for all inclinations as well. Both low obliquity asteroids, 0° and 176°, have Sun-synchronous orbits only at a range of 36° and 144°, while the 90° case has no Sun-synchronous orbits from 72° and 102°. Therefore it seems that Sun-synchronous orbits are stable for all inclinations unless the asteroid has an obliquity parallel, anti-parallel, or perpendicular to the orbit pole. Being parallel results in no equatorial Sun-synchronous orbits, while being perpendicular to the orbit results in no stable terminator plane orbits. All of these results were validated by observing the orbits of the asteroid centered orbit rotating-frame to see if the precession of the longitude of the ascending node was fixed.

5.5.2 Modified Laplace Plane

In Figure 5.16a, many initial conditions are shown for an asteroid with $\epsilon = 176°$, and a natural satellite that is 3.75 m in diameter with a semi-major axis of 2 km. Each data point

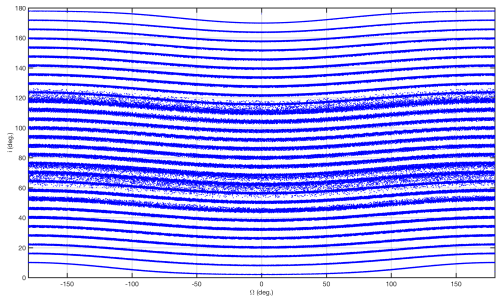

(a) $\epsilon = 0°$

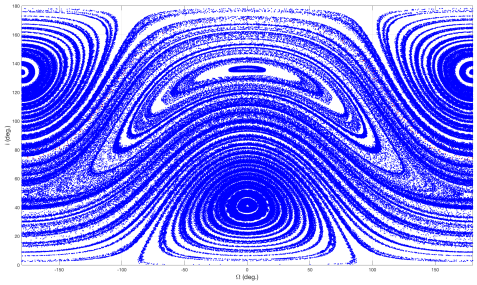

(b) $\epsilon = 45°$

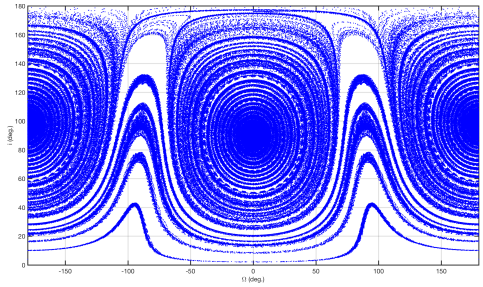

(c) $\epsilon = 90°$

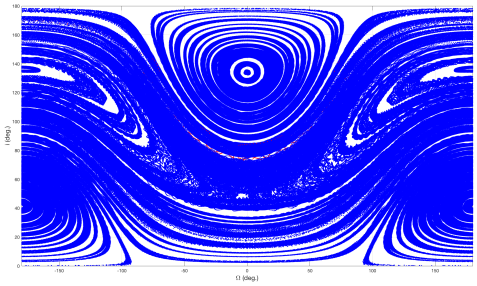

(d) $\epsilon = 135°$

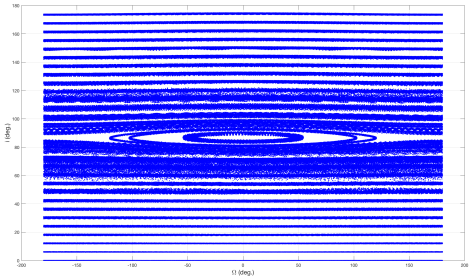

(e) $\epsilon = 176°$

Figure 5.16: Inclination vs. longitude of the ascending node for $a = 2\ km,\ D = 3.75\ m$ for 1000 years. The higher obliquity asteroids, have the motion of the natural satellite orbits oscillating around the Laplace plane, and therefore their longitude of the ascending node is bounded. Figure (a), has a small retrograde obliquity, therefore the longitude of the ascending node is not bounded to the Laplace plane.

represents an inclination and a longitude of ascending node at a specific time in any given orbit. The sum of all the data yield information on which orbital regions are stable/unstable or if longitude of periapsis precesses 360° or less. Figure 5.16 have the inclination and longitude of the ascending node defined from the equator of the asteroid. In Figure 5.16a, there is one equilibrium at $\Omega = 0°$ and $i = 90°$, there are some orbits that will oscillate around the equilibrium, but most precess a full $\Omega = 360°$. At an obliquity of 0° there are three Lapalce equilibria, however if the initial condition isn't directly on the Laplace plane, the orbit will precess 360 °. Figure 5.16b-c with $\epsilon = 45°$ and $\epsilon = 135°$ respectively have three modified Laplace equilibria, where the majority of possible orbits will oscillate around one of these three equilibria. The only difference between $\epsilon = 45°$ and $\epsilon = 135°$ is that the equilibria at a given inclination will shift the longitude of the ascending node 180°. At $\epsilon = 90°$, more initial conditions will precess around the Laplace plane compared to the other obliquities. It appears that higher obliquity asteroids will have natural satellites larger than 1 m diameter mostly oscillating around the modified Laplace plane, and therefore will be bounded in the longitude of the ascending node, while the same asteroid at low obliquities will precess 360°.

5.5.3 Kozai Resonance

If the Sun-synchronous stable orbits are taken away from the summary plots of the stability, the instability due to the Kozai resonance can be observed. The Kozai resonance can cause instability around the natural satellite. Because of the exchange between inclination and eccentricity, some inclinations are large enough that the maximum eccentricity capable of impact or collision will be reached at some point in the orbit. In chapter 4, it is discussed that the Kozai resonance and how it caused instability for high inclination orbits from $78° - 102°$. Also investigated is if this resonance causes instability for the other obliquities. For the intermediate obliquities,45° and 135°, the Kozai resonance does not cause any instability as can be seen in Figure 5.17. The Kozai resonance was originally modeled with averaged

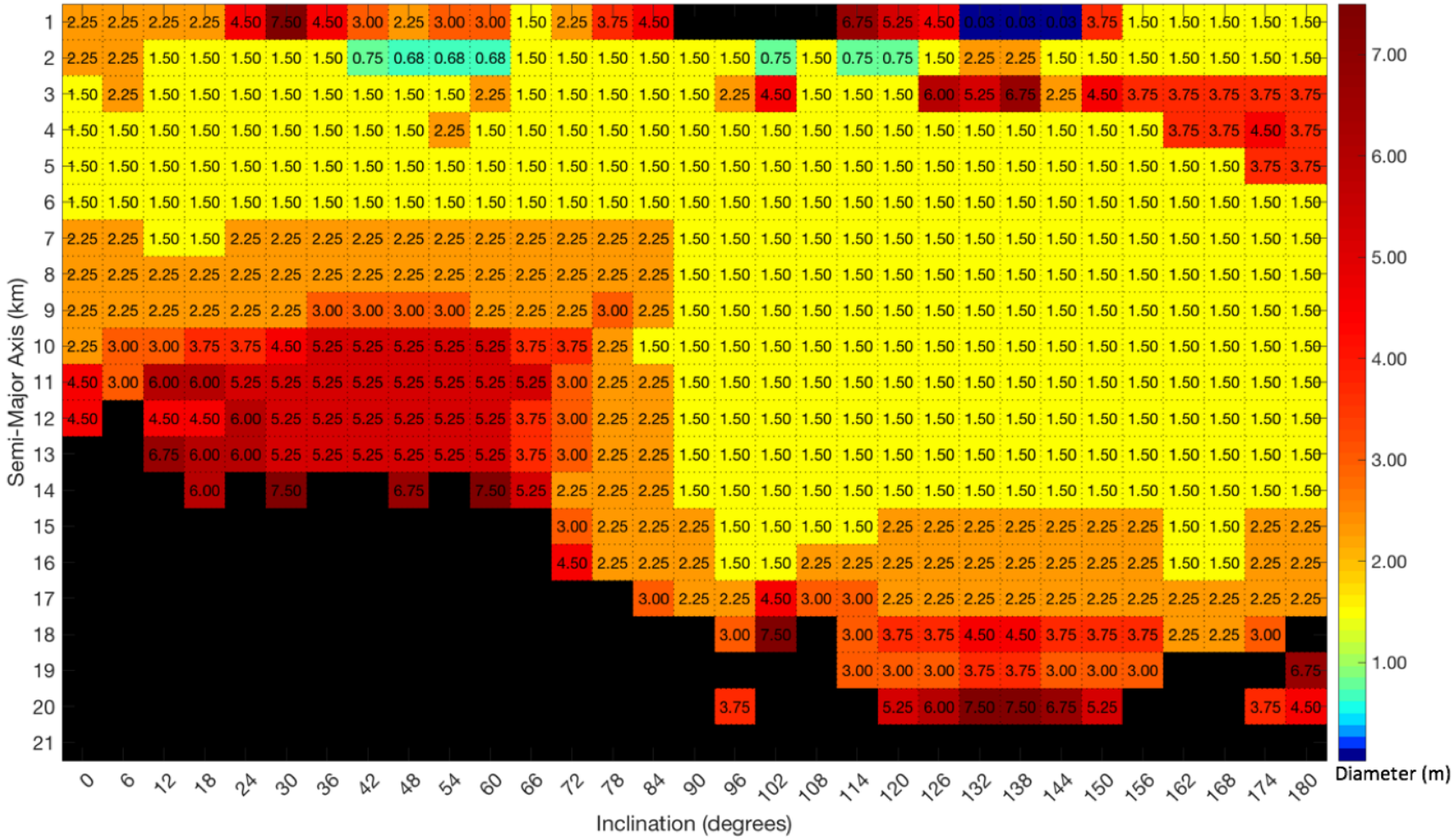

Figure 5.17: This figure summarizes the overall results without Sun-synchronous orbits for an asteroid with obliquity of 45°. For each semi-major axis and inclination simulated, the minimum natural satellite diameter is determined and shown with a corresponding color, where blue is the smallest diameter to red being the largest. Larger diameter objects may exist at the same semi-major axis and inclination.

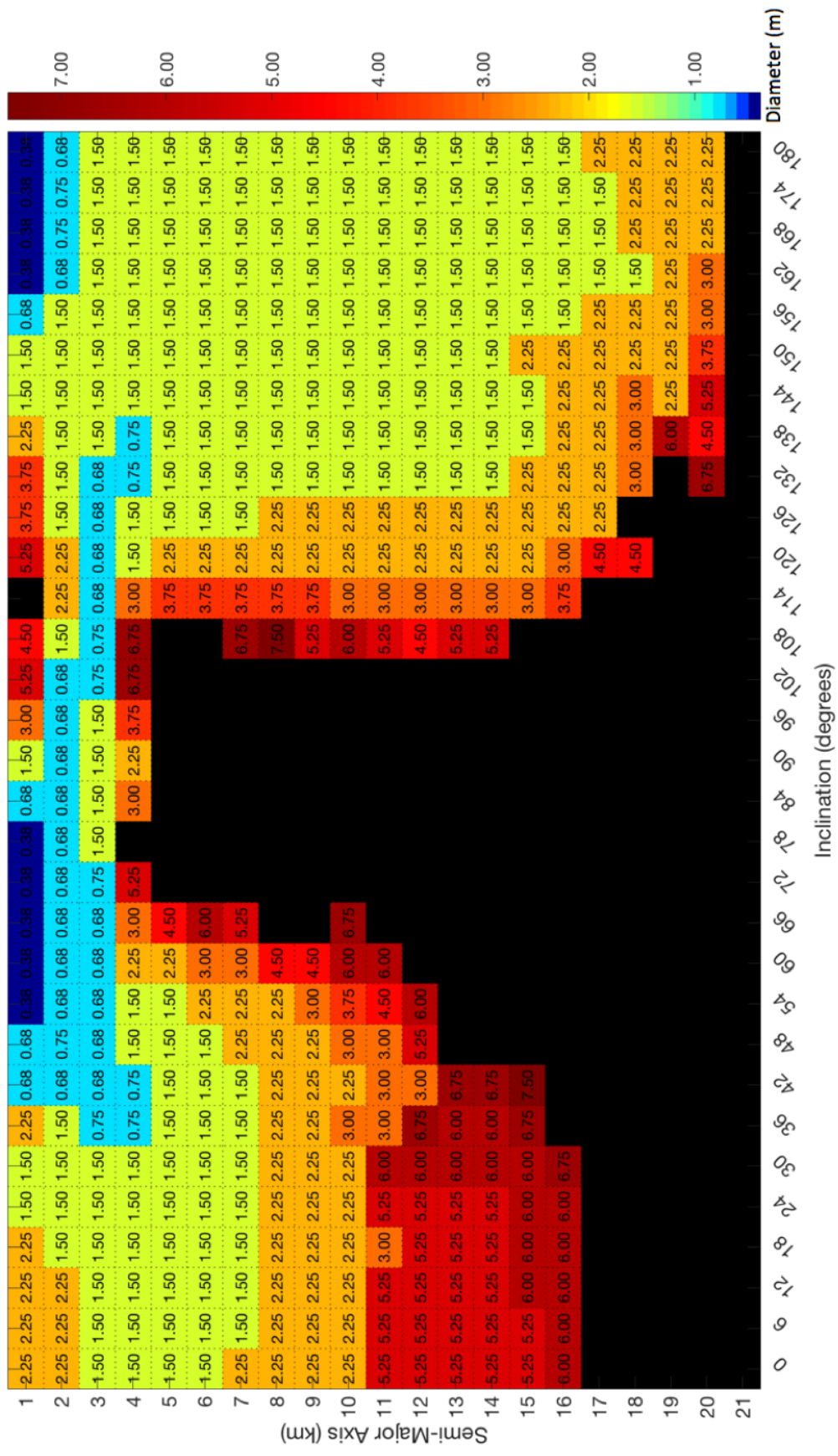

Figure 5.18: This figure summarizes the overall results without Sun-synchronous orbits for an asteroid with obliquity of 0°. For each semi-major axis and inclination simulated, the minimum natural satellite diameter is determined and shown with a corresponding color, where blue is the smallest diameter to red being the largest. Larger diameter objects may exist at the same semi-major axis and inclination.

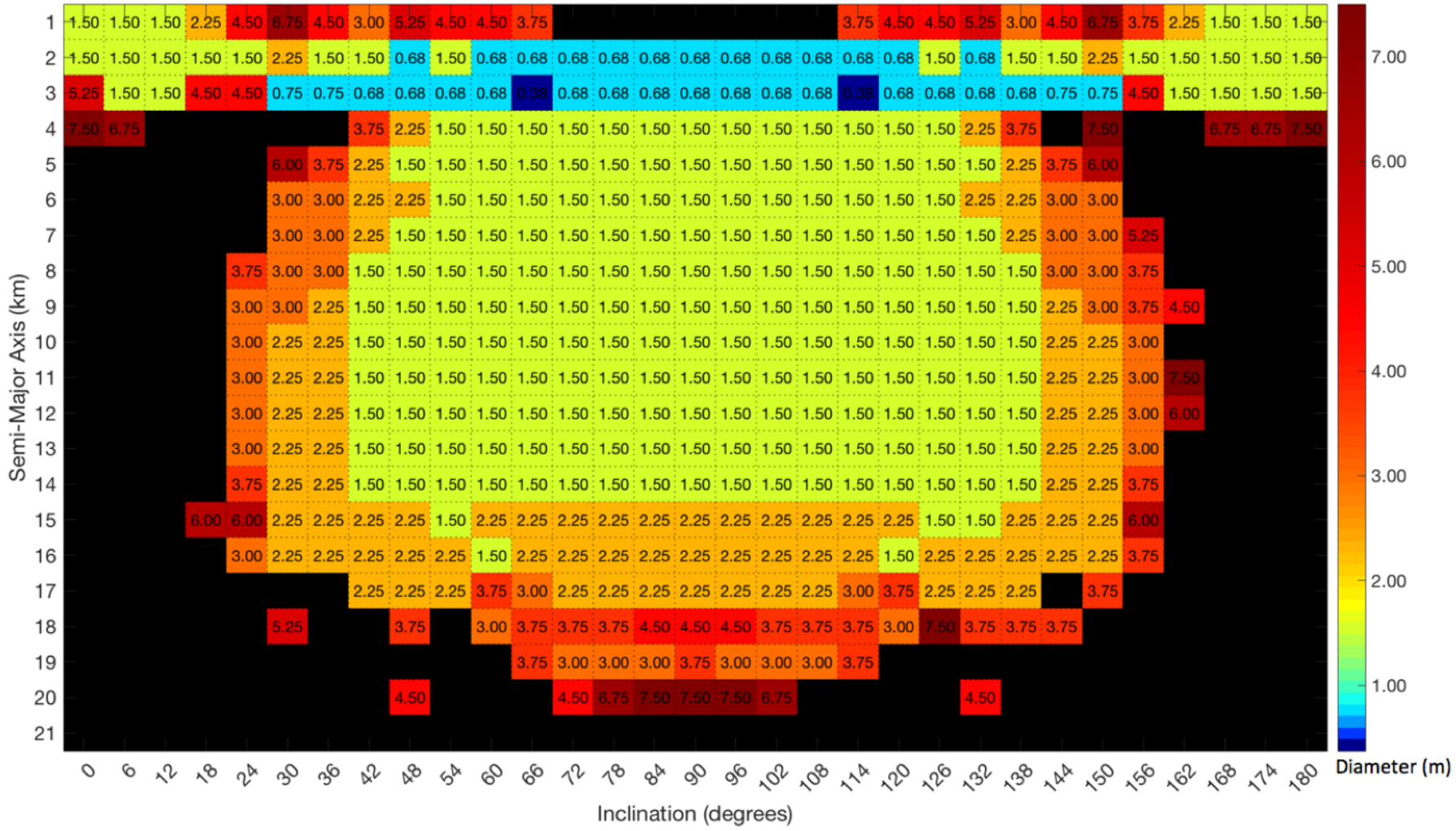

Figure 5.19: This figure summarizes the overall results without Sun-synchronous orbits for an asteroid with obliquity of 0°. For each semi-major axis and inclination simulated, the minimum natural satellite diameter is determined and shown with a corresponding color, where blue is the smallest diameter to red being the largest. Larger diameter objects may exist at the same semi-major axis and inclination.

equations with third body perturbations only. Perhaps adding the perturbations of an oblate spheroid at some given obliquity will disrupt the Kozai resonance.

Bennu has an expected obliquity that is very near equatorial. This obliquity had the Kozai resonance present according to the simulations. The same is the case for no obliquity, $\epsilon = 0°$, as seen in Figure 5.18. It appears the Kozai resonance here creates instability for the identical high inclination orbits as was observed with the $\epsilon = 176°$ case. The interesting result is when the obliquity is 90°, which can be viewed in Figure 5.19. The Kozai resonance seems to have cause instability to orbits that are very near the equator of the orbit. At first, this seems counterintuitive because the Kozai resonance affects high inclination orbits. However, the results shown in Figure 5.19 are in the asteroid-centered equatorial frame. Since the obliquity of the asteroid is 90°, an equatorial orbit is technically a 90° orbit in the asteroid-centered orbit-frame. Since the Kozai resonance is only affected by third-body perturbations, the high inclination is relative to the orbit-frame, not the equator. Therefore it seems the Kozai resonance just causes instability to the satellite at high inclinations if the asteroid is very close to having no obliquity or the rotation pole is perpendicular to the orbit pole.

5.6 Conclusion

By varying the obliquity of the asteroid, there are several differences between where natural satellites will be stable and what orbital phenomena are causing stability or instability. The conclusions of these simulations are:

- Sun-synchronous orbits yield stable orbits for natural satellites less than 1 m in diameter for all asteroid obliquities. Also, $\epsilon = 176°$, $\epsilon = 90°$, and $\epsilon = 0°$ had Sun-synchronous orbits only for a range of inclinations, while $\epsilon = 45°$ and $\epsilon = 135°$ have Sun-synchronous orbits for all inclinations.

- The high oblquity cases, $\epsilon = 45°$ and$\epsilon = 90°$, $\epsilon = 135°$, have natural satellites greater

than 1 meter oscillating around the Laplace plane, while the low oblquity case will have the longitude of the ascending node precess 360°.

- Kozai instability region only exists for the $\epsilon = 176°$, $\epsilon = 0°$, and $\epsilon = 90°$ asteroids.

Chapter 6

Binary asteroids in the Laplace Plane

6.1 Introduction

In Chapter 1 a brief history of the non-gravitational forces that can cause secular changes on an asteroid's orbit over an extended period is given. These non-gravitational forces are the main contributors to why the asteroid population is what is observed today. There have been numerous papers published to describe the processes that form binary systems, contact binaries, asteroid pairs, or ternary systems [70, 72, 78, 80, 102]. Cuk and Burns first presented the non-gravitational force, BYORP, in 2005 [68]. This force was an extension of YORP from a single asteroid to a binary system. Thermal reemission causes the YORP effect due to solar radiation pressure "...on irregularly shaped bodies that results in a torque that will cause secular effects to the spin-rate and direction of an asteroid" [56]. YORP is responsible for driving the spin-rate and spin-direction of an asteroid, where it is the sole contributor to increasing centrifugal accelerations on a "rubble pile" to a particular spin rate that causes fission. This spin rate is determined by the largest separation distance between the mass centers of the fissioned component and the main body [77]. YORP is a crucial component of the contact binary cycle as it is responsible for separating the asteroid into a binary system. BYORP is similar to YORP in that it is due to thermal reemission of solar radiation pressure. However, instead of an asymmetrical asteroid, there is a binary system with a spherical central body and an asymmetrical secondary. For the thermal reemission to have any secular effects, the binary needs to be synchronous, or the orbit of the secondary is

equal to the rotation of the primary. This synchronicity will cause the binary to have secular growth or contraction of the semi-major axis and for the eccentricity to be dampened [74].

In this chapter, the non-gravitational force, BYORP, with the classical Laplace plane also discussed in previous chapters are combined. "The classical Laplace plane is the mean reference plane about whose axis the pole of a satellite's orbit precesses." [82]. Suppose there are just two perturbations on a primary body and it's satellite: J_2 of the primary asteroid and third body perturbations from the Sun. Precession of angular momentum of the satellite from J_2 will rotate about the primary body's polar axis, while the precession of angular momentum due to 3^{rd} body perturbations will precess around the primary's orbit pole. If the orbit pole and the primary pole is not aligned, there exists a frozen orbit where the two precession caused by these perturbations will balance each other. This frozen orbit lies along the Laplace surface and is defined by its orbital radius and inclination, or Laplace angle. This frozen orbit will change inclination for a given orbital radii. As the orbit is near the primary body, J_2 is the dominant perturbation, and therefore the inclination will be near the equator. Likewise, as the orbit increases in distances, the 3rd body perturbations will be the dominating perturbation and the inclination will go towards the orbit plane of the primary[82]. The classical Laplace plane has been applied to a multitude of evolutionary theories in planetary science from the formation of planetary rings, natural satellites, and satellites that are formed from circumplanetary disks of gas and dust [82, 83, 88, 103, 104, 105, 106]. Now it will be investigated that the evolution of binary systems through BYORP expanding the binary asteroid along the Laplace plane, and thus changing the secondary's inclination.

The study of the Laplace plane and BYORP yields very standard results of BYORP expanding the secondary along the Laplace plane. However, the Laplace plane for specific orientations of the primary asteroid's obliquity and the secondary's orbital radius will eventually come to an instability region. This instability region will rapidly increase the eccentricity of the orbit till the binary system impacts. The effects of this region may play a

Table 6.1: Asteroid model properties

Parameter	Value
Semi-Major Axis	1 AU
Graviational Parameter	157.035 m^3/s^2
Major Radius	750 m
Minor Radius	670 m

role in the formation of contact binaries and may even create a cycle where the asteroid will go through the YORP process to create a binary system and then BYORP with the Laplace plane to cause the system to become a contact binary again.

6.2 Implementation

The model of the binary system will include solar tides, an oblate spheroid primary, and a constant force BYORP model as presented in Equation 2.49. For more information on the BYORP model and the coefficients used, please refer back to Chapter 2. The binary system modeled uses parameters such as the J_2 coefficient and BYORP coefficients of the observed binary system, 1999 KW_4. However, the obliquity of the primary, mass, and size of the primary and binary will change depending on the simulation. For most simulations, the mass of the primary will reflect that in Table 6.1 unless otherwise noted.

The binary system will be numerically simulated for a large number of initial conditions. The program to simulate these results will be written in C and MATLAB will be used to analyze data. The numerical simulation in C will take advantage of the GNU Scientific Library, which has a suite of functions used to integrate ordinary differential equations. The numerical analysis is done using a Runge-Kutta Prince-Dormand (8, 9) method. Simulations will run till the secondary impacts or escapes from the primary. The initial model uses mass, and radii of KW_4 along with the 0^{th} order BYORP coefficient[25]. A summary of values used can be seen in Table 6.1.

6.3 BYORP Expansion along the Laplace plane

First, it is important to model if as BYORP expands the secondary, it will expand along the Laplace plane. When an asteroid fissions into a binary, the secondary must go through some processes to reach a synchronous state to be expanded or contracted by BYORP. If the binary has a mass ratio $\lesssim 0.2$, then the secondary will go through a second fission and tidal effects to settle into a synchronous orbit. From observations, mass ratios $\lesssim 0.2$ have an orbital radius of 1.5-3 primary radii. For mass ratios $\gtrsim 0.2$, tides will dampen the system to a double synchronous binary with an orbit between 2-8 primary radii [78]. Therefore, to test if the binary follows the Laplace plane, a synchronous binary between 1.5 and eight primary radii with an initial inclination on the Laplace plane is simulated. Four examples are shown in Figure 6.1 for four different primary obliquities: 25°, 45°, 65°, and 85°. In Figure 6.1, the numerical results follow the analytical solution and increase in inclination along the Laplace surface.

The examples in Figure 6.1 all follow the Laplace plane, however, they all have initial orbital radii greater than six primary radii. If the initial orbital radius began at $\lesssim$4.7 primary radii, they would enter into the evection resonance. The evection resonance occurs when the longitude of periapsis of the satellite is equivalent to the orbital period of the primary or planet [91]. The evection resonance causes a substantial increase in eccentricity. Our model of the secondary is simply a point-mass that has a constant secular force that expands its orbit. This model does not account for libration of the secondary's rotation and the possibility of the secondary having the shape of an ellipsoid. Without the libration being modeled, the evection resonance can exist and keep the binary from expanding, since the resonance will cause the binary to lose synchronicity [68]. However, once libration is added, it is impossible for prograde binaries to be captured into an evection resonance and retrograde systems will only be captured temporarily [72]. Therefore, although the evection resonance exists in our simplified model, it will not have any effect on the outcome of the binary system once the

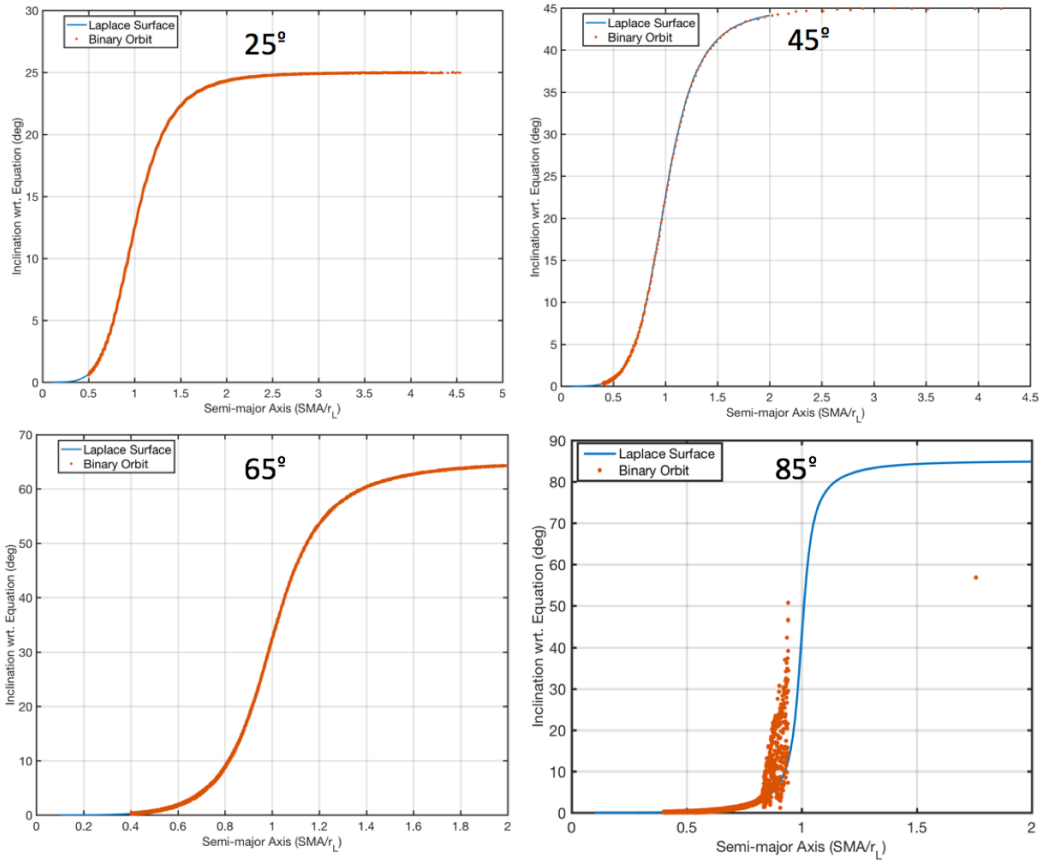

Figure 6.1: Examples of 4 different obliquities following the Laplace plane when expanded with BYORP acceleration. The red, numerical data follow the blue analytical solutions solved using Equation 3.20. For the 85°, the the Laplace plane instability region and stops its evolution.

rotation of the secondary is also included in the model. Therefore our model will always start our initial conditions outside the evection resonance, assuming once libration is added to the model, it may begin with any initial state and get the results without the evection resonance.

The model used to see if BYORP would expand the binary along the Laplace plane started with initial conditions on the Laplace plane. However, current theories suggest that if the secondary fissions, it will most likely separate from the equator of the object [25, 107]. Therefore, the inclination of the binary may be offset from the Laplace place by a couple of degrees instead of lying directly on the Laplace plane. The farthest observed orbital radii for a binary system is ten primary radii [79]. At ten primary radii, the Laplace plane will be $1^\circ - 3^\circ$ inclined to the equator. In Figure 6.2, the secondary began its orbit on the equator at 0.7 Laplace radii, or ~ 11 primary radii. At this point the Laplace plane is 5° from the equator. Even with a 5° difference in inclination, the secondary still followed the Laplace surface as BYORP expanded the orbit, but the orbit varies more in inclination as it expands. Therefore the binary system can settle into a double-synchronous orbit along the equator or within $\sim 5^\circ$ of the Laplace surface and still expand along the surface. To have an 5° difference between the Laplace angle and the equator, the primary needs to have an obliquity at the lower range of the unstable region. As the obliquity approaches 90°, the Laplace surface will approach being discontinuous where prior to one Laplace radii, the Laplace angle is 0° and after one Laplace radius the Laplace angle is 90°, or equal to the obliquity. For example, if the obliquity is 75°, the Laplace radii at which the Laplace angle is 5° is at 0.77 Laplace radii or approximately 13 primary radii. For $q > 0.2$, the clear majority of binary asteroids will settle at primary radii equal or less than 8 primary radii, or 0.55 Laplace radii, which is well within the bounds of when the Laplace angle is greater than 5° [78]. Therefore the limitations of the binary not following the Laplace plane because of a difference in inclination will be very rare for obliquities near 90°. This demonstrates that the secondary can remain on the equator once it settles into a synchronous orbit, but still

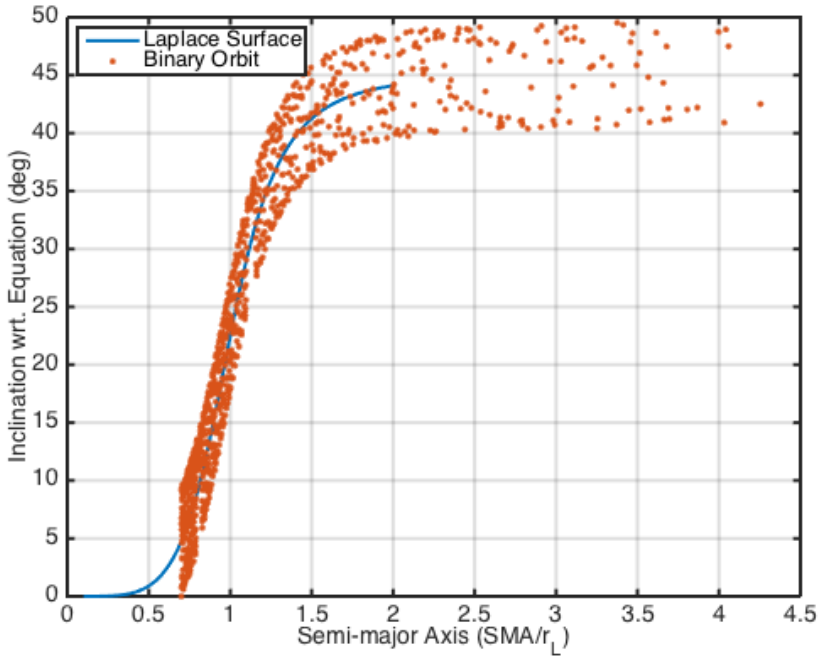

Figure 6.2: The analytical solution for the Laplace surface is given in blue. In red is inclination change of the secondary as the semi-major axis increases due to BYORP expansion. The initial orbit for the secondary was at ~ 11 primary radii and an inclination of $0°$. This demonstrates that the secondary can remain on the equator once it settles into a double-synchronous orbit, but still follow the Laplace surface as the orbit expands.

follow the Laplace surface as the orbit expands.

In Figure 6.1, an obliquity of 85° follows the Laplace plane till approximately 0.8 Laplace radii or ∼13 primary radii and then begins to have a more chaotic evolution in inclination and semi-major axis. This is due to the Laplace plane instability region. The instability region is first discussed in Chapter 3 and the instability region is shown in yellow in Figure 3.2 is unstable for obliquity angles above 68.875° and Laplace radii from 0.9 to 1.25. To understand the instability region in Figure 3.2, the code ran for a multitude of initial conditions and determined the maximum eccentricity of the satellite in 1000 years. The results of this can be seen in Figure 6.3. In this region, within 1000 years some initial conditions reach an eccentricity of one after the 1000 years. The area of the instability region that caused the most eccentricity growth was between Laplace radii of 0.95-1.0, or 16-17 primary radii and for primary obliquities between $76° - 107°$. If a binary asteroid has a primary with a high obliquity between $77° - 105°$, BYORP can expand the orbit along the Laplace plane, enter this instability region and re-impact the primary. From this information, it was determined there may exist a contact binary-binary asteroid cycle.

6.4 Contact Binary-Binary Cycle

Of near-Earth asteroids (NEA) greater than 200 m, 10% are contact binaries [81]. Of the currently observed contact binaries, 9 out of 14 have known obliquities between $50° - 130°$ [108]. A summary of contact binaries and binary asteroids and their properties can be seen in the Johnston Archive website [109]. Therefore, the existence of high obliquity asteroids required for this cycle has been observed. This high obliquity along with radiative forces that drastically affect the evolution of NEA will provide the mechanisms in which this cycle is possible.

The asteroid of interest for this cycle will be between 100 m and 10 km and therefore will be a "rubble pile" asteroid. A "rubble pile" is a collection of boulders of various sizes bounded by gravity [17, 18]. Previous missions to asteroids such as Hayabusa's exploration

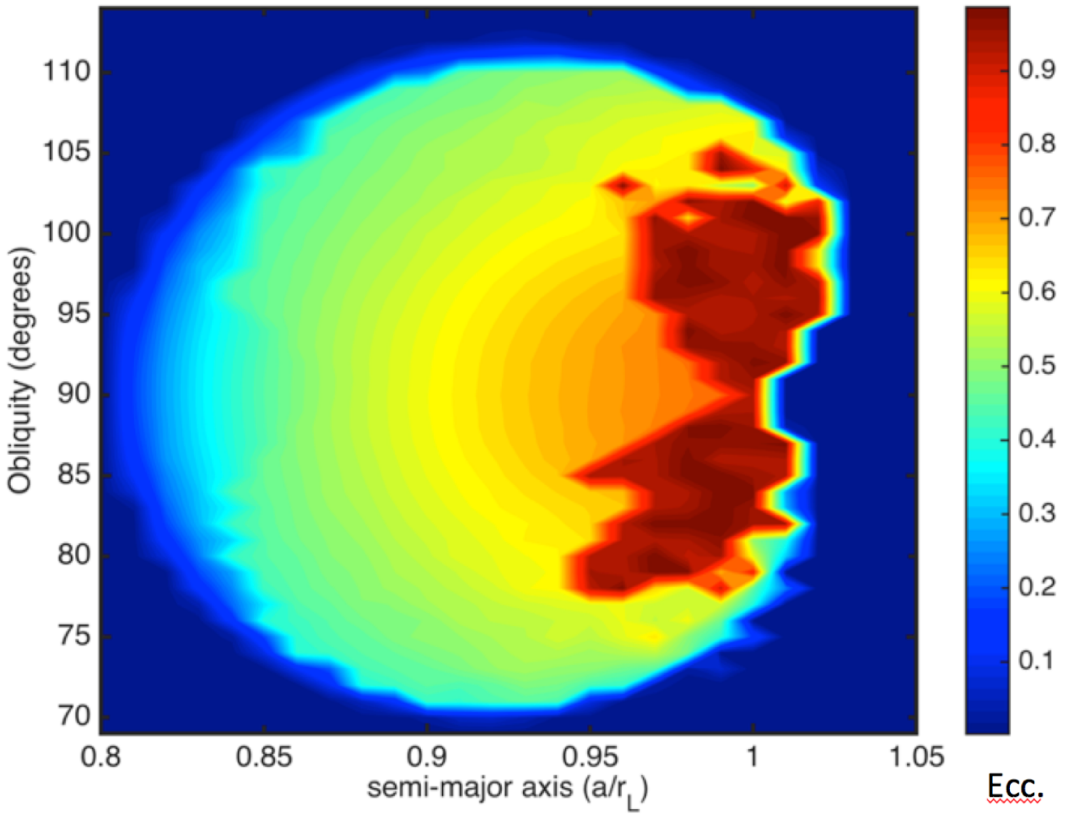

Figure 6.3: Eccentricity displayed as a contour plot after 1000 years. In the most unstable regions, the eccentricity goes to unity even in this short amount of time.

of Itokawa and NEAR Shoemaker's flyby of Mathilde as well as radar imaging of KW_4, show that the bulk density of these asteroids is lower than that of a monolith rock; providing observational evidence of the existence of rubble pile asteroids [14, 21, 25].

The binary would also have to have a mass-ratio greater than 0.2. To observe a contact binary, the size differences between the two lobes need to be large enough to observe. This also excludes a lot of complicated dynamics with mass-ratios less than 0.2 where there can be secondary fission or the secondary escape/impacts the primary before reaching a synchronous orbit. Because of the large mass ratio, the binaries will always enter a double-synchronous orbit and begin BYORP expansion at 2-8 primary radii [78].

The cycle begins with a contact binary asteroid that has an obliquity of $\sim 90^\circ$ with YORP increasing the rotation rate of the asteroid. A contact binary that is affected by YORP will drive the asteroid to obliquities of 0° and 90° with a nearly equal chance of going to either obliquity. [56]. This asteroid will eventually spin up to a period of $\sim$2.2 h that will result in a disruption of the self-gravitating "rubble pile" asteroid. [79] It is assumed that this disruption will cause the contact binary to fission into a binary system with a mass-ratio of 0.2 or larger. The binary system will then go through a tidal process that will end with the binary system being double synchronous [78]. Because the system is double synchronous, the binary will have the non-gravitational force, BYORP, expand the orbit of the binary. As the binary orbit radius expands, the inclination of the orbit will follow the Laplace surface, which is stable to precession due to third-body perturbations from the Sun and the primary's oblateness. Even if the secondary does not begin directly on the Laplace surface, as the orbit radii expands, its inclination will oscillate around the Laplace plane equilibrium. As the orbit expands along the Laplace surface, the secondary will eventually enter the Laplace plane instability region at approximately 14.8-16 R_p. The orbit will quickly grow in eccentricity and eventually lose synchronous lock and stop expanding the orbit. The eccentricity will continue to grow beyond 0.9 due to this instability region. The orbit will elongate and intersect the primary resulting in an impact of the two asteroids. This contact

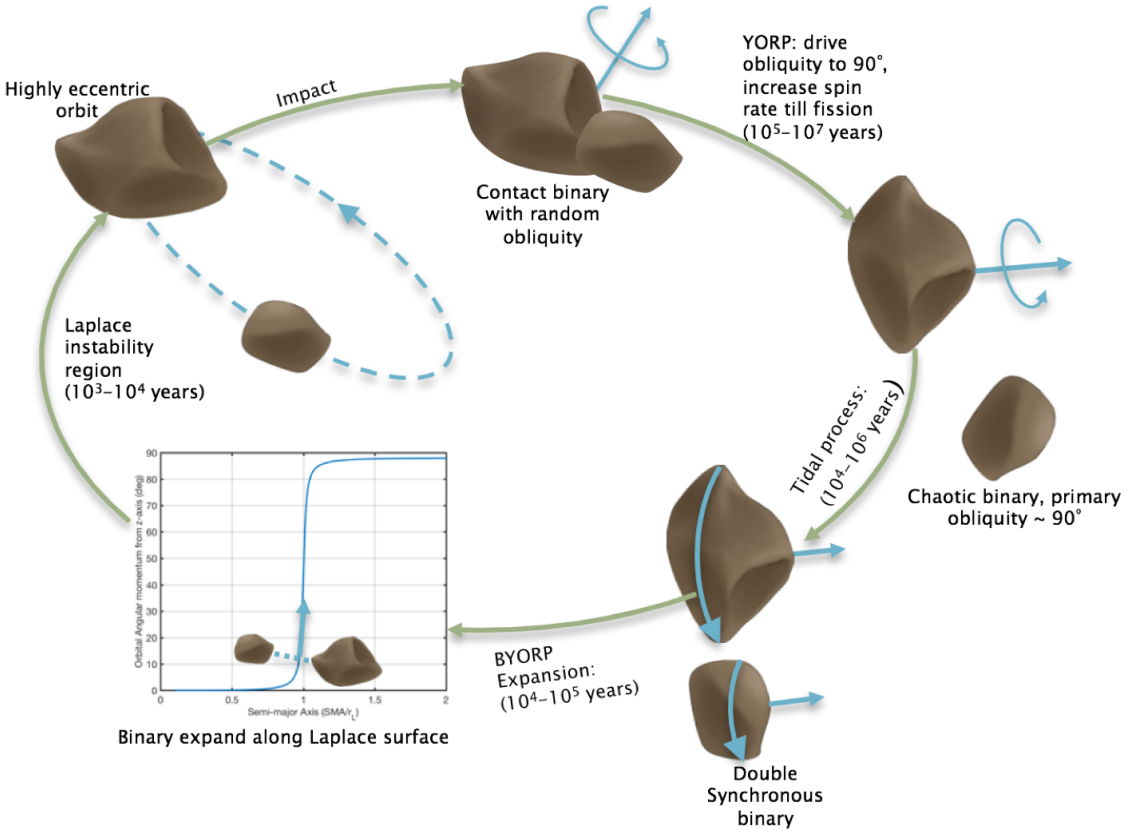

Figure 6.4: 1. Begin with contact binary. Contact binary is driven to an obliquity of 90° and its rotation rate is spinning up due to YORP. 2. Fissions into chaotic binary, where the tidal process will dissipate the energy in the system. 3. The binary system will settle into a double-synchronous binary. From there, the binary will expand due to BYORP. It will follow the Laplace plane as it expands. 4. The orbit will expand, increasing in orbital radii and inclination until it reaches the Laplace plane instability region. 5. The Laplace plane instability region will cause a rapid growth in the orbital eccentricity of the binary system until it leads to an impact, causing a contact binary.

binary will have a new obliquity, that varies from $\sim 40^\circ - 140^\circ$. Then the process repeats itself, with the contact binary being driven by YORP again to an obliquity of 90°. This process is summarized in Figure 6.4.

6.4.1 YORP Process

The cycle begins with a contact binary. This binary will have the non-gravitational force, YORP, altering the rotation state of the asteroid. YORP will change the obliquity angle of the asteroid as well as the spin-rate. First, the obliquity angle will be driven to either 90° or 0°/180° with an approximately equal chance of going to either spin pole[56]. There is also a 6.9% chance of the asteroid being driven to an intermediate obliquity as well. For this cycle to begin, it is necessary that YORP drives the asteroid to an obliquity of or near 90°. This is because eventually, the Laplace plane instability region will play a role in the cycle by driving the secondary to re-impact the primary asteroid. For this instability region to exist, the obliquity of the primary must be between $76^\circ - 107^\circ$. Therefore, an asteroid driven by YORP to 90° will be at an obliquity angle that lies in this region. Secondly, YORP will drive this asteroid to either increase or decrease its spin-rate, with a lesser likelihood that a permanent spin-up of the asteroid to occur. However, for fission of the asteroid to occur, the asteroid needs to spin up to a period of approximately ~ 2.2 h that will result in a disruption of the self-gravitating "rubble pile" asteroid. [79].

6.4.2 Binary Fission leading to large mass-ratio systems

Once the object is at a high obliquity near 90° and is rotating at approximately ~ 2.2 h period, the increasing spin-rate will fission into a binary. The next step in the cycle is for tidal processes discussed in Jacobson and Scheeres to cause the binary to settle into a double-synchronous binary. For a double-synchronous binary, the mass-ratio of the secondary to the primary must be $q > 0.2$ [78]. There are a couple of reasons why only these higher mass-ratios are studied. The first is that contact binaries can only be observed if the

mass-ratio is high enough to see the contact binary is made of two parts. This ensures that our hypothesis is focused on the currently observed contact binaries with high obliquities. Secondly, the process for tides to dampen a chaotic binary is more straightforward for higher mass-ratios. If the secondary has a high enough mass-ratio, it cannot be ejected from the exchanges of angular momentum and energy through spin-orbit coupling. This is much more severe for mass-ratios $q \lesssim 0.2$ where it can cause the secondary to eject from the system[78]. The eccentricity/momentum exchange for higher mass-ratios reduces the eccentricity of the system and therefore keeps the secondary from escaping or producing a secondary fission event. Tidal Dissipations eventually dampens the libration in the system, such that the binary system is double-synchronous [78]. Double-synchronous systems will have both the primary and secondary period equivalent to the orbit. Low mass-ratios can have secondary fission and can result in multiple end states such as a stable ternary, asteroid pairs or a reshaped asteroid[56]. Third, a double-synchronous binary may have a better lock on synchronicity compared to a regular synchronous binary. This will cause the binary to continue to expand into the instability region of the Laplace plane even with eccentricity growth. By continuing to expand into the region, it will reach the center where the eccentricity can grow to near parabolic and eventually result in an impact.

6.4.3 BYORP Expansion

Once the binary system has settled into a double-synchronous orbit, the BYORP force due to this synchronicity will have secular motion that will either expand or contract the system. This all depends on the shape of the binary, but it is assumed that the binary will expand. It is assumed that the secondary will settle into an orbit close enough to the Laplace plane, that the secondary will oscillate in inclination around the Laplace surface as the orbit expands due to BYORP.

As the binary expands along the classical Laplace plane, it will eventually reach the instability region of the Laplace plane. This happens when the secondary is $14.8 - 16\ r_p$

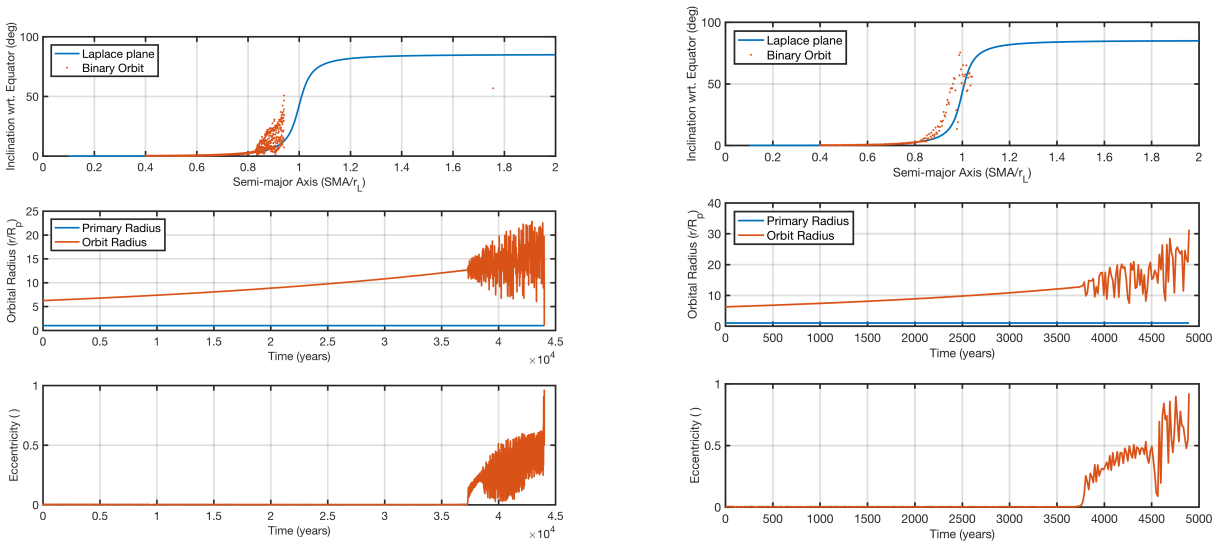

(a) $A_0 = 1400\ m^2$ (b) $A_0 = 14,000\ m^2$

Figure 6.5: a.) The left figure gives three plots for a binary orbit where A_0 is 1400 m^2 b.) gives the same three plots for $A_0 = 14,000\ m^2$. The higher A_0 crosses the instability region and increases the eccentricity to 0.5, but not high enough to impact the primary. The secondary will eventually escape the primary. a.) The less asymmetric secondary with a lower A_0 value will reach an eccentricity of almost 1 which will result in an impact before leaving the instability region.

from the primary. Also, the obliquity of the primary must be between 76° and 107° for the secondary to expand into the Laplace instability region, which is the case for our binary system where the obliquity should be near 90°. At this point, the eccentricity of the binary will increase until it is highly eccentric, > 0.85, that it results in an impact. But, there are issues with BYORP that may cause the eccentricity to rise, but not enough to result in an impact.

BYORP could expand the orbit too quickly. The acceleration of BYORP is dependent on the asymmetric shape of the secondary. The more asymmetric the shape, the faster BYORP will expand the orbit. Also, because the binary is double-synchronous, the shape of the primary can also enhance or reduce the BYORP effect due to their rotations being equal, and this can also play a part in how fast the secondary expands away from the primary [74]. This asymmetry is simply represented by the value of A_0. The value of A_0 is important because if A_0 is too large, the acceleration may be fast enough to cause the binary to expand through the instability region without increasing eccentricity to a high enough value that there is an impact. An example of this can be seen in Figure 6.5. In Figure 6.5a.) the value of A_0 is low enough that the expansion of BYORP takes $25,000$ years to grow to 10 primary radii, while in Figure 6.5b.) the value of A_0 is a magnitude greater resulting in the same orbital radii growth to happen in 2500 years. The rate of expansion of the latter case will be so fast it will enter and leave the Laplace instability region before eccentricity increases to a value that results in impact. Therefore, the asymmetry of the secondary must be slow enough to allow for the eccentricity growth to occur during BYORP expansion. However, the secondary must not be too symmetric that A_0 is small, and the time to expand takes longer than the lifetime of a binary where a flyby of a planet could severely disrupt the system.

If the secondary expands through the instability region of the Laplace plane, the eccentricity increases, which may cause the secondary to lose synchronous lock with the primary. If the binary loses lock, the binary system with cease to expand due to BYORP. This could

help increase the number of impacts because asymmetric secondaries that expand too quickly could lose lock and cause the binary to remain in the Laplace plane instability region. This would cause the eccentricity to grow and lead to an impact with the primary. However, this could also reduce impacts because the binary may lose lock too soon. The instability region is only capable of growing the eccentricity high enough to cause instability at radii above 14.8 primary radii. However, the instability region begins at 13.3 primary radii and therefore may get trapped in the area where the eccentricity may only grow to an eccentricity of 0.4. Thus, it will need to simulate the loss of synchronicity to understand how this changes the process of eccentricity growth. Random initial conditions were simulated with initial radii between $0.35 - 0.85\ r_L$ and primary obliquities of $75° - 110°$. Parameters are altered such as $A_0 = 1400\ m^2$ and $A_0 = 14,000\ m^2$ as well as the inclination being on the Laplace plane or the equator. It is not known what value of eccentricity will cause the binary to lose lock, but it is assumed, for now, that it is an eccentricity of either 0.05 or 0.1. A summary of the impacts is in Table 6.2. For the binary to lose synchronous lock at 0.05, the slower rate of expansion ($A_0 = 1400$ m^2) will effect the possibility of impacts with a 50% increase in binary impacts. The difference in impacts is also reduced 10% if the initial orbit is on the equator as opposed to the Laplace plane. According to Table 6.2, if synchronous lock is lost at an eccentricity of 0.1, the loss of synchronous lock will cause an increase in impacts regardless of the value of A_0. Therefore, it seems that once in the instability region, eccentricity will continue to grow and eventually result in an impact. The initial conditions that did not impact for the cases where eccentricity of 0.1 caused the synchronicity to lose lock are summarized in Figure 6.6 . Regardless of the parameters dictating the simulation, it appears that the only initial states that do not impact are at the extremes on the obliquity ranges of the instability region. Therefore, perhaps because it is on the peripheries of the instability region displayed in Figure 6.3, sometimes the eccentricity increases enough to cause impact and sometimes it does not. However, once the obliquity is between $77° - 102°$, there will be an impact regardless of losing synchronicity or not.

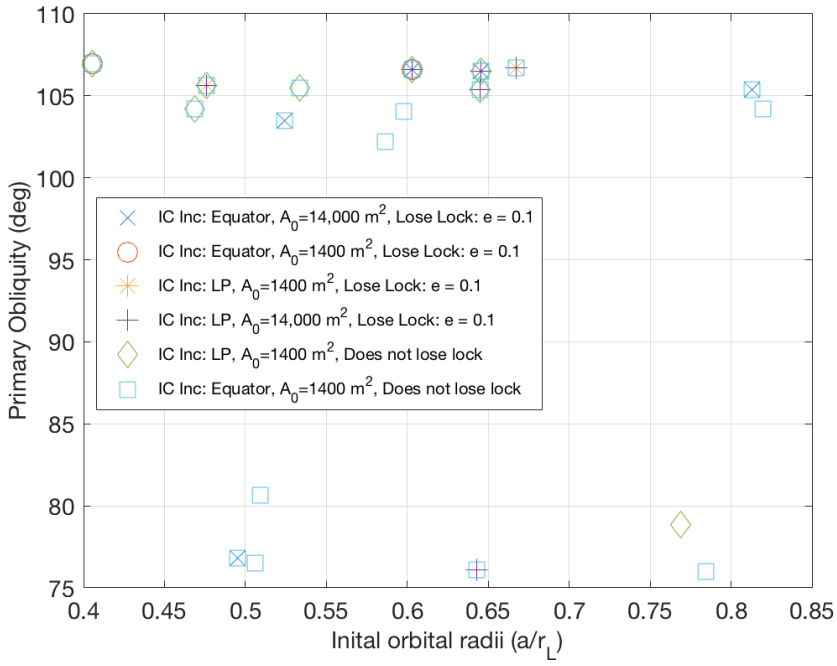

Figure 6.6: The initial conditions for orbital radii and obliquity for the binary systems that did not impact. These are all on the extreme values of obliquity for the Laplace instablity region.

Table 6.2: Percent of initial conditions that impacted asteroid.

A_0	Initial Inclination	Eccentricity lose Synchronous Lock	Percent Impact
1400	Laplace Plane	0.05	92
14,000	Laplace Plane	0.05	39
1400	Equator	0.05	82
14,000	Equator	0.05	28
1400	Laplace Plane	0.1	98
14,000	Laplace Plane	0.1	94
1400	Equator	0.1	98
14,000	Equator	0.1	94

6.4.4 Impact state obliquity distribution

If the binary system impacts, the new rotational state of this contact binary must be determined. This can be easily determined by conservation of angular momentum, where the orbital and rotational angular momentum becomes just the final rotational angular momentum:

$$\frac{m_1 m_2}{m_1 + m_2} \boldsymbol{r} \times \boldsymbol{v} + I_i \Omega_i \hat{\boldsymbol{\omega}}_i = I_f \Omega_f \hat{\boldsymbol{\omega}}_f. \tag{6.1}$$

Where $\boldsymbol{r}$ and $\boldsymbol{v}$ is the final Cartesian state of the orbit before impact, I is the moment of inertia, Ω is the angular velocity and $\hat{\boldsymbol{\omega}}$ is the spin-pole direction. The moment of inertia of a sphere is $I = \frac{2}{5} m_1 r_1^2$. It is assumed that the secondary has a negligible rotational angular momentum. The final moment of inertia is the sum of the two asteroids moments of inertia plus their moments of inertia around their center of mass. It is assumed that the final contact binary will be two spherical bodies resting on each other, such that the distance between the two sphere's centers are $\boldsymbol{R_1} + \boldsymbol{R_2}$. To determine the primary angular velocity, it can be assumed that the system is double-synchronous while the eccentricity of the orbit is low. Therefore, it can be assumed that the spin-rate of the primary is equal to the mean motion of the orbit, or $\sqrt{\frac{Gm_1}{a^3}}$. To determine the value of a for the mean motion, the semi-major axis right before the eccentricity drastically spikes in Figure 6.7 is found. This value is chosen

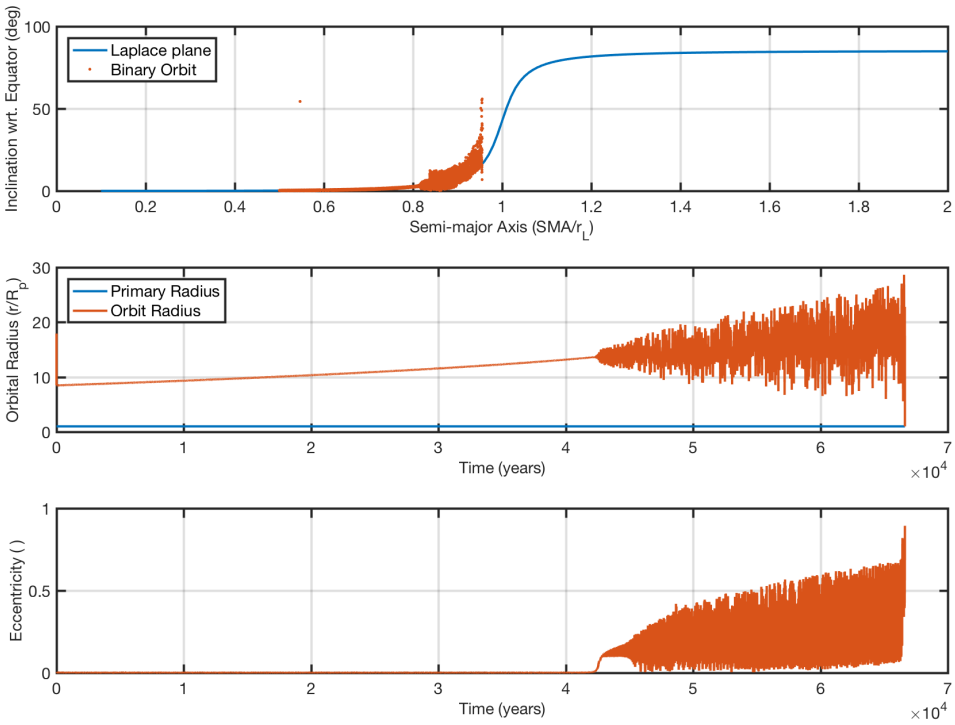

Figure 6.7: The semi-major axis and eccentricity grow for a binary system. The semi-major axis shows the increase in orbital radii due to BYORP for the binary, while eccentricity growth shows the increase in eccentricity due to the Laplace instability region.

because BYORP will lose synchronicity, so this is the last moment it can be assumed that the primary spin state is equal to the secondary orbit.

It is determined that the final states for 200 varying initial conditions that begin with the expansion of the orbit through BYORP at a given radius from $0.35 - 0.85\ r_L$ and for primary obliquities from $75° - 110°$. Half the initial conditions start with an inclination that is on the Laplace plane, while the other half begins on the equator.

The result for the final state versus the initial state is in Figure 6.8. The final obliquities vary from $23° - 150°$, with no correlation between the initial state and the final state of the contact binary. This means that the ultimate determination of this cycle repeating itself is from YORP driving the obliquity to 90° and not the final state of impact for the contact binary.

For these same simulations, the periods of the contact binary are also computed and can be seen in Figure 6.9. Most contact binaries have a final period between 14 and 14.5 hours, while there are several even in the 16-17 hours range. This is much slower than the period that is required to cause another binary system, and therefore YORP will have to spin up the asteroid for the cycle to continue.

The impact velocity varies depending on the mass of the objects, but if the primary is under 2 km in diameter, the impact velocity will be less than 1 m/s. A binary the size of KW_4 with a mass-ratio of 0.2 with its secondary, will have an impact velocity of 0.73 m/s.

6.4.5 Timescales of binary-contact binary cycle

In this section, it is determined that the relative lengths of time it takes for YORP to spin up the contact binary to fission and the time BYORP takes to expand the binary into the instability region. If one time period is significantly longer than the other, then the majority of observations will be of the state with a longer time. Both YORP and BYORP processes time scales can be analytically determined. The YORP induced spin rate of acceleration on

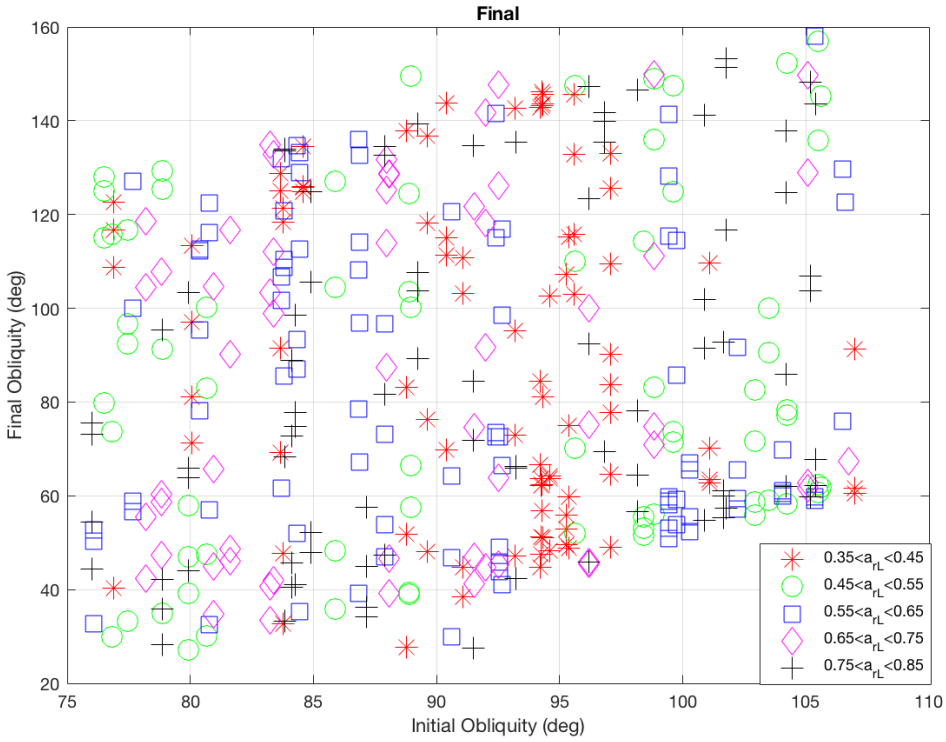

Figure 6.8: The final obliquities of the contact binary as a function of the inital oblquity of the primary while as a binary system. Regardless of the intial orbit radii or obliquity, the final obliquity appears random, except for the maximum and minimum range of the final obliquity trending upwards as the initial obliquity increases.

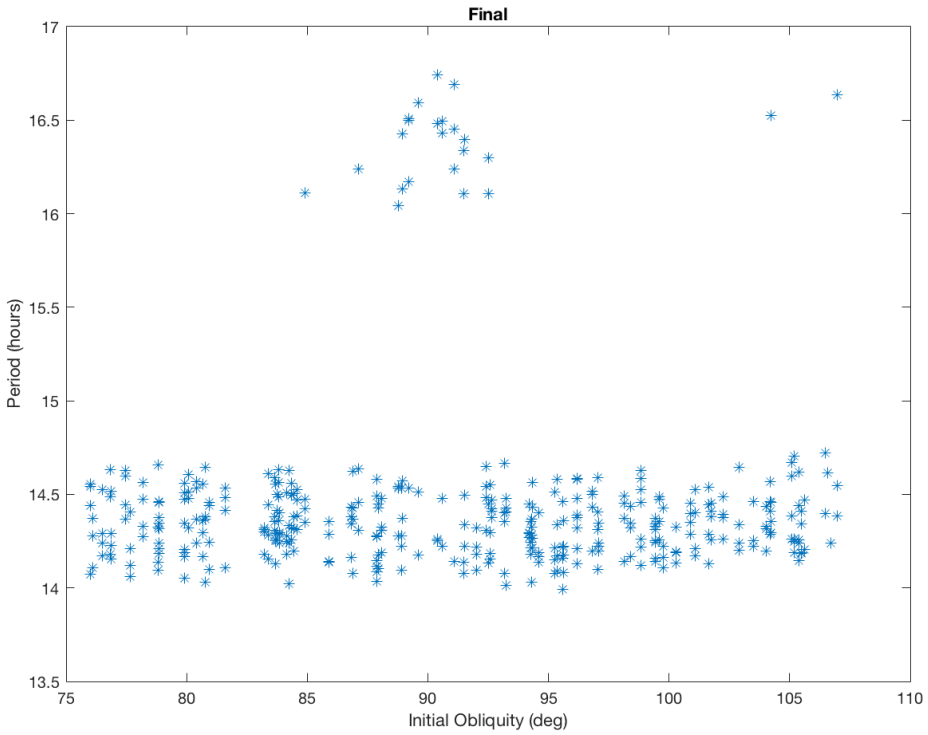

Figure 6.9: Most of the final periods of the contact binary are clustered at 14-14.5 hours, while there are some around 16-17 hours. These are too slow to cause a binary, and therefore will need to have the spin-rate increased by BYORP.

the contact binary can be represented by

$$\dot{\omega} = \frac{3P_\phi}{4\pi a_s^2\sqrt{1-e_s^2}}\frac{C}{\rho R_a^2}, \tag{6.2}$$

where ρ is the density of the contact binary and C ranges from 0.001 to 0.01 and represents a non-dimensional constant that is a function of the shape and obliquity of the asteroid's body [60]. This can be integrated to give the time for YORP to reach a spin rate that allows the contact binary to fission as

$$T_y = (\omega_f - \omega_i)\frac{4\pi a_s^2\sqrt{1-e_s^2}}{3P_\phi}\frac{\rho R_a^2}{C}. \tag{6.3}$$

An analytical equation given in McMahon and Scheeres gives the year averaged rates for secular expansion/contraction of the semi-major axis as

$$\bar{\dot{a}} = \frac{P_\phi}{a_s^2\sqrt{1-e_s^2}}\frac{a_p\sqrt{\mu p_s}}{m_p\mu}[\hat{\boldsymbol{y}}_b \cdot \bar{\boldsymbol{A}}_0], \tag{6.4}$$

where μ is the gravitational parameter of the system and p_s is the semi-latus rectum of the system's orbit around the Sun. Integrating this equation gives the time that it takes BYORP to expand/contract the orbit from an initial to final semi-major axis:

$$T_b = \left(\frac{1}{\sqrt{a_i}} - \frac{1}{\sqrt{a_f}}\right)\frac{a_s^2 m_p\sqrt{\mu}}{P_\phi A_0}. \tag{6.5}$$

Depending on the value of C and if A_0 is 1400 m^2, τ_y/τ_b is between ~ 44.5 and ~ 445.3. Therefore, the system will spend 1-2 orders of magnitude more time as a contact binary then as a binary system. For a primary with a radius of $R = 650$ m, a binary will take 10^4 years to expand, while YORP will take $10^5 - 10^6$ years to reach a spin rate that will cause fission. Figure 6.10 shows the analytically determined time to expand from 2.0 primary radii to 13.5 primary radii (0.8 Laplace radius) over the time YORP takes to reach 2.2 hour spin-rate. The secondary's initial orbital radii starts close to the primary so that it takes a long amount of time to expand BYORP to the instability region. This final primary radius of

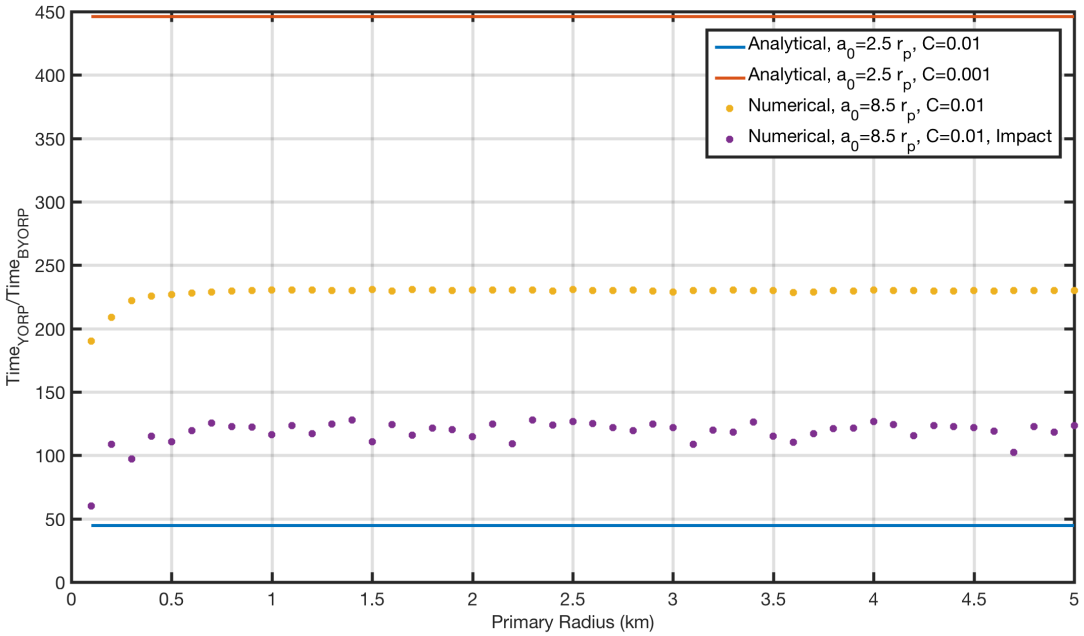

Figure 6.10: The ratio between time spent in the YORP process over time spent in the BYORP process.The yellow data is the time it takes numerical simulations to expand from 0.5 r_L-0.8 r_L or 8.5r_p to 13.5 r_p, while the purple data is the same numerical expansion but include the time in the instability region to the impact as well. The solid red and blue lines give the range of time ratios for an expansion from 2.0 r_p to 13.5 r_p.

$13.5R_p$ is approximately where the instability region begins. The bounds of the possible ratio T_{YORP}/T_{BYORP} are given in Figure 6.10 for the maximum and minimum value of C to represent the YORP coefficient. In between are two numerical sets of data. The yellow data is the time ratio between YORP and BYORP to expand from $8.5R_p$ to 13.5 R_p for asteroid diameters from 200 km to 10 km. In purple, is the same simulation, but includes the time in the instability region after losing synchronous lock till the time of impact. From this, it can be seen that the time spent in the instability region takes about the same amount of time to an order of magnitude less time than BYORP expansion.

6.4.6 Discussion

The contact binary cycle would provide a theory of maintaining the current population of contact binaries. If something in this cycle were observed, a contact binary spinning up due to YORP with any obliquity will most likely be seen, but also trending toward an end state obliquity of 90°. If the binary portion was witnessed the binary part of the cycle, BYORP would be expanding the orbit and although the Laplace plane changes the inclination of the orbit, the orbit will most likely be at a low inclination generally below 10°. The higher inclination orbits will not be observed unless the binary already has a higher eccentricity and does not have a synchronous orbit.

6.5 Conclusion and Future Work

6.5.1 Conclusion

It has been determined that a binary system can follow the Laplace plane as it expands with BYORP, even if it is not directly on the Laplace plane. If the obliquity of the primary has an obliquity between $68.875° - 111.125°$, the binary will enter the Laplace instability region and grow in eccentricity. If the obliquity is between $77° - 105°$, the eccentricity will eventually grow to above 0.9 causing an eventual impact or escape. These conclusions were

applied to create a new hypothesis on contact binary creation that keeps them in cycles of fission and formation.The necessary conditions for the contact binary cycle to exist:

(1) Mass ratio, $q \gtrsim 0.2$, to ensure no second fission or secondary escape. Ensures that binary will settle into a double-synchronous orbit.

(2) The asymmetry of the secondary is such that the orbit of the binary expands as opposed to contracts.

(3) The secondary settles near the Laplace plane within 5° inclination or on the equator $\lesssim 10$ primary radii.

(4) The primary has an obliquity between $76° - 107°$, so that the orbit expands into the unstable region of the Laplace plane that results in collisions.

(5) After impact, YORP drives the obliquity to 90° and spins up the period of the contact binary.

The binary cycle begins with a contact binary that is spinning up and its obliquity is being driven to 90° due to YORP. Once YORP spins up the asteroid to a period of 2.2 hours, the asteroid will fission. The binary is chaotic, but due to $q \gtrsim 0.2$, the tidal process will yield a double-synchronous binary. This binary will expand due to BYORP along the Laplace plane. Once the binary reaches an orbital distance of approximately 13.3 primary radii, the secondary has entered the Laplace plane instability region. This will cause the binary orbit to increase in eccentricity. First, the binary will lose synchronous lock, and the orbit will stop expanding. Next, since the orbit is now stranded in the instability region, the orbital eccentricity will eventually grow until the orbit intersects the primary body resulting in an impact. The impact will result in a contact binary with a slow rotation and an obliquity between $30° - 150°$. For the cycle to continue, YORP will need to drive the contact binary to an obliquity of 90° and spin up the rotation of the asteroid.

6.5.2 Future Work

What was presented in this chapter is a very simplified model, the next step would be to include the libration of the two bodies to see how this affects the cycle's evolution. This will provide more conclusive timing on when precisely the binary system is most likely to lose its synchronicity once the eccentricity increases. The obliquity of the primary may also need to be incorporated into the model of BYORP since a double synchronous orbit includes the mutual effect of solar re-emission on both the primary and secondary. Finally, YORP driving the cycle back to a 90° obliquity is a crucial part of the cycle, but current work proposes it is a coin toss between 90° and 0°/180° or leans more towards final states of 0°/180°. It would be interesting to determine if there exists a mechanism in which contact binaries would be driven more towards 90° or if this cycle will only have a 50% chance of continuing each time it reaches the YORP portion of the cycle.

Chapter 7

Conclusion and Future Work

7.1 Conclusion

7.1.1 Natural and Artificial Satellites

This dissertation applied known models of solar radiation pressure to near-Earth asteroids to explore the stability to impact or escape of natural and artificial satellites around these bodies. This dissertation also presented the novel application of the classical Laplace plane to the evolution of a binary asteroid through BYORP expansion. This use of the Laplace plane created a hypothesis for contact binary-binary cycles that would help explain the current population of contact binaries in the NEA population as well as explain the broad range of obliquities found in observed contact binary populations.

The research provided in this dissertation used a model of spherical harmonics of the asteroid, third-body perturbations from the Sun, and solar radiation pressure to characterize the stability of natural satellites around the asteroid Bennu, the future destination of the OSIRIS-REx spacecraft. Previous work has investigated binary asteroid systems with satellites large enough not to be directly impacted by SRP or studied particles such as dust or 1 cm sized debris. This research looks at the stability of satellites small enough to be affected by SRP and incapable of being seen from Earth observations, but large enough to be dangerous if a collision with a spacecraft were to take place, ranging in size from 1 cm to 15 m in diameter. Three orbital phenomena have been discussed that lead to stability or instability of the satellite: modified Laplace plane, Kozai resonance, and Sun-synchronous

orbits. The modified Laplace plane created a frozen orbit that was stable for satellites larger than 1.5 m, while the Sun-synchronous orbits created stability for objects under 1 m in diameter at inclinations between $36° - 144°$. The Kozai resonance caused instability for large objects over 1.5 m in diameter at high inclinations between $78° - 102°$. Objects less than 1 meter in size are constrained to orbits 13 km or less. These objects will be the most difficult to see during the natural satellite survey during approach.

The research of natural satellite stability was also applied to other asteroids such as KW_4 without the secondary and Vesta as well as asteroids with various obliquities of 0°, 45°, 90°, 135°. This research provided insight into how the obliquity will change natural satellite stability as a whole. There were three main findings from this work. First, sun-synchronous orbits were stable for all inclinations for asteroids with spin-poles not aligned or perpendicular to the orbit pole, $\epsilon = 45°$ and $\epsilon = 135°$. While $\epsilon = 0°$ and $\epsilon = 176°$ were only stable from $36° - 144°$. $\epsilon = 90°$ had stable Sun-synchronous orbits except from $78° - 102°$. Along the same trend, the Kozai resonance instability did not exist for $\epsilon = 45°$ and $\epsilon = 135°$, while the aligned and perpendicular obliquities to the orbit pole did have the Kozai resonance instability. Finally, the further the obliquity angle was from aligning with the orbit-pole, the more possible orbits would precess around the Laplace plane and therefore have bounded precession in longitude of the ascending node. At $\epsilon = 90°$, most orbits had precession of Ω bounded to the Laplace plane, while $\epsilon = 0°$ had none.

A subset of mass-to-area ratios from our natural satellite research that overlapped with artificial satellites was discussed. It is confirmed that the terminator plane is the best long-term stable orbit for a spacecraft mission to an asteroid. There are stable orbits that are Sun-synchronous, which precess in inclination around the terminator plane. However, the significant precession in inclination and the growth of eccentricity that occur in these orbits make them too unpredictable for spacecraft missions. Also, the modified Laplace plane was determined not to be an option for a spacecraft orbit at NEA, unless the NEA is one of the few asteroids greater than ~5 km in diameter. However, the modified Laplace plane could

easily be implemented as a spacecraft orbit at a main-belt asteroid with any obliquity for any object over ~ 5 km in diameter.

7.1.2 Binary Asteroids

The dissertation also discussed the possibility of binary asteroids expanding due to BYORP acceleration along the classical Laplace plane. The work confirmed that the secondary would maintain an inclination synonymous with the Laplace surface with a model of an oblate spheroid primary, solar tides, and a constant-force BYORP model. This is also true if the satellite is displaced from the Laplace surface. The inclination of the secondary would just oscillate around the Laplace surface as it expanded away from the primary. However, with obliquities between $68.875^\circ - 111.125^\circ$, the secondary will eventually enter the Laplace plane instability region where the orbit eccentricity will increase. If the obliquity is between $77^\circ - 105^\circ$, the eccentricity will become high enough to cause the secondary to impact the primary.

From this information, a contact binary-binary cycle was proposed. The cycle begins with a contact binary that will spin up, and its obliquity will be driven to $\sim 90^\circ$ due to BYORP. Once the rotational period of the asteroid reaches ~ 2.2 hours, the asteroid will fission. The binary system will be chaotic until tides bring the binary into a double-synchronous orbit. The secondary will expand along the Laplace plane where it will eventually reach the Laplace plane instability region. Once the secondary enters this area, it will increase in eccentricity, lose synchronicity and ultimately impact the secondary. This creates a contact binary with any obliquity that will be subject to YORP increasing the spin rate.

7.2 Future Work

7.2.1 Natural and Artificial Satellites

The research presented in this dissertation has made progress on these topics, however, with research, there are always more questions to ask and problems to solve. The work accomplished on natural satellite stability purposefully places the issue, "How would a natural satellite get into this orbit?" outside the bounds of the research goals. However, if most satellites come from rocks or boulders leaving the equatorial bulge at the equator; how would a natural satellite evolve to have a terminator plane orbit? Also, one initial parameter that is ignored is the eccentricity. The eccentricity of an orbit can often make it more stable to perturbations. For example, the terminator plane orbit requires a non-zero eccentricity to be stable to SRP. Therefore, exploring how this increases stability for the natural satellites would be beneficial to investigate.

7.2.2 Binary Asteroids

The binary asteroid system model with BYORP is a simple model that does not include the libration of the two asteroids. This would help determine exactly when the binary will stop being synchronous due to increases in eccentricity. Because the binary is double-synchronous, the rotation of the primary also would affect the secular motion of the secondary. But the primary has a high obliquity, which may change how thermal re-emission from the primary contributes to BYORP. Finally, a significant portion of the cycle relies on the assumption that YORP will spin up the asteroid and drive the obliquity to 90° and BYORP will expand, not contract, the binary system. Therefore, the cycle has a certain probability during the BYORP or YORP process that the cycle will stop because the asteroid is oriented the wrong way, and the asymmetry causes the opposite to happen. There may be a mechanism that causes the cycle to have a high probability of ending in states that allow the cycle to continue. Either way, it is essential to understand the chances of the cycle

stopping at each step of the contact binary evolution.

Bibliography

[1] A Morbidelli, W.˜F. Bottke Jr., C Froeschlé, and P Michel. Origin and Evolution of Near-Earth Objects. Asteroids III, pages 409–422, 2002.

[2] A. Mainzer, T. Grav, J. Bauer, J. Masiero, R. S. McMillan, R. M. Cutri, R. Walker, E. Wright, P. Eisenhardt, D. J. Tholen, T. Spahr, R. Jedicke, L. Denneau, E. DeBaun, D. Elsbury, T. Gautier, S. Gomillion, E. Hand, W. Mo, J. Watkins, A. Wilkins, G. L. Bryngelson, A. Del Pino Molina, S. Desai, M. Go'mez Camus, S. L. Hidalgo, I. Konstantopoulos, J. A. Larsen, C. Maleszewski, M. A. Malkan, J. C. Mauduit, B. L. Mullan, E. W. Olszewski, J. Pforr, A. Saro, J. V. Scotti, and L. H. Wasserman. NEOWISE Observations of Near-Earth Objects: Preliminary Results. The Astrophysical Journal, 156(Shoemaker 1983), 2011. ISSN 0004-637X. doi: 10.1088/0004-637X/743/2/156. URL `http://arxiv.org/abs/1109.6400{%}0Ahttp://dx.doi.org/10.1088/0004-637X/743/2/156`.

[3] Gustav Witt. Entdeckung eine neuen Planeten 1898 DQ. Astronomische Nachrichten, 147:141, 1898.

[4] A. R. Hinks. Sun, Parallax of the, from Photographs of Eros. Monthly Notices of the Royal Astronomical Society, 69:544, 1905.

[5] S. H. Jones. Eros, Observations of, at the Opposition 1930-31. Monthly Notices of the Royal Astronomical Society, 90:724, 1930.

[6] J. H. Lieske. Mass of the Earth-Moon System from Observations of Eros, 1893-1966. The Astronomical Journal, 73:628, 1968.

[7] E. Rabe and M. P. Francis. The Earth+Moon Mass and Other Astronomical Constants from the Eros Motion 1926-1965. The Astronomical Journal, 72:856, 1967.

[8] E. von Oppolzer. Vorläufige Mittheilung uber photometrische Messungen des Planeten (433) Eros. Astronomische Nachrichten, 154:309–312, 1901.

[9] D. Vokrouhlický, W. F. Bottke, and D. Nesvorný. The Spin State of 433 Eros and its Possible Implications. Icarus, 175(2):419–434, 2005. ISSN 00191035. doi: 10.1016/j.icarus.2004.11.017.

[10] G. Krug, W., Schrutka-Rechtenstamm. Untersuchungen uber Gestalt und Größe des Planetoiden Eros. Zeitschrift für Physik, 13:1–12, 1937.

[11] M. Pilcher, Belton. J. S., J. Veverka, P. Thomas, P. Helfenstein, D. Simonelli, Chapman. C., M. E. Davies, R. Greeley, R. Greenberg, J. Head, S. Murchie, K. Klaasen, T. V. Johnson, A. McEwen, D. Morrison, and G. F. Neukum. Galileo Encounter with 951 Gaspra: First Pictures of an Asteroid. Science, 257:1992, 1992. URL http://www.jstor.org/stable/2880122.

[12] M.J.S. Belton, C.R. Chapman, P.C. Thomas, M.E. Davies, R. Greenberg, K. Klaasen, D. Byrnes, L. D'Amario, S. Synnott, T.V. Johnson, A. McEwen, W.J. Merline, D.R. Davis, J.-M. Petit, A. Storrs, J. Veverka, and B. Zellner. Bulk Density of Asteroid 243 Ida from the Orbit of its Satellite Dactyl, 1995. ISSN 00280836.

[13] C.R. Chapman, J. Veverka, P.C. Thomas, K. Klaasen, M.J.S. Belton, A. Harch, A. McEwen, T.V. Johnson, P. Helfenstein, M.E. Davies, W.J. Merline, and T. Denk. Discovery and Physical Properties of Dactyl, a Satellite of Asteroid 243 Ida, 1995. ISSN 00280836.

[14] D. K. Yeomans. Estimating the Mass of Asteroid 253 Mathilde from Tracking Data During the NEAR Flyby. Science, 278(5346):2106–2109, 1997. ISSN 00368075. doi: 10.1126/science.278.5346.2106. URL http://www.sciencemag.org/cgi/doi/10.1126/science.278.5346.2106.

[15] J. Veverka, P. Thomas, A. Harch, B. Clark, J. F. Bell Iii, B. Carcich, J. Joseph, and M. Robinson. NEAR Encounter with Asteroid 253 Mathilde: Overview. International Journal of Solar System Studies, 16(1):3–16, 1999. ISSN 00191035. doi: 10.1006/icar.1999.6120. URL http://linkinghub.elsevier.com/retrieve/pii/S0019103599961201.

[16] P. Michel. Collisions and Gravitational Reaccumulation: Forming Asteroid Families and Satellites. Science, 294(5547):1696–1700, 2001. ISSN 00368075. doi: 10.1126/science.1065189. URL http://www.sciencemag.org/cgi/doi/10.1126/science.1065189.

[17] D. C. Richardson, P. Elankumaran, and R. E. Sanderson. Numerical Experiments with Rubble Piles: Equilibrium Shapes and Spins. Icarus, 173(2):349–361, 2005. ISSN 00191035. doi: 10.1016/j.icarus.2004.09.007.

[18] P. Tanga, C. Comito, P. Paolicchi, D. Hestroffer, A. Cellino, A. Dell'Oro, D. C. Richardson, K. J. Walsh, and M. Delbo. Rubble-Pile Reshaping Reproduces Overall Asteroid Shapes. The Astrophysical Journal, 706(1):L197–L202, 2009. ISSN 0004-637X. doi: 10.1088/0004-637X/706/1/L197. URL http://stacks.iop.org/1538-4357/706/i=1/a=L197?key=crossref.ed0c866c65a19f79c6eedab394e1106b.

[19] D. K. Yeomans. Radio Science Results During the NEAR-Shoemaker Spacecraft Rendezvous with Eros. Science, 289(5487):2085–2088, 2000. ISSN 00368075. doi: 10.

1126/science.289.5487.2085. URL http://www.sciencemag.org/cgi/doi/10.1126/science.289.5487.2085.

[20] J. Veverka. NEAR at Eros: Imaging and Spectral Results. Science, 289(5487):2088–2097, 2000. ISSN 00368075. doi: 10.1126/science.289.5487.2088. URL http://www.sciencemag.org/cgi/doi/10.1126/science.289.5487.2088.

[21] A. Fujiwara, J. Kawaguchi, D. K. Yeomans, M. Abe, T. Mukai, T. Okada, J. Saito, H. Yano, M. Yoshikawa, D. J. Scheeres, O. Barnouin-Jha, A. F. Cheng, H. Demura, R. W. Gaskell, N. Hirata, H. Ikeda, T. Kominato, H. Miyamoto, A. M. Nakamura, R. Nakamura, S. Sasaki, and K. Uesugi. The Rubble-Pile Asteroid Itokawa as Observed by Hayabusa. Science, 312(5778):1330–1334, 2006. ISSN 0036-8075. doi: 10.1126/science.1125841. URL http://www.sciencemag.org/cgi/doi/10.1126/science.1125841.

[22] H. Demura, S. Kobayashi, E. Nemoto, N. Matsumoto, M. Furuya, A. Yukishita, N. Muranaka, H. Morita, K. Shirakawa, M. Maruya, H. Ohyama, M. Uo, T. Kubota, T. Hashimoto, J. Kawaguchi, A. Fujiwara, J. Saito, S. Sasaki, H. Miyamoto, and N. Hirata. Pole and Global Shape of 25143 Itokawa. Science, 312(5778):1347–1349, 2006. ISSN 0036-8075. doi: 10.1126/science.1126574. URL http://www.sciencemag.org/cgi/doi/10.1126/science.1126574.

[23] D. J. Scheeres. Rotational Fission of Contact Binary Asteroids. Icarus, 189(2):370–385, 2007. ISSN 00191035. doi: 10.1016/j.icarus.2007.02.015.

[24] P. Chodas. Center for Near Earth Object Studies Discovery Statistics, 2017.

[25] Steven. J. Ostro, J.-L. Margot, L. A. M. Benner, J. D. Giorgini, D. J. Scheeres, E. G. Fahnestock, S. B. Broschart, J. Bellerose, M. C. Nolan, C. Magri, P. Pravec, P. Scheirich, R. Rose, R. F. Jurgens, E. M. De Jong, and S. Suzuki. Radar Imaging of Binary Near-Earth Asteroid (66391) 1999 KW4. Science, 314(5803):1276–1280, 2006. ISSN 0036-8075. doi: 10.1126/science.1133622. URL http://www.sciencemag.org/cgi/doi/10.1126/science.1133622.

[26] L. Benner. Binary and Ternary Near-Earth Asteroids Detected by Radar, 2017. URL https://echo.jpl.nasa.gov/{~}lance/binary.neas.html.

[27] D.S. Lauretta. OSIRIS-REx: Sample Return from Asteroid (101955) Bennu. Springer, (101955), 2017. doi: DOI10.1007/s11214-017-0405-1.

[28] Y. Tsuda, M. Yoshikawa, M. Abe, H. Minamino, and S. Nakazawa. System Design of the Hayabusa 2-Asteroid Sample Return Mission to 1999 JU3. Acta Astronautica, 91:356–362, 2013. ISSN 00945765. doi: 10.1016/j.actaastro.2013.06.028. URL http://dx.doi.org/10.1016/j.actaastro.2013.06.028.

[29] D. J. Scheeres. Orbital Motion in Strongly Perturbed Environments: Applications to Asteroid, Com
Springer, 2012. ISBN 978-3642032554.

[30] A.F. Cheng, P. Michel, C. Reed, A. Galvez, and I. Carnelli. DART : Double Asteroid Redirection Test. European Planetary Science Congress, 7:23–28, 2012.

[31] A Galvez, I Carnelli, P Michel, A F Cheng, C Reed, S Ulamec, J Biele, P Abell, and R Landis. AIDA: The Asteroid Impact & Deflection Assessment Mission. European Planetary Science Congress, 8, 2013. URL http://meetingorganizer.copernicus.org/EPSC2013/EPSC2013-1043.pdf.

[32] B Chauvineau, P Farinella, and F Mignard. Planar Orbits about a Triaxial Body - Application to Asteroidal Satellites, 1993. ISSN 00191035.

[33] D. J. Scheeres. Dynamics about Uniformly Rotating Triaxial Ellipsoids: Applications to Asteroids. Icarus, 110:225–238, 1994.

[34] W. M. Kaula. Theory of Satellite Geodesy. Blaisdell, Boston, 1966.

[35] D.J. Scheeres, S.J. Ostro, R.S. Hudson, E.M. DeJong, and S. Suzuki. Dynamics of Orbits Close to Asteroid 4179 Toutatis. Icarus, 132(1):53–79, 1998. ISSN 00191035. doi: 10.1006/icar.1997.5870. URL http://linkinghub.elsevier.com/retrieve/pii/S001910359795870X.

[36] D. J. Scheeres, B. G. Williams, and J. K. Miller. Evaluation of the Dynamic Environment of an Asteroid: Applications to 433 Eros. Advances in the Astronautical Sciences, 102 II(3):835–848, 1999. ISSN 00653438. doi: 10.2514/2.4552.

[37] Harry Dankowicz. Some Special Orbits in the Two-Body Problem with Radiation Pressure. Celestial Mechanics & Dynamical Astronomy, 58(4):353–370, 1994. ISSN 09232958. doi: 10.1007/BF00692010.

[38] D. J. Scheeres. Satellite Dynamics about Small Bodies: Averaged Solar Radiation Pressure Effects. Journal of the Astronautical Sciences, (47):25–46, 1999. URL http://www-personal.umich.edu/{~}scheeres/reprints/JAS{_}sunpert.pdf.

[39] D. J. Scheeres and F. Marzari. Spacecraft Dynamics in the Vicinity of a Comet. Journal of the Astronautical Sciences, 50(1):35–52, 2002. ISSN 00219142. URL http://www-personal.umich.edu/{~}scheeres/reprints/JAS{_}comet{_}far{_}rev.pdf.

[40] D.J. Scheeres. Satellite Dynamics about Asteroids. In AAS / AIAA Space Flight Mechanics Meeting, 1994.

[41] D. J. Scheeres. Orbit Mechanics About Asteroids and Comets. Journal of Guidance, Control, and Dynamics, 35(3):987–997, may 2012. ISSN 0731-5090. doi: 10.2514/1.57247. URL http://arc.aiaa.org/doi/abs/10.2514/1.57247.

[42] D. J. Scheeres. Design , Dynamics and Stability of the OSIRIS-REx Sun-Terminator Orbits. In AAS / AIAA Space Flight Mechanics Meeting, pages 1–20, 2013.

[43] K. Richter and H. U. Keller. On the Stability of Dust Particle Orbits around Cometary Nuclei, 1995. ISSN 00191035.

[44] D. J. Scheeres. Orbits Close to Asteroid 4769 Castalia. Icarus, 121(1):67–87, 1996. ISSN 00191035. doi: 10.1006/icar.1996.0072. URL http://linkinghub.elsevier.com/retrieve/pii/S001910359690072X.

[45] D. P. Hamilton and J. A. Burns. Orbital Stability Zones about Asteroids. Icarus, 92 (1):118–131, 1991. ISSN 10902643. doi: 10.1016/0019-1035(91)90039-V.

[46] D. P. Hamilton and J. A. Burns. Orbital Stability Zones about Asteroids II. The Destabilizing Effects of Eccentric Orbits and of Solar Radiation. Icarus, 96:43–64, 1991.

[47] M. C. Nolan, C. Magri, E. S. Howell, L. A. M. Benner, J. D. Giorgini, C. W. Hergenrother, R. S. Hudson, D. S. Lauretta, J.-L. Margot, S. J. Ostro, and D. J. Scheeres. Shape Model and Surface Properties of the OSIRIS-REx Target Asteroid (101955) Bennu from Radar and Lightcurve Observations. Icarus, 226(1):629–640, 2013. ISSN 00191035. doi: 10.1016/j.icarus.2013.05.028. URL http://dx.doi.org/10.1016/j.icarus.2013.05.028.

[48] C. W. Hergenrother, M. A. Barucci, O. Barnouin, B. Bierhaus, R. P. Binzel, W. F. Bottke, S. Chesley, B. C. Clark, B. E. Clark, E. Cloutis, C. Drouet, M. Delbo, J. Emery, B. Gaskell, E. Howell, L. Keller, M. Kelley, J. Marshall, P. Michel, M. Nolan, B. Rizk, D. Scheeres, D. Takir, D. D. Vokrouhlický, E. Beshore, and D. S. Lauretta. The Design Reference Asteroid for the OSIRIS-REx Mission Target (101955) Bennu. arXiv preprint arXiv: ..., (101955), 2014.

[49] W. K. Hartmann, P. Farinella, D. Vokrouhlický, S. J. Weidenschilling, A. Morbidelli, F. Marzari, D. R. Davis, and E. Ryan. Reviewing the Yarkovsky Effect: New Light on the Delivery of Stone and Iron Meteorites from the Asteroid Belt. Meteoritics & Planetary Science, 34(S4):A161–A167, 1999. ISSN 10869379. doi: 10.1111/j.1945-5100.1999.tb01761.x. URL http://doi.wiley.com/10.1111/j.1945-5100.1999.tb01761.x.

[50] D. P. Rubincam. Asteroid Orbit Evolution due to Thermal Drag. Journal of Geophysical Research, 100(E1):1594–1595, 1995. ISSN 01480227. doi: 10.1029/94JE02411.

[51] D. P. Rubincam. Yarkovsky Thermal Drag on LAGEOS. Journal of Geophysical Research: Solid Earth, 93(B11):13805–13810, 1988. ISSN 01480227. doi: 10.1029/JB093iB11p13805. URL http://doi.wiley.com/10.1029/JB093iB11p13805.

[52] J. A. O'Keefe. Tektites and their Origin. Elsevier, 1976.

[53] V. V. Radzievskii. A Mechanism for the Disintegration of Asteroids and Meteorites. Doklady Akademii Nauk SSSR, 29:162–170, 1952.

[54] S. J. Paddack. Rotational Bursting of Small Celestial Bodies: Effects of Radiation Pressure. Journal of Geophysical Research, 74(17):4379–4381, 1969.

[55] D. Rubincam. Radiative Spin-up and Spin-down of Small Asteroids. Icarus, 148(1): 2–11, 2000. ISSN 00191035. doi: 10.1006/icar.2000.6485. URL http://linkinghub.elsevier.com/retrieve/doi/10.1006/icar.2000.6485.

[56] D. Vokrouhlický and D. Capek. YORP-Induced Long-Term Evolution of the Spin State of Small Asteroids and Meteoroids: Rubincam's Approximation. Icarus, 159(2):449–467, 2002. ISSN 00191035. doi: 10.1006/icar.2002.6918. URL http://www.sciencedirect.com/science/article/B6WGF-46THB2H-M/2/8e8514cac64857a7541ba253f0fe16f2.

[57] D. Čapek and D. Vokrouhlický. The YORP Effect with Finite Thermal Conductivity. Icarus, 172(2):526–536, 2004. ISSN 00191035. doi: 10.1016/j.icarus.2004.07.003.

[58] D. J. Scheeres. The Dynamical Evolution of Uniformly Rotating Asteroids Subject to YORP. Icarus, 188(2):430–450, 2007. ISSN 00191035. doi: 10.1016/j.icarus.2006.12.015.

[59] D. J. Scheeres and S. Mirrahimi. Rotational Dynamics of a Solar System Body under Solar Radiation Torques. Celestial Mechanics and Dynamical Astronomy, 101(1-2): 69–103, 2008. ISSN 09232958. doi: 10.1007/s10569-007-9116-3.

[60] D. J. Scheeres. Disaggregation of Small, Cohesive Rubble Pile Asteroids due to YORP. Icarus, 2017. ISSN 10902643. doi: 10.1016/j.icarus.2017.05.029.

[61] M. Kaasalainen, J. urech, B. D. Warner, Y. N. Krugly, and N. M. Gaftonyuk. Acceleration of the Rotation of Asteroid 1862 Apollo by Radiation Torques. Nature, 446(7134):420–422, 2007. ISSN 0028-0836. doi: 10.1038/nature05614. URL http://www.nature.com/doifinder/10.1038/nature05614.

[62] S. C. Lowry, A. Fitzsimmons, P. Pravec, D. Vokrouhlický, H. Boehnhardt, P. A Taylor, J.-L. Margot, A. Galád, M. Irwin, J. Irwin, and P. Kusnirák. Direct Detection of the Asteroidal YORP Effect. Science, 316(April):272–274, 2007. ISSN 0036-8075. doi: 10.1126/science.1229223.

[63] P. A. Taylor, J.-L. Margot, D. Vokrouhlický, D. J. Scheeres, P. Pravec, S. C. Lowry, A. Fitzsimmons, M. C. Nolan, S. J. Ostro, L. A. M. Benner, J. D. Giorgini, and C. Magri. Spin Rate of Asteroid (54509) 2000 PH5 Increasing Due to the YORP Effect. Science, 316(April):274–277, 2007. ISSN 0036-8075. doi: 10.5061/dryad.5t110. Supplementary.

[64] O. Golubov and Y. N. Krugly. Tangential Component of the Yorp Effect. The Astrophysical Journal, 752(1):L11, 2012. ISSN 2041-8205. doi: 10.1088/2041-8205/752/1/L11. URL http://stacks.iop.org/2041-8205/752/i=1/a=L11?key=crossref.0a13b483b02dd05dd52a6282966dc4af.

[65] O. Golubov, D. J. Scheeres, and Yu. N. Krugly. A Three-Dimensional Model of Tangential Yorp. The Astrophysical Journal, 794(1):22, 2014. ISSN 1538-4357. doi: 10.1088/0004-637X/794/1/22. URL http://stacks.iop.org/0004-637X/794/i=1/a=22?key=crossref.b2ff6772941868ece5239bf8e0defeea.

[66] P. Ševeček, O. Golubov, D. J. Scheeres, and Yu. N. Krugly. Obliquity Dependence of the Tangential YORP. Astronomy & Astrophysics, 592:A115, 2016. ISSN 0004-6361. doi: 10.1051/0004-6361/201628746. URL http://arxiv.org/abs/1605.06959{%}0Ahttp://dx.doi.org/10.1051/0004-6361/201628746{%}5Cnhttp://www.aanda.org/10.1051/0004-6361/201628746.

[67] O. Golubov and D. J. Scheeres. New Results on Spin Evolution due to the YORP Effect. In Division of Planetary Sciences Meeting 49, Provo, UT, 2017.

[68] Matija Ćuk and Joseph A. Burns. Effects of Thermal Radiation on the Dynamics of Binary NEAs. Icarus, 176(2):418–431, 2005. ISSN 00191035. doi: 10.1016/j.icarus.2005.02.001.

[69] J.-L. Margot. Binary Asteroids in the Near-Earth Object Population. Science, 296 (5572):1445–1448, 2002. ISSN 00368075. doi: 10.1126/science.1072094. URL http://www.sciencemag.org/cgi/doi/10.1126/science.1072094.

[70] P. Pravec, D. Vokrouhlický, D. Polishook, D. J. Scheeres, A. W. Harris, A. Galád, O. Vaduvescu, F. Pozo, A. Barr, P. Longa, F. Vachier, F. Colas, D. P. Pray, J. Pollock, D. Reichart, K. Ivarsen, J. Haislip, A. Lacluyze, P. Kusnirák, T. Henych, F. Marchis, B. Macomber, S. A. Jacobson, Y. N. Krugly, A. V. Sergeev, and A. Leroy. Formation of Asteroid Pairs by Rotational Fission. Nature, 466(7310):1085–8, 2010. ISSN 1476-4687. doi: 10.1038/nature09315. URL http://dx.doi.org/10.1038/nature09315.

[71] M Ćuk. Formation and Destruction of Small Binary Asteroids. The Astrophysical Journal Letters, pages 57–60, 2007. ISSN 0004-637X. doi: 10.1086/516572. URL http://iopscience.iop.org/1538-4357/659/1/L57.

[72] Matija Ćuk and David Nesvorný. Orbital Evolution of Small Binary Asteroids. Icarus, 207(2):732–743, 2010. ISSN 00191035. doi: 10.1016/j.icarus.2009.12.005.

[73] J. McMahon and D. Scheeres. Secular Orbit Variation due to Solar Radiation Effects: A Detailed Model for BYORP. Celestial Mechanics and Dynamical Astronomy, 106 (3):261–300, 2010. ISSN 09232958. doi: 10.1007/s10569-009-9247-9.

[74] J. McMahon and D. Scheeres. Detailed Prediction for the BYORP Effect on Binary Near-Earth Asteroid (66391) 1999 KW4 and Implications for the Binary Population. Icarus, 209(2):494–509, oct 2010. ISSN 00191035. doi: 10.1016/j.icarus.2010.05.016. URL http://linkinghub.elsevier.com/retrieve/pii/S0019103510002083.

[75] P. Pravec. Fast and Slow Rotation of Asteroids. Icarus, 148(1):12–20, 2000. ISSN 00191035. doi: 10.1006/icar.2000.6482. URL http://linkinghub.elsevier.com/retrieve/doi/10.1006/icar.2000.6482.

[76] D. J. Scheeres. Stability of the Planar Full 2-body Problem. Celestial Mechanics and Dynamical Astronomy, 104(1-2):103–128, 2009. ISSN 09232958. doi: 10.1007/s10569-009-9184-7.

[77] D. J. Scheeres. Minimum Energy Asteroid Reconfigurations and Catastrophic Disruptions. Planetary and Space Science, 57(2):154–164, 2009. ISSN 00320633. doi: 10.1016/j.pss.2008.03.009.

[78] S. A. Jacobson and D. J. Scheeres. Dynamics of Rotationally Fissioned Asteroids: Source of Observed Small Asteroid Systems. Icarus, 214(1):161–178, jul 2011. ISSN 00191035. doi: 10.1016/j.icarus.2011.04.009. URL http://linkinghub.elsevier.com/retrieve/pii/S0019103511001448.

[79] P. Pravec and A. W. Harris. Binary Asteroid Population. 1. Angular Momentum Content. Icarus, 190(1):250–259, 2007. ISSN 00191035. doi: 10.1016/j.icarus.2007.02.023.

[80] D. Vokrouhlicky and D. Nesvorny. Pairs of Asteroids Probably of a Common Origin. The Astronomical Journal, 136(1):280–290, 2008. ISSN 0004-6256. doi: 10.1088/0004-6256/136/1/280. URL http://stacks.iop.org/1538-3881/136/i=1/a=280?key=crossref.fabdae875c2c028c38f7a34bc26de547.

[81] L. A. M. Benner, M. C. Nolan, S. J. Ostro, J. D. Giorgini, D. P. Pray, A. W. Harris, C. Magri, and J.-L. Margot. Near-Earth Asteroid 2005 CR37 : Radar Images and Photometry of a Candidate Contact Binary. Icarus, 182:474–481, 2006. doi: 10.1016/j.icarus.2006.01.016.

[82] S. Tremaine, J. Touma, and F. Namouni. Satellite Dynamics on the Laplace Surface. The Astronomical Journal, 137(3):3706–3717, mar 2009. ISSN 0004-6256. doi: 10.1088/0004-6256/137/3/3706. URL http://stacks.iop.org/1538-3881/137/i=3/a=3706?key=crossref.7166da0a6724d0175f85d1c362264064.

[83] A. J. Rosengren and D. J. Scheeres. Laplace Plane Modifications Arising From Solar Radiation Pressure. The Astrophysical Journal, 786(1):45, may 2014. ISSN 0004-637X. doi: 10.1088/0004-637X/786/1/45. URL http://stacks.iop.org/0004-637X/786/i=1/a=45?key=crossref.0890dae4f8368622f8e7fd4658c5dd03.

[84] Y. Kozai. Secular Perturbations of Asteroids with High Inclination and Eccentricity. The Astronomical Journal, 67(9):591–598, 1962. ISSN 0717-6163. doi: 10.1007/s13398-014-0173-7.2.

[85] A. Abad and E. Lacruz. Computing Derivatives of a Gravity Potential by using Automatic Differentiation. Celestial Mechanics and Dynamical Astronomy, 117(2):187–200, 2013. ISSN 09232958. doi: 10.1007/s10569-013-9505-8.

[86] marquis de Laplace, Pierre Simon. Traite de Mecanique Celeste. Paris (Courcier), Volume 4(Book 8), 1805.

[87] R. R. Allan and G. E. Cook. The Long-Period Motion of the Plane of a Distant Circular Orbit. The Royal Society, Proceedings Series A, 280(1380):97–109, 1964.

[88] William R. Ward. Orbital Inclination of Iapetus and the Rotation of the Laplacian Plane. Icarus, 46(1):97–107, 1981. ISSN 10902643. doi: 10.1016/0019-1035(81)90079-8.

[89] A. R. Dobrovolskis. The Laplace Plane of Uranus and Pluto, 1993.

[90] A. J. Rosengren and D. J. Scheeres. On the Milankovitch Orbital Elements for Perturbed Keplerian Motion. Celestial Mechanics and Dynamical Astronomy, 118 (3):197–220, jan 2014. ISSN 0923-2958. doi: 10.1007/s10569-013-9530-7. URL http://link.springer.com/10.1007/s10569-013-9530-7.

[91] D. Brouwer and G. M. Clemence. Methods of Celestial Mechanics. London, 1961.

[92] S. M. Rieger and D. J. Scheeres. Laplace Plane Dynamics with Solar Radiation Pressure in the Vicinity of an Asteroid. In AIAA/AAS Astrodynamics Specialists Conference, 2014.

[93] S. R. Chesley, D. Farnocchia, M. C. Nolan, D. Vokrouhlický, P. W. Chodas, A. Milani, F. Spoto, B. Rozitis, L. A. M. Benner, W. F. Bottke, M. W. Busch, J. P. Emery, E. S. Howell, D. S. Lauretta, J.-L. Margot, and P. A. Taylor. Orbit and Bulk Density of the OSIRIS-REx Target Asteroid (101955) Bennu. Icarus, 235(101955):5–22, 2014. ISSN 10902643. doi: 10.1016/j.icarus.2014.02.020.

[94] Ryan P Russell and Demyan Lantukh. Heliotropic Orbits with Zonal Gravity and Shadow Perturbations : Application at Bennu. 39(9), 2016. doi: 10.2514/1.G001279.

[95] Demyan Lantukh, Ryan P Russell, and Stephen Broschart. Heliotropic orbits at oblate asteroids : balancing solar radiation pressure and J2 perturbations. pages 171–190, 2015. doi: 10.1007/s10569-014-9596-x.

[96] Stephen B Broschart, Gregory Lantoine, and Daniel J Grebow. Quasi-Terminator Orbits near Primitive Bodies. 120(2):195–215, 2014. doi: 10.1007/s10569-014-9574-3.

[97] Stephen B Broschart and Benjamin F Villac. Identification of Non-Chaotic Terminator Orbits near 6489 Golevka. pages 1–20, 2009.

[98] Benjamin Villac. Applications of Chaoticity Indicators to Stability Analysis around Small Bodies. (949):1813–1832, 2009.

[99] Benjamin F Villac, Katherine Yi-yin Liu, and Stephen B Broschart. Numerical Exploration of Small-Body Orbiter Dyncamics using Chaoticity Indicators. pages 1603–1622, 2009.

[100] D. Rabinowitz, E. Helin, K. Lawrence, and S. Pravdo. A Reduced Estimate of the Number of Kilometre-Sized Near-Earth Asteroids. Nature, 403(6766):165–166, 2000. ISSN 00280836. doi: 10.1038/35003128.

[101] S. M. Rieger, D. J. Scheeres, and B. Barbee. Orbital Stability Regions for Hypothetical Natural Satellites of 101955 Bennu (1999 RQ36). In 26th AAS/AIAA Space Flight Mechanics Meeting,, Napa, CA, 2016.

[102] S. A. Jacobson, D. J. Scheeres, and J. McMahon. Formation of the Wide Asynchronous Binary Asteroid Population. The Astrophysical Journal, 780:60, 2013. ISSN 0004-637X. doi: 10.1088/0004-637X/780/1/60. URL http://stacks.iop.org/0004-637X/780/i=1/a=60?key=crossref.f796260887d953984d85e7b931b949b8{%}5Cnpapers3://publication/doi/10.1088/0004-637X/780/1/60.

[103] Peter Goldreich. Inclination of Satellite Orbits about an Oblate Precessing Planet. The Astronomical Journal, 70(1):5–9, 1965.

[104] P. Goldreich. History of the Lunar Orbit. Reviews of Geophysics, 4(4):411–439, 1966. ISSN 19449208. doi: 10.1029/RG004i004p00411.

[105] J. A. Burns, P. Hamill, J. N. Cuzzi, and R.H. Durisen. On the "Thickness" of Saturn's Rings Caused by Satellite and Solar Perturbations and be Planetary Recession. The Astronomical Journal, 84(11):1783–1801, 1979.

[106] A. R. Dobrovolskis, N. J. Borderies, and T. Y. Steiman-Cameron. Stability of Polar Rings Around Neptune. Icarus, 81(1):132–144, 1989. ISSN 10902643. doi: 10.1016/0019-1035(89)90130-9.

[107] Kevin J. Walsh and Derek C. Richardson. A Steady-State Model of NEA Binaries formed by Tidal Disruption of Gravitational Aggregates. Icarus, 193(2):553–566, 2008. ISSN 00191035. doi: 10.1016/j.icarus.2007.08.020.

[108] M. W. Busch and Et. Al. Radar Imaging and Shape Modeling of Contact-Binary Near-Earth Asteroids 11066 Sigurd, 2000 YF29, and 2004 XL14. in prep, 2017.

[109] Robert Johnston. Asteroids with Satellites. URL http://www.johnstonsarchive.net/astro/asteroidmoons.html.

[110] D. S. Lauretta, A. E. Bartels, M. A. Barucci, E. B. Bierhaus, R. P. Binzel, W. F. Bottke, H. Campins, S. R. Chesley, B. C. Clark, B. E. Clark, E. A. Cloutis, H. C. Connolly, M. K. Crombie, M. Delbo, J. P. Dworkin, J. P. Emery, D. P. Glavin, V. E. Hamilton, C. W. Hergenrother, C. L. Johnson, L. P. Keller, P. Michel, M. C. Nolan, S. A. Sandford, D. J. Scheeres, A. A. Simon, B. M. Sutter, D. Vokrouhlicky, and K. J. Walsh. The OSIRIS-REx Target Asteroid (101955) Bennu: Constraints on its Physical, Geological, and Dynamical Nature from Astronomical Observations. Meteoritics and Planetary Science, 50(4):834–849, 2015. ISSN 10869379. doi: 10.1111/maps.12353.

[111] J. Kawaguchi. Summary of Guidance , Navigation and Control Achievement in its Proximity Phase. AIAA/AAS Astrodynamics Specialist Conference, (August):1–8, 2006. doi: 10.2514/6.2006-6533.

[112] K. J. Walsh, D. C. Richardson, and P. Michel. Rotational Breakup as the Origin of Small Binary Asteroids. Nature, 454(7201):188–191, 2008. ISSN 0028-0836. doi: 10.1038/nature07078.

[113] P. Pravec, P. Scheirich, P. Kušnirák, L. Šarounová, S. Mottola, G. Hahn, P. Brown, G. Esquerdo, N. Kaiser, Z. Krzeminski, D. P. Pray, B. D. Warner, A. W. Harris, M. C. Nolan, E. S. Howell, L. A M Benner, J. L. Margot, A. Galád, W. Holliday, M. D. Hicks, Yu N. Krugly, D. Tholen, R. Whiteley, F. Marchis, D. R. DeGraff, A. Grauer, S. Larson, F. P. Velichko, W. R. Cooney, R. Stephens, J. Zhu, K. Kirsch, R. Dyvig, L. Snyder, V. Reddy, S. Moore, Š Gajdoš, J. Világi, G. Masi, D. Higgins, G. Funkhouser, B. Knight, S. Slivan, R. Behrend, M. Grenon, G. Burki, R. Roy, C. Demeautis, D. Matter, N. Waelchli, Y. Revaz, A. Klotz, M. Rieugné, P. Thierry, V. Cotrez, L. Brunetto, and G. Kober. Photometric Survey of Binary Near-Earth Asteroids. Icarus, 181(1):63–93, 2006. ISSN 00191035. doi: 10.1016/j.icarus.2005.10.014.

Appendix A

Tabulated Results for Natural Satellites

Table A.1: Range of stable natural satellite diameters for semi-major axes 1-5 km.

	Semi-major axis (km)				
	1	2	3	4	5
i°	Diameter (m)				
0	0.3-15	1.5-15	1.5-15	1.5-15	1.5-15
6	0.3-15	1.5-15	1.5-15	1.5-15	1.5-15
12	0.3-15	1.5-15	1.5-15	1.5-15	1.5-15
18	0.45-15	1.5-15	1.5-15	1.5-15	1.5-15
24	0.6, 1.5-15	1.5-15	1.5-15	1.5-15	1.5-15
30	1.5-15	1.5-15	1.5-15	1.5-15	1.5-15
36	1.5-15	1.5-15	0.075, 1.5-15	0.15, 1.5-15	0.225, 1.5-15
42	2.25-15	1.5-15	0.075, 1.5-15	0.15, 0.675-15	0.15-0.225, 1.5-15
48	3.75-15	0.03, 1.5-15	0.0525-0.675, 1.5-15	0.075-0.225, 1.5-15	0.15-0.3, 1.5-15
54	3.75-15	0.03-0.06, 1.5-15	0.0375-0.15, 0.675-15	0.0675-0.225, 1.5-15	0.15-0.3, 1.5-15
60	5.25-15	0.03-0.0675, 1.5-15	0.045-0.15, 0.675-15	0.0675-0.3, 1.5-15	0.15-0.375, 1.5-15
66	15	0.0225-0.075, 2.25-15	0.0375-0.15, 0.675-0.75, 3-15	0.06-0.3, 2.25-15	0.15-0.375, 2.25-15
72	5.25-15	0.015-0.075, 1.5-15	0.0375-0.225, 0.75, 2.25, 15	0.06-0.3, 6.75-15	0.15-0.375, 6-15
78	0.0075, 5.25-15	0.015-0.075, 0.675-15	0.03-0.225, 1.5-15	0.06-0.3	0.15-0.45
84	0.0075, 5.25-15	0.015-0.075, 0.6-15	0.03-0.225, 1.5-15	0.0525-0.3, 3-15	0.15-0.45
90	1.5-15	0.015-0.075, 0.6-15	0.03-0.225, 1.5-15	0.0525-0.375, 3-15	0.15-0.45
96	0.75-15	0.015-0.075, 0.6-15	0.03-0.225, 1.5-15	0.0525-0.3, 3.75-15	0.15-0.45
102	0.0075, 0.75-15	0.015-0.075, 0.525-15	0.03-0.225, 1.5-15	0.0525-0.3	0.15-0.45
108	0.375, 0.525-15	0.015-0.075, 0.525-15	0.0375-0.15, 0.75-3, 6.75-15	0.06-0.3, 6.75-15	0.15-0.45, 5
114	0.375-15	0.015-0.0675, 0.525-15	0.0375-0.15, 0.675-0.75, 2.25-15	0.06-0.3, 2.25-15	0.15-0.375, 3-15
120	0.525-15	0.0225-0.06, 0.525-15	0.0375-0.15, 0.6-15	0.0675-0.3, 1.5-15	0.15-0.375, 2.25-15
126	0.375-15	0.0225-0.0525, 0.525-15	0.045-0.15, 0.6-15	0.0675-0.225, 1.5-15	0.15-0.375, 1.5-15
132	0.6-15	0.75-15	0.045-0.075, 0.6-15	0.075-0.225, 0.75-15	0.15-0.3, 1.5-15
138	0.75-15	0.675-15	0.045-0.075, 1.5-15	0.075-0.15, 0.675-15	0.15-0.225, 1.5-15
144	3.0-15	1.5-15	0.0525-0.0675, 0.75-15	0.675-15	0.15-0.225, 1.5-15
150	15	1.5-15	1.5-15	1.5-15	0.75-15
156	1.5, 5.25-15	1.5-15	1.5-15	1.5-15	1.5-15
162	2.25-15	1.5-15	1.5-15	1.5-15	1.5-15
168	2.25-15	2.25-15	1.5-15	1.5-15	1.5-15
174	2.25-15	2.25-15	1.5-15	1.5-15	1.5-15

Table A.2: Range of stable natural satellite diameters for semi-major axes 11-15 km.

	Semi-major axis (km)				
	11	12	13	14	15
i°	Diameter (m)				
0	1.5-15	1.5-15	1.5-15	1.5-15	1.5-15
6	1.5-15	1.5-15	1.5-15	1.5-15	1.5-15
12	1.5-15	1.5-15	1.5-15	1.5-15	1.5-15
18	1.5-15	1.5-15	1.5-15	1.5-15	1.5-15
24	1.5-15	1.5-15	1.5-15	1.5-15	1.5-15
30	1.5-15	1.5-15	1.5-15	1.5-15	1.5-15
36	1.5-15	1.5-15	1.5-15	1.5-15	2.25-15
42	1.5-15	1.5-15	1.5-15	1.5-15	1.5-15
48	1.5-15	1.5-15	1.5-15	1.5-15	1.5-15
54	0.525- 0.6, 1.5-15	1.5-15	1.5-15	2.25-15	2.25-15
60	0.525-0.75, 2.25-15	0.675, 2.25-15	2.25-15	2.25-15	2.25-7.5
66	0.525-0.75, 2.25-15	0.6-0.75, 3-15	2.25-15	3.0-15	3, 5.25-6, 7.5-15
72	0.45-0.75, 3.75-15	0.6-0.75, 3-15	0.75, 3.75-6.75, 15	3.75-6.75, 15	3.75
78	0.45-0.75	0.675-0.75	-	-	-
84	0.525-0.75	0.675	-	-	-
90	0.6-0.675	-	-	-	-
96	0.675-0.75	0.75	-	-	-
102	-	-	-	-	-
108	0.75	-	-	-	-
114	15	-	15	-	-
120	6.0-15	15	15	-	-
126	3.75, 5.25-15	-	-	-	-
132	3.75-15	15	15	15	15
138	3.0-15	7.5-15	7.5-15	7.5-15	7.5-15
144	3-3.75, 5.25-15	6.75-15	6.0-15	6.75-15	6.75-15
150	3, 6-15	6.0-15	6.0-15	6.0-15	6.0-15
156	3, 5.25-15	5.25-15	5.25-15	6.0-15	6.0-15
162	5.25-15	5.25-15	5.25-15	5.25-15	5.25-15
168	5.25-15	5.25-15	5.25-15	5.25-15	5.25-15
174	5.25-15	5.25-15	5.25-15	5.25-15	5.25-15

Table A.3: Range of stable natural satellite diameters for semi-major axes 20 and 25 km.

	Semi-major axis (km)	
	20	25
i°	Diameter (m)	
0	2.25-15	6-7.5
6	3.0-15	6-6.75
12	2.25-15	6.75, 15
18	3.0-15	6.0-15
24	2.25-15	-
30	2.25-15	-
36	2.25-3, 5.25-6, 15	-
42	3	-
48	5.25	-
54	-	-
60	-	-
66	-	-
72	-	-
78	-	-
84	-	-
90	-	-
96	-	-
102	-	-
108	-	-
114	-	-
120	-	-
126	-	-
132	-	-
138	-	-
144	-	-
150	-	-
156	-	-
162	-	-
168	-	-
174	-	-